Earth Surface Processes and Landforms

Evaluation of aDcp processing options for secondary flow identification at river junctions

Journal:	*Earth Surface Processes and Landforms*
Manuscript ID	ESP-19-0030.R2
Wiley - Manuscript type:	Research Article
Date Submitted by the Author:	31-Jul-2019
Complete List of Authors:	Moradi, Gelare; UNIL, Institute of Earth Surface Dynamics, Faculty of Geosciences and Environment Vermeulen, Bart; Universiteit Twente Departement Civil Engineering, Water Engineering and Management Department Rennie, Colin; University of Ottawa, Civil Engineering Cardot, Romain; UNIL, Institute of Earth Surface Dynamics, Faculty of Geosciences and Environment Lane, Stuart; UNIL, Institute of Earth Surface Dynamics, Faculty of Geosciences and Environment
Keywords:	Acoustic Doppler current profiler, Secondary circulation, River confluences, River junctions
Note: The following files were submitted by the author for peer review, but cannot be converted to PDF. You must view these files (e.g. movies) online.	
ESP-19-0030.R2.zip	

“For the ESPL special issue: Measuring and numerical modelling of hydro-morphological processes in open-water”

Evaluation of aDcp processing options for secondary flow identification at river junctions

Gelare Moradi [1], Bart Vermeulen[3], Colin D. Rennie [2], Romain Cardot [1], Stuart N. Lane[1]

1: University of Lausanne - Institute of Earth Surface Dynamics (UNIL - IDYST) Université de Lausanne - IDYST Quartier Mouline - Bâtiment Géopolis - Switzerland

2: Civil Engineering Department, University of Ottawa

3: Water Engineering and Management Department, University of Twente, the Netherlands

Abstract

Secondary circulation in river confluences results in a spatial and temporal variation of fluid motion and a relatively high level of morphodynamic change. Acoustic Doppler current profiler (aDcp) vessel-mounted flow measurements are now commonly used to quantify such circulation in shallow water fluvial environments. It is well established that such quantification using vessel-mounted aDcps requires repeated survey of the same cross-section. However, less attention has been given to how to process these data. Most aDcp data processing techniques make the assumption of homogeneity between the measured radial components of velocity. As acoustic beams diverge with distance from the aDcp probe, the volume of the flow that must be assumed to be homogeneous between the beams increases. In the presence of secondary circulation cells, and where there are strong rates of shear in the flow, the homogeneity assumption may not apply,

especially deeper in the water column and close to the bed. To reduce dependence on this assumption, we apply a newly-established method to aDcp data obtained for two medium-sized (~60-80 m wide) gravel-bed river confluences and compare the results with those from more conventional data processing approaches. The comparsion confirms that in the presence of strong shear our method produces different results to more conventional approaches. In the absence of a third set of fully independent data, we cannot demonstrate conclusively which method is best, but our method involves less averaging and so in the presence of strong shear is likely to be more reliable. We conclude that it is wise to apply both our method and more conventional methods to identify where data analysis might be impacted upon by strong shear and where inferences of secondary circulation may need to be made more cautiously.

Keywords

Acoustic Doppler current profiler

Secondary circulation

River confluences

River junctions

Introduction

Acoustic Doppler current profilers (aDcps) are now used widely to measure river flow in three-dimensions, notably for the quantification of secondary flows. Applications have been made to river bedforms (e.g., Parsons et al., 2005; Kostaschuk et al., 2009; Shugar et al., 2010), bends (e.g., Dinehart and Burau, 2005; Kasvi et al., 2013; Vermeulen et al., 2014a, 2015; Engel and Rhoads, 2016; Knox and Latrubesse, 2016; Kasvi et al., 2017; Lotsari et al., 2017; Parsapour-Moghaddam and Rennie, 2018), junctions (e.g., Parsons et al., 2007; Lane et al., 2008; Szupiany et al., 2009; Riley and Rhoads, 2012; Riley et al., 2015; Gualtieri et al., 2017), bifurcations (e.g., Parsons et al., 2007; Szupiany et al., 2012), canyons (e.g., Alvarez et al., 2017; Tomas et al., 2018; Venditti et al., 2014), deltas (e.g., Czuba et al., 2011) and gravity currents (e.g., Garcia et al., 2007; Garcia et al., 2012). Research has also shown the need to make repeat section measurements (e.g., Szupiany et al., 2007; Jackson et al., 2008) and also to process these data carefully, (Muste et al., 2004; Rennie and Church 2010; Tsubaki et al., 2012; Parsons et al., 2013; Petrie et al., 2013). Such processing must take into account positioning (Rennie and Rainville, 2006) and orientation (Zhao et al., 2014) errors, and the treatment of repeat section measurements (e.g., Szupiany et al., 2007; Jackson et al., 2008).

This paper is concerned with recent observations regarding the inference of secondary flows from aDcp data and concerns regarding the assumption that flow is homogenous in the fluid volumes defined by the acoustic beams emitted from an aDcp and used to calculate any one point estimate (Vermeulen et al., 2014b). Acoustic beams are reflected by suspended particles, which, if moving, cause a Doppler shift in beam frequency, which is then detected at the sensor. This shift is directional so each beam measures the radial velocity, which is the velocity of particle motion parallel to the acoustic path. This can be assumed to be the flow velocity if the particle motion is identical to fluid motion. In order to resolve flow in more than one direction, aDcps require at least three acoustic beams to estimate three Cartesian components of velocity. The radial velocities originating from the beams are traditionally analyzed for a single measurement cycle at a single depth at a time (Vermeulen et al., 2014b). The velocity then applies to the volume of fluid defined by the beams at each depth. Flow within this volume is assumed to be homogeneous. However, as the beams spread from the sensor, depth bins increase in horizontal size (Rennie et al., 2002). This means that: (1) bins further from the sensor are likely to produce less reliable velocities because the bin size is greater and the flow within bins is more likely to be heterogeneous (Gunawan et al., 2011); and (2), even in smaller bins, velocities may be less reliable in zones of strong shear where also the within-bin flow is less likely to be homogeneous. In a river where measurements are made throughout the flow depth, the maximum shear may be close to the bed, where the beam divergence may also be greatest.

One solution to this problem accounts for first order shear within the flow volume (e.g. Marsden and Ingram, 2004) through a Taylor expansion of the coordinate transform used to determine the Cartesian velocity components. Under this solution, flow is allowed to vary linearly within the bin, but the bin's volume becomes potentially larger with distance from the sensor. Vermeulen et al. (2014b) developed and tested a second solution. As explained in detail below, multiple radial (beam) velocity measurements within a single bin are put through a Cartesian transform to obtain a localized within-bin three-dimensional velocity. This method strongly reduces the volume over which homogeneity should be assumed and Vermeulen et al. (2014b) found that this significantly impacted interpretations of secondary velocities in the presence of strong shear. In this paper, we seek to quantify the effects of this method for the measurement of secondary flow in two medium-sized river junctions (c. 60-80 m post-junction channel width). River junctions are associated with very strong shear (e.g. Best and Roy, 1991; Biron et al., 1993, 1996a, 1996b; Sukhodolov and Rhoads, 2001; Rhoads and Sukhodolov, 2004, 2008; Konsoer and Rhoads, 2014; Sukhodolov et al., 2017), as well as well-developed secondary circulation (e.g. Ashmore et al., 1992; Rhoads and Kenworthy, 1995, 1998; Rhoads and Sukhodolov et al., 2001; Lane et al., 2008; Riley and Rhoads, 2012; Riley et al., 2015). Thus, understanding how to process effectively the aDcp data used to describe them is of paramount importance.

Methods for estimating Cartesian velocity components from aDcp data

In this section, we describe the two different methodological approaches used in this study to estimate Cartesian velocity components: (1) Method A, the Vermeulen et al., (2014b) method; and (2) Method B, the conventional method. Common to all methods is the assumption that data are available from repeat measurement of the same cross-section, as has been shown to be critical for obtaining reliable estimates of secondary circulation from aDcp data (Szupiany et al., 2007), particularly when single transect measurements are not close enough together.

Method A: based on Vermeulen et al., (2014b)

Application of the Vermeulen et al. (2014b) method requires mapping of radial beam velocity data onto a predefined mesh. This mesh requires both a bottom topography or bathymetric model, and an upper limit just below the water surface. As the measurements were made using several repeat transects for each cross section, the first step is to define a mean cross section for each set of individual transects (boat tracks). The second step is to define a grid mesh for this mean cross section. Third, all measured beam velocities are projected on to this cross section mesh. Finally, the beam velocities within each mesh cell are then used to resolve a Cartesian velocity for the mesh cell. Errors that influence these steps can be estimated.

The first step is estimation of the mesh extremes, both the lower boundary or bathymetry model and the upper boundary near the water surface. To generate the bathymetry model we use depth soundings collected with the aDcp. We recognize that each beam may register a different distance of the stream bed from the sounder, especially as we are dealing with bathymetrically irregular cross-sections. Specifically, for each bottom track sounding within each transect, we use the UTM coordinates obtained with a coupled differential GPS (dGPS), the range of each bottom track beam return, and the instrument tilt to estimate the bed elevation and horizontal position of each beam impingement point on the bed. These bed positions are combined together to identify an initial mean transect. Provided a point is within a certain distance from the initial mean cross-section, LOWESS interpolation (Appendix A) is applied, which has the effect of defining a bathymetric model that gives most weight to points that appear to be closer to the cross-section. It is important to note that this mean transect is not necessarily orthogonal to the primary flow direction and so will not yield true primary and secondary flow estimates without further correction. We address this below.

Once the initial bathymetric model is defined, we estimate a unique vector using the initial mean transect; that is the principal direction of the scatter cloud of all x and y UTM positions at the bed. This unique vector points in the direction of the largest eigenvector of the covariance matrix of all UTM positions (*t*). We then calculate the mean UTM position

(p_{mean}) for each set of individual transects and the difference between each measured beam position (p_b) and the mean position. The dot product of these obtained values and the unique vector is then used to define the projection of each UTM position in the direction of the unique vector. To identify the final mean cross section, we sum up all individual projected vectors and obtain the best fit to all available data (Figure 1).

To define the upper boundary of the mesh, we estimate the elevation of the water surface. As there is a blanking distance at the surface of the water during the measurement, we then remove this blanking distance, taken as 0.30 m. Thus, the mesh has also a blanking distance and the upper part of the cross-section is, strictly, the upper limit of available data, not the water surface.

"Figure1"

The second step uses the defined bathymetric model and available velocity bins within the measured area (not influenced by side lobes, and below the blanking distance) to define a cross-section mesh. The side-lobe interference is caused by the striking of the channel bed by side-lobe energy from each of the acoustic beams. This side-lobe energy has strong reflections from the bed, which result in echoes that overwhelm the signal from scatters near the bed. The thickness of the side-lobe layer is typically 6-7% of the measured depth (Morlock, 1996).

To generate the mesh, the cross section is initially subdivided into vertical slices with equal widths (Δn). For each slice, the simplest definition of mesh cell thicknesses (Δz) divides each vertical equally. These verticals are converted to non-dimensional σ coordinates using following equation:

157 $$\sigma=1-\left(\frac{p_v.\boldsymbol{k}-\eta}{p_b.\boldsymbol{k}-\eta}\right) \quad \text{(Vermeulen et al. 2014b)} \quad (1)$$

158 where p_v stands for velocity measurement positions (m), p_b is the corresponding bed position (m) that is found using velocity measurement horizontal positions and applying the bathymetric model, $\boldsymbol{k}$ is the upward pointing unit vector and η are the water surface fluctuations around the mean water level at which z=0.

162 However, because of beam spreading and differences in the distance of the sounder from the bed, which varies with position of the sounder, this tends to produce a highly heterogeneous number of measurements in each cell within the mesh. The alternative, adopted here, is to allow mesh cell thickness to vary through the water column such that there is a roughly equal number of beam velocities contributing to each mesh cell (see Figure 2 for a typical distribution).

168 As the river bed form is varying, to follow its shape, each mesh cell is considered to be a cuboid with 6 edges, two on the left side, two in the middle and two on the right side. To define these edges, the first step is to define the middle point of each mesh cell. Once defined, by calculating the slope for each half part of the mesh cell, edges can be obtained. The mesh cell faces are then calculated on the basis of adjacent verticals and the mesh cell upper and lower boundaries.

174 To identify the beams that contribute to each mesh cell, an index for each beam velocity is defined, which shows its associated mesh cell, using the projection of each radial velocity onto the estimated mean cross section (Figure 2).

177 “Figure 2”

178 In the third step, the radial velocities for each beam (**b**) that contribute to each mesh cell

179 (the N beam velocities) have to be transformed into Cartesian velocities (v_x, v_y and v_z)

180 using:

181 $$\begin{pmatrix} b_1 \\ \vdots \\ b_N \end{pmatrix} = \begin{pmatrix} q_1 \\ \vdots \\ q_N \end{pmatrix} . \begin{pmatrix} v_x \\ v_y \\ v_z \end{pmatrix} \leftrightarrow \mathbf{b} = Q.\mathbf{u} \qquad (2)$$

182 where **q** is a unit vector which describes the direction of the acoustic beam.

183 To obtain the raw beam velocities, we use matrix transformations obtained from the raw

184 data to transform measured velocities in XYZ coordinates into beam velocities. The

185 Vermeulen et al., (2014b) method includes in the transformations an explicit treatment of

186 the random errors due to internal and external factors and the bias (systematic errors)

187 caused by the measurement system and the nature of river flow (Tsubaki et al., 2012).

188 Random errors include those that come from sampling a time-varying flow in the presence

189 of strong gradients and represent a form of aliasing. By adding a combined term of errors

190 ε, (2) becomes:

191 $$\mathbf{b} = Q\mathbf{u} + \varepsilon \qquad (3)$$

192 A least squares solution is fitted to (3) that minimizes the sum of the square of the errors.

193 The optimal estimation ($\hat{\mathbf{u}}$) for (**u**) is then given by the normal equation:

194 $$\hat{\mathbf{u}} = Q^{+}\mathbf{b} + \varepsilon \qquad (4)$$

195 where Q^{+} can be defined as:

196 $$Q^{+} = (Q^{T}Q)^{-1}Q^{T} \qquad (5)$$

To solve three Cartesian velocity components, we need at least three equations. Each beam measurement in a mesh cell adds an equation. Where enough beam velocities are collected in a mesh cell and the equations are different from each other (beam velocities are measured from different directions), the velocity can be estimated. To check whether this is the case, the matrix describing the system of equations can be analyzed. In the processing we use the rank which indicates how many unknowns can be solved from the system of equations. When the rank is three, the three Cartesian velocities can be solved. Where the rank of the matrix is one or two, the system cannot be solved. Where the system of equations is overdetermined, the obtained solution is a matrix with more equations (rows) than unknowns (columns). The velocity can be solved using the generalized inverse of the matrix and in such a way that the sum of squared errors is minimized. As this combined term of errors also contains information about the turbulence and accuracy of the measurements, we can obtain the covariance matrix of the velocity components:

$$\hat{\varepsilon}=\mathbf{b} - Q\hat{\mathbf{u}} \tag{6}$$

$$\mathrm{var}(\hat{\mathbf{u}})=\frac{\hat{\varepsilon}^T\hat{\varepsilon}(Q^TQ)^{-1}}{N-3} \tag{7}$$

and the variance of the velocity across the section can be then estimated as:

$$\mathrm{var}(\mathbf{u})=\frac{\mathrm{var}(\hat{\mathbf{u}})}{N} \tag{8}$$

Method B: the standard aDcp method

As the Doppler shift is directional, it can only measure radial velocities. With the standard method, to determine Cartesian velocity components, radial velocities then have to be resolved into three orthogonal velocity vectors. To do so, at least three beam velocities pointed in known directions are required. Also, because the beams are measuring different water profiles along their individual slant ranges, the assumption of horizontal homogeneity must be taken into account. Hence, in the standard method, the three dimensional velocity for each depth bin for each ping can be solved for a typical four-beam system using the following equations (Mueller and Wagner, 2009):

$$V_x=\frac{(b_3-b_1)}{\sqrt{2}\sin\theta} \tag{9}$$

$$V_y=\frac{(b_4-b_2)}{\sqrt{2}\sin\theta} \tag{10}$$

$$V_z=\frac{-(b_1+b_3)}{(2\cos\theta)}=\frac{-(b_2+b_4)}{(2\cos\theta)} \tag{11}$$

where V_y is the cross stream velocity assuming beam 3 is pointed upstream, V_x is the streamwise velocity, V_z is the vertical velocity, b_1, b_2, b_3 and b_4 are the radial velocities measured in beams 1,2,3 and 4 respectively and θ is the tilt angle of the beams referenced to vertical. These data should then be corrected for pitch and roll angles, obtained from the internal inclinometer and the heading angle from the internal compass. Velocity outputs are already corrected for ship velocities.

To compare results obtained using Method B with those of Method A, we use the same mean cross section built for Method A, as well as the same bathymetric model and the same mesh. Each measured velocity vector is assigned to the appropriate mesh cell by projecting its 3D position (horizontal position and depth) onto the mean cross section mesh. We then average x, y, and z components of all velocities measured within a mesh cell to obtain the mean velocity vector for the mesh cell.

Methodology

This paper is motivated by the need to acquire three-dimensional data from junctions of tributaries with a main river stem, here the River Rhône, western Switzerland, and so the need to identify methods for reliably obtaining Cartesian velocities from aDcp data. The Rhône tributaries typically have very high bedload transport rates for short periods of time, leading to the formation of very large tributary mouth bars downstream of their junctions with the main river. These bars are maintained for weeks or months such that at lower tributary flow, with negligible sediment supply, there is a legacy effect of previous high momentum tributary events upon junction morphology and secondary flow formation.

For this paper, we used a specially-designed rope and pulley system to collect aDcp data from the junction of two tributaries with the Rhône (Figure 3).

“Figure 3”

The Lizerne is a Rhône tributary of almost 20 km length that flows south-westward from the western slopes of the Tête Noire (2451m) or La Fava (2612m), in the Bernese Alps. This river is heavily regulated for hydropower with sediment extracted upstream of the junction. As a result, there is negligible sediment supply and no evidence of point bar formation. It reaches the Rhône between Ardon and Vétroz, forming a 90° junction angle and it has a bed that is nearly concordant with the Rhône.

The Grande Eau is a second tributary of the Rhône River which has a length of 26 km and takes its source on the Vaud side of the Les Diablerets and flows into the Rhône River with a 70° confluence angle, near Aigle. The Grande Eau bed is 1.5 m higher than the Rhône such that it is markedly discordant.

In this section, we: (1) describe the aDcp used to collect data; (2) describe how the aDcp was deployed; and (3) outline the analytical approaches used to interpret the results from the different methods. Although the method is valid for any aDcp that has an onboard compass and potential for differential GPS positioning, as is standard with most aDcps, we use a Sontek M9 aDcp in this study.

The Sontek M9 aDcp

The SonTek M9 aDcp is a nine-transducer system with three acoustic frequencies, configured as two sets of four profiling beams (3 MHz and 1 MHz transducers in Janus configurations) and one vertical beam (0.5 MHz Echo sounder) for depth measurements (SonTek YSI, 2010). It uses these two sets of four beams to provide raw radial velocity samples. These beams are equally spaced at 90º azimuth angles and are projected at an angle θ of 25 º off the vertical axis (SonTek YSI, 2000). For the standard configuration, the four beams encompass a sampling diameter of 93% of the distance from the aDcp (7% of side-lobe) (SonTek YSI, 2000).

The output velocities from the SonTek M9 Riversurveyor are either in Cartesian coordinates (XYZ) that are relative to sensor orientation or in Earth coordinates (ENU) for a SonTek system with compass and tilt sensors. These raw velocity data in Earth coordinates or XYZ coordinates are already corrected for the ship motion. To apply Method A to Sontek output data, as this method is based on radial velocities, it is necessary to transform these output velocities to radial velocities. To do so, we add ship velocities to these output velocities and then apply the inverses of the instrument’s matrix coordinate transformations (obtained from MATLAB files output by the SonTek data collection software RiverSurveyor). As the survey is being undertaken using a moving vessel, these radial velocities then have to be corrected again for the boat velocity. There are two key methods for doing this. The first uses the bottom tracking to measure the boat velocity relative to the river bed, under the assumption that the latter is stationary (i.e. there is no bedload transport). The second tracks the boat position using differential GPS (dGPS, e.g. Zhao et al., 2014). In this study, we corrected all raw beam velocities for ship velocities, using dGPS as we could not exclude the possibility of there being bedload transport.

To apply Method B in this study, we use the raw velocity data in Earth coordinates and we correct it for pitch and roll angles, obtained from internal inclinometer and heading angle data for the internal compass. For SonTek M9 aDcps, pitch is a y-axis rotation and roll an x-axis rotation.

Depending on the water depth and velocity, the Sontek M9 firmware changes the acoustic operating frequency and the water profiling mode on-the-fly, thus the number of sampled points in the vertical varies automatically from one profile to the next. Specifically, when the water is shallower than 0.75 m and the maximum velocity is less than 0.4 ms^{-1}, the M9 reports data acquired with a 3 MHz frequency using the pulse coherent mode to obtain a 2cm depth measurement resolution. For deeper situations, this frequency changes to 1 MHz pulse coherent pings using a 6cm aDcp cell size. If the maximum velocity is greater than 0.4 ms^{-1} then SmartPulse (i.e., broadband) mode is utilized, with the 3 MHz beams if depth is less than 5 m and the 1MHz beams if depth is greater than 5m, with the aDcp cell size optimized based on the current water depth. As a result of these on-the-fly changes, each measured profile has a different number of aDcp cells and different aDcp cell sizes. Hence, to correct the aDcp cell size variability, for both methods A and B there is the need to define a cross-sectional mesh and to project the measured velocities to this mesh. For Method A we use the beam velocity vertical positions in a non-dimensionalized coordinate system using equation 1, within the predefined mesh explained in section 2.1.

Deployment of the Sontek M9 in the river junctions

The survey work was undertaken in two junctions of the Swiss River Rhône, the Lizerne-Rhône confluence in August 2017 and the Grande Eau-Rhône confluence in May 2018, using a Sontek M9 vessel mounted aDcp and a specially-designed rope-pulley system (Figure 3c). The survey was spatial, monitoring 11 cross-sections from upstream of the junction to its downstream at the Lizerne-Rhône confluence with a Momentum ratio (Mr) of 0.018 (Figure 3a) and 11 cross-sections at the Grande Eau-Rhône confluence with a Mr of 0.022 (Figure 3b). Table 1 shows the general characteristics of these two confluences on the date of the measurements.

“Table 1”

As proposed previously by Dinehart and Burau (2005), Szupiany et al. (2007), Gunawan et al. (2011) and Vermeulen et al., (2014b) at least five repeats are required to have a robust estimation of secondary velocities. Hence, in this paper, data are processed for cross-section 6 at the Lizerne-Rhône confluence (Figure 3a), and for cross section 3 at the Grande Eau-Rhône confluence (Figure 3b). Identification of the minimum number of repeat transects necessary per cross-section was undertaken using cross-section 9 at the Lizerne-Rhône confluence (Figure 3a), which involves 16 repetitions. We noted that after application of Method A, the standard deviation of velocity stabilized with six repetitions, which is the number we adopt for this study.

Bin position error determination

Application of Method A requires estimation of the error terms in (2). The size of the sampling volume in each beam is determined by the size of the bin used. As the SonTek M9 aDcp uses different bin sizes depending on the water track frequency (section 2.1.3), these volumes could vary. Applying Method A might improve the velocity estimation for large measurement volumes at depth, as it does not rely on the homogeneity assumption. But as bins with a small number of velocity measurements will have greater error, this method can estimate velocities with error. Also, if the beam velocity distribution within each mesh cell is not linear, as averaging is made in the middle of each mesh cell, it can introduce error in velocity estimation. Thus, it is necessary to calculate a minimum necessary mesh cell size when applying Method A.

Method B is inherently limited by spatial averaging due to the potential use of divergent beams and the associated homogeneity assumption. In other words, one must assume that the velocity is homogeneous over the horizontal domain defined by beam divergence (Eq.12). Method A has the advantage that velocities are recorded within an individual beam depth bin, thus no spatial averaging between beams is required. However, in order for Method A to overcome the uncertainty induced by spatial averaging inherent to Method B, it is essential that the bin location is known explicitly. Error in bin location can be induced by dGPS position and or tilt sensor (pitch and roll) errors. We therefore compare possible bin position errors using Method A to beam divergence obtained from Method B to indicate when Method A should be advantageous over Method B.

Beam divergence is the spatial separation of the beams due to the Janus configuration of the beams with beam angles of 25°. This divergence determines the sampling volume that must be considered homogeneous for Method B and can be calculated using equation 12:

$$x_b=2d\tan\theta \qquad (12)$$

where d is the depth in m and θ is the beam angle which for a SonTek aDcp is 25°. The aDcp dGPS is used to reference the velocity measurements in space and to estimate the ship velocity. If dGPS is used for ship velocity, this introduces errors in measurement of the absolute water velocity (because ship velocity is subtracted from the water velocity measured in the reference frame of the aDcp). This uncertainty introduces error in velocity calculations.

To estimate the errors due to dGPS and the tilt sensors, in this study we assume normally distributed random errors with a standard deviation of ±1° for tilt sensors, based on manufacturer specifications, and a normally distributed displacement error measured by the dGPS for the dGPS positions (as a function of satellite configuration during measurement), and we apply a Monte Carlo approach which we run 100 times sampling under these uncertainties. Each time we calculate the estimated secondary velocity differences as compared with the original secondary velocities.

To be able to reduce the uncertainty due to velocity estimation using Method A compared to Method B, the errors induced in Method A related to GPS uncertainty and tilt sensors must be less than the errors in Method B due to beam divergence and the homogeneity assumption. Hence, Method A can be used if the error associated with a minimum aDcp cell size is in between the error due to beam divergence and the maximum estimated error due to the GPS and tilt sensors. Otherwise using this method introduces more error in velocity estimations than using Method B.

Data interpretation

Methods A and B, described above, were applied to the Sontek M9 data, to determine Cartesian velocities (v_x, v_y and v_z). As our interest is in process estimation, here we describe the methods we apply to the Cartesian velocities to estimate processes relevant to junction dynamics. In order to distinguish between primary and secondary components of flow, we need to rotate the initial mean transect. Options for doing this are reviewed in Lane et al. (2000) and we do not assess them here, but rather apply the zero net cross stream discharge definition (Lane et al., 2000). By calculating the mean values of the *x* and *y* velocity components (*U* and *V*), we then calculate the velocity magnitude (*v*). By rotating these velocity components to the direction of the cross-stream velocity, using the unique vector ($\boldsymbol{\sigma}$), primary velocity vectors ($\boldsymbol{v_p}$) and secondary velocity vectors ($\boldsymbol{v_s}$) then can be estimated.

$$v=\sqrt{U^2+V^2} \tag{13}$$

$$\begin{pmatrix}\sigma_x\\ \sigma_y\end{pmatrix}=\begin{pmatrix}U\\ V\end{pmatrix}/v \tag{14}$$

where σ_x and σ_y are sin and cos of the angle between the section angle and east.

$$\boldsymbol{v}_p=\sigma_x\boldsymbol{v}_x+\sigma_y\boldsymbol{v}_y \tag{15}$$

$$\boldsymbol{v}_s=-\sigma_y\boldsymbol{v}_x+\sigma_x\boldsymbol{v}_y \tag{16}$$

However, secondary circulation is all flow that is orthogonal to the primary flow and not just horizontal flow; there should be not net secondary flux in a section; and so correction should also consider vertical velocities. Thus, we extend these relationships to include vertical velocities:

$$\begin{pmatrix} \sigma_{x,1} & \sigma_{x,2} & \sigma_{x,3} \\ \sigma_{y,1} & \sigma_{y,2} & \sigma_{y,3} \\ \sigma_{z,1} & \sigma_{z,2} & \sigma_{z,3} \end{pmatrix} = \begin{pmatrix} U \\ V \\ W \end{pmatrix} / v \quad (17)$$

where: *U*, *V* and *W* are the mean velocities of *x*, *y* and *z* velocity components, respectively and *v* is the magnitude of the velocity which can be obtained using:

$$v=\sqrt{U^2+V^2+W^2} \quad (18)$$

$$\boldsymbol{v}_p=\sigma_{x,1}\boldsymbol{v}_x+\sigma_{x,2}\boldsymbol{v}_y+\sigma_{x,3}\boldsymbol{v}_z \quad (19)$$

$$\boldsymbol{v}_s=\sigma_{y,1}\boldsymbol{v}_x+\sigma_{y,2}\boldsymbol{v}_y+\sigma_{y,3}\boldsymbol{v}_z \quad (20)$$

$$\boldsymbol{v}_v=\sigma_{z,1}\boldsymbol{v}_x+\sigma_{z,2}\boldsymbol{v}_y+\sigma_{z,3}\boldsymbol{v}_z \quad (21)$$

To estimate velocity gradients, and to correct for weak curvature with the survey method at the edges of each transect line (e.g. Figure 3), all data have been transformed into row and column coordinates (η and ζ) using the following transformation:

$$\begin{pmatrix} \frac{\partial}{\partial n} \\ \frac{\partial}{\partial z} \end{pmatrix} = \begin{pmatrix} \frac{\partial \eta}{\partial n} & \frac{\partial \zeta}{\partial n} \\ \frac{\partial \eta}{\partial z} & \frac{\partial \zeta}{\partial z} \end{pmatrix} \begin{pmatrix} \frac{\partial}{\partial \eta} \\ \frac{\partial}{\partial \zeta} \end{pmatrix} \quad (22)$$

where *n* and *z* are horizontal and vertical coordinates on the section plane, respectively (Vermeulen et al., 2014b).

Results

Primary and secondary velocities

Primary and secondary velocities estimated using methods A and B for the Lizerne-Rhône confluence appear to be similar at cross-section 6 (Figures 4a and 4b) and the differences in estimated secondary flows are minor. The differences are most pronounced between -10 and 5 m, in the middle of the main channel.

These primary and secondary velocity patterns show higher differences at cross-section 3 of the confluence of Grande Eau-Rhône (Figures 4c and 4d) despite it having a similar momentum ratio to the Lizerne during measurement. Primary velocities differ significantly between methods A and B: (1) at greater distance from the aDcp because the bins contain larger volumes of water assumed to be homogenous; and (2) at the edges of the cross-section where there are more beam velocity measurements (contours in Figures 4c and 4d). Secondary velocity vectors estimated using Method A indicate flow convergence at the surface and flow descending towards the riverbed throughout the centre of the channel (Figure 4c). This is due to a high degree of bed discordance between the Grande Eau and the Rhône, which increases the penetration of the tributary flow into the main channel over the junction, and which forms a zone of high lateral and vertical shear, on the one hand, and main channel narrowing because of penetration of the tributary mouth bar on the other hand. The secondary velocity vectors estimated by Method B show a weaker penetration of the tributary flow into the main channel, which results in a reverse flow towards the bank on the tributary side of the channel at the surface of the mixing interface (Figure 4d). In this case, the core of the secondary circulation is located in the middle of the main channel and closer to the inner bank.

“Figure 4”

Figure 5 and Figure 6 quantify the differences in primary and secondary velocity patterns estimated using methods A and B, for the Lizerne-Rhône confluence. Figures 5a and 5c and Figures 6a show that almost 4% of mesh cells have a relative difference in primary velocities between methods A and B of more than 10%. These differences can exceed 0.2 ms^{-1} and so they are relatively small. Velocity differences are more pronounced in estimated secondary velocities, with almost 82% of mesh cells having a difference of more than 10%, and almost 37% of mesh cells having a difference of more than 50% (Figure 5b, 5d and 6b).

“Figure 5”

“Figure 6”

At the Grande Eau-Rhône confluence, these differences are greater as compared with those of the Lizerne-Rhône confluence. Figures 7a, 7c and 8a show that these differences for primary velocities exceed 0.4 ms^{-1} in the zone of high vertical and lateral shear and near the inner bank. Almost 20% of the mesh cells have a relative difference in primary velocities between methods A and B of more than 10%. The secondary velocity differences are more pronounced between these two methods. Figures 7b and 7d show differences with a magnitude of 0.4 ms^{-1} near the edges and near the bed. Almost all the mesh cells have a difference in estimated secondary velocities between two methods. Figure 8b shows that almost 93% of the mesh cells have a relative difference of 10% between methods A and B. although this value decreases to 55% for a relative difference of 90% between these two methods.

“Figure 7”

“Figure 8”

Velocity gradients

As Figure 9 shows, there is a strong relationship between lateral gradient in secondary velocities and differences between the secondary velocities estimated using methods A and B for both the Lizerne-Rhône and the Grande Eau-Rhône confluences. This is because a stronger velocity gradient increases the probability that the assumption of flow homogeneity within a bin is likely to fail. Indeed, the marked differences between methods A and B at the Grande Eau confluence (Figure 7) are also in a zone of strong lateral shear.

“Figure 9”

Number of repeat transects

One way to reduce data fluctuations due to random errors and turbulence, during the measurement using moving vessel aDcps, is to average by using several repeat transects together in one cross section. As each estimated velocity measurement is a single sample in time, adding in a repeat section adds in an additional estimated velocity measurement. Under [8], this should cause the variance to increase, despite the number of measurements used in its estimation increasing, until the point at which there are enough repeats to capture the effects the range of scales of variation in turbulence impacting the measurement. Then, this variance will become stable. At this stage we can consider the number of repeats as the minimum number required to have a robust estimation of secondary velocity vectors that is to have reached estimates of velocity that are asymptotic on this stable state.

Here we apply both methods A and B to the survey of 16 repeats at cross-section 9 in Figure 3a at the Lizerne-Rhône confluence. To allow a reasonable comparison, three mesh cells in the middle of the cross section, and at three different depths (near the surface, middle depth and near the bed) have been chosen (Figure 11). Results show that by using Method A, after six repeats, a stable variance of the velocity estimator is obtained at the Lizerne-Rhône confluence (Figure 11a). Many more repeats are needed using Method B (Figure 11b) and this is likely because Method B uses fewer measurements per mesh cell. These results also show a higher standard deviation of the velocity estimation near the surface, using Method A and before achieving the stable situation. This can be explained by the fact that near the surface Method A is more sensitive to errors caused by positioning, while near the bed, hence with distance from the sounder, as the beam spread increases, the improvement obtained using Method A is more pronounced (Figure 11a).

"Figure 10"

"Figure 11"

DGPS and tilt sensor uncertainty analysis

As explained above a normally distributed random error has been applied 100 times to both dGPS positioning (by adding a random offset) and tilt sensors (by changing pitch and roll angles randomly) and the secondary velocities have been estimated using Method A for each perturbed dataset. As Figure 12 shows, the magnitude of errors related to dGPS accuracy are higher than those related to tilt sensor accuracy, for both confluences. These values can reach ±0.03 ms^{-1} and confirms the earlier finding of Rennie and Rainville (2006) which showed that GPS corrections can have average errors of about ±0.03 ms^{-1} (Figures 12a and 12c). These magnitudes are also higher near the surface and near the bed for the Lizerne-Rhône confluence (Figure 12a). Near the surface, as there fewer measurements that can contribute to the estimation of aDcp position and tilt, uncertainties in dGPS data will have a greater effect. Near the bed, as the velocity gradient is higher, errors will be greater as well. Figure 12c shows higher magnitudes near the surface at cross-section 3 in Figure 3b for the Grande Eau-Rhône confluence.

Errors related to tilt sensor uncertainty are higher where there is a higher velocity gradient. This is related to the fact that within the mesh cells with higher velocity gradients, as the velocity distribution is not linear, and as averaging is made in the middle of the mesh cell, it is more probable that the velocity will be affected by sensor inaccuracies of bin positioning, and so be in error (Figures 12b and 12d).

"Figure 12"

Homogeneity assumption analysis

Figure13 shows the maximum inhomogeneity allowance, using Method B for both case studies. These results are obtained by dividing the velocity gradient obtained from equation 22 by the divergence of the beams from equation 12. They confirm that, for the homogeneity assumption to be valid and thus error to be minimized using Method B, the maximum mesh cell size, which can be used is as small as 5cm near the bed. Clearly, this is impossible as the configuration of the beams using aDcps always results in beam divergence greater than 5cm.

"Figure 13"

Primary and secondary flow patterns

In this section, we compared estimated primary and secondary velocities using methods A and B for other cross sections in Figure 3 for both river confluences.

Figure 14 shows the results for cross sections 4, 5 and 7 (in Figure 3a) at the Lizerne-Rhône confluence. These cross sections also show similar results in primary and secondary velocity patterns for both methods A and B. Figure15 shows different patterns in primary and secondary velocities estimation using Method A and B for cross sections 4,6 and 8 in Figure 3b at the Grande Eau-Rhône confluence. Method A leads to the identification of a stronger and more coherent tributary penetration at cross-section 4 and weaker upwelling mid-channel, giving the impression of less intense secondary circulation (Figure 15). At section 6, flow towards the true left across the shallow top of the tributary mouth bar is identified and is coherent with Method A. At the channel-scale there is general flow convergence reflecting channel narrowing (Figure 15). When using Method B, these patterns are less coherent and flow is towards the true right in the vicinity of the tributary mouth bar. These patterns are repeated for section 8 (Figure 15).

“Figure 14”

“Figure 15”

Discussion

In this paper we used data collected with boat-mounted aDcp technology at two confluences of the Swiss river Rhône, both with similar and very low momentum ratios (0.018, 0.022) and analysed these using two different methods, A and B, to estimate Cartesian velocity components. Method A is based on a methodological approach developed by Vermeulen et al. (2014b). It differs by treating explicitly each individual beam velocity based on its position within a predefined mesh. Results show that this method reduces the volume over which the flow must be assumed to be homogenous (Fig 13). It can, but not necessarily does, result in differences in estimated primary and secondary velocities as compared with the more traditional method (B in this study), that involves determining velocities by averaging data from the spreading beams. Our results show that these differences are more pronounced in estimated secondary velocities than primary velocities and are higher where there is a greater lateral velocity gradient (Figure 9). The comparison between the two case studies shows that even though both confluences have a very low momentum ratio, as the confluence of the Grande Eau-Rhône has a more complex shear zone, likely due to the effects of bed discordance, and there are more significant differences in the estimation of primary and secondary velocities. This is related to the extent to which spreading of the aDcp measurement beams influences the secondary velocities, particularly in relation to lateral gradients in flow conditions. More standard methods (Method B in this study) are valid if the flow is completely homogenous over the diameter of the fluid column that the beams spread. This diameter varies over depth and is largest near the bed. In the case of the Grande Eau-Rhône confluence where stronger lateral velocity gradients exist in the flow, individual beams will not be measuring homogenous conditions, particularly near the bed and in the zone of high shear near the inner bank, because the spread of the beams may be greater in diameter than the width of the zone of lateral velocity variation. In this case, as Method A involves less spatial-averaging than Method B, it may provide more accurate information on the flow behavior, but such a conclusion really needs a third and independent method to confirm it. At the Lizerne-Rhône confluence, even though the momentum ratio is similar to Grande Eau-Rhône confluence, there is only more localized shear in the flow and a simplified shear zone (Figure 9). In such a situation, using Method B to detect the large scale patterns of secondary flow may be more advantageous, because it involves more spatial averaging.

569 The above discussion suggests that whether or not high rates of later shear influence the
570 potential importance of Method A depends on distance from the aDcp: with more
571 divergence at greater depths, lower levels of lateral shear are likely to be acceptable.
572 Figures 16a and 16b quantifies the relationship between lateral velocity gradient, depth
573 and the magnitude of the relative differences in secondary velocities estimated using
574 methods A and B for the cross-section 6 of the Lizerne-Rhône and cross-section 3 of the
575 Grande Eau-Rhône confluences, respectively. At the Lizerne-Rhône confluence, as the
576 zone of high lateral shear is absent, even though there is a strong relationship between
577 the magnitude of the relative differences in secondary velocities estimated using methods
578 A and B and the depth (Figure 16a), their relationship with the lateral velocity gradients is
579 poor. In contrast, for the case of the Grande Eau-Rhône confluence (Figure 16b), where
580 increasing the lateral velocity gradient and depth results in higher relative differences in
581 secondary velocities. Thus, the need to use Method A will depend on the case being used
582 and the extent to which there is lateral shear at greater distances from the aDcp. This is
583 why whilst it may be tempting to introduce some kind of shear or velocity gradient
584 threshold to identify when Method A might be preferable, to do so would be misleading as
585 the threshold will also depend on the distance of the shear from the aDcp.

586 “Figure 16”

587 Results also confirm that several repeat transects are indispensable to provide a robust
588 estimation of secondary circulation and to reduce the effect of spatial inhomogeneity and
589 temporal variations. Although Method A reduces the minimum number of repeat transects
590 needed to estimate the secondary velocities, a larger number of these minimum repeat
591 transects (6 or more repeats for Lizerne-Rhône confluence) appeared to be required. This

is higher than in the earlier findings of Szupiany et al. (2007) and Vermeulen et al., (2014b) who argue that 5 repeats are enough to have a robust estimation of the turbulence averaged velocity. We also note that an even number of repeats may be important to avoid directional bias in dGPS positions.

Since Method A is based on the position of beams, if the bin position errors related to dGPS accuracy as well as sensor tilt are greater than homogeneity errors associated with beam divergence, standard Method B is more reliable. This is likely to be the case particularly in rivers shallower than those studied here and where high resolution is required due to large velocity gradients. In rivers of the scale studied here, and deeper, by increasing the mesh cell size, we can still have sufficient data to estimate velocity vectors, and the effects dGPS and tilt sensor errors have a minor effect. This confirms the earlier findings by Vermeulen et al., (2014b), which showed that Method A provides the greatest improvement where the aDcp cell size is much smaller than the beam spread. We are not yet in a position to identify the depth at which Method A becomes preferable to Method B, and again this will depend on other parameters such as the intensity of shear and so may not be readily generalizable between confluences.

The difficulty of identifying the depths of rivers and intensities of shear that make one method preferable over another precludes adoption of simple quantitative guidance on which method to use when. As both methods have some disadvantages, we argue that both methods should be applied. If they give similar results, then there should be confidence in both. If and where they differ, analysis should be undertaken to identify why, and hence which method is likely to be preferable. Association of the differences in primary and secondary velocities inferred between the two methods with estimates of shear intensity and with estimated tilt and positioning errors should then help decide whether Method A or Method B is preferable in a particular case. This preference may vary between confluences but also through time at a confluence, if shear or flow depth changes significantly between survey dates.

Finally, we wish to emphasise that the impact of averaging is only one element that must be considered in obtaining reliable primary and secondary clow estimates in river confluences. Other issues, such as the rotation method needed to distinguish primary and secondary circulation, remain important and should be considered routinely.

Conclusions

This paper shows the advantage of working with the radial (beam) velocity measurements of an aDcp within each bin prior to averaging them across a given volume of fluid (Method A) as opposed to identify volumes of fluid and assuming bend homogeneity within them (Method B). Such a treatment is important where there are strong velocity gradients in the flow as with river channel confluences. In the first of our case-study confluences, the Lizerne-Rhône, a very small tributary joined the main river, and the pattern of primary and secondary velocities obtained with methods A and B were relatively similar, more so for primary velocities. But for a second confluence, the Grande Eau-Rhône, with a similar momentum ratio, there were much larger differences. We attributed this to the formation of much stronger shear at this confluence. Method A also appeared to reduce the number of repeat transects needed to estimate secondary velocities reliably. The main downside is that Method A is more sensitive to errors related to positioning. Thus, good dGPS accuracy and precision are required to perform a robust estimation of velocity.

In smaller/shallower rivers, Method B may be acceptable indeed preferable as it is less sensitive to GPS errors. In larger rivers, Method A may be necessary, especially in the presence of strong shear at the confluence. Choice between these methods should be based upon an initial screening of the extent to which there is strong shear in the flow as well as the extent to which bins further from the aDcp are influenced by beam divergence.

Appendix A

The LOWESS model is a locally weighted polynomial regression, which at each point and in the range of dataset, a low degree polynomial is fitted to a subset of the data, using weighted least squares. This polynomial fit gives more weight to points closer to the point whose response is being estimated. The value of the regression function for the point is then obtained by evaluating the local polynomial using the explanatory variable values for that data point. The LOWESS fit is complete after regression function values have been computed for each of the *n* data points. Many of the details of this method, such as the degree of the polynomial model and the weights, are flexible (“Local regression,” n.d.).

Acknowledgements

This paper benefited from constructive and detailed suggestions from two anonymous reviewers and Editor Mike Kirkby. The work was supported by Swiss National Science Foundation Grant 200021_160020. The codes used may be obtained upon request to Gelare Moradi.

References

Alvarez, L. V., Schmeeckle, M.W., Grams, P.E., 2017. A detached eddy simulation model for the study of lateral separation zones along a large canyon-bound river. J. Geophys. Res. Earth Surf. 122, 25–49. https://doi.org/10.1002/2016JF003895.

Ashmore, P.E., Ferguson, R.I., Prestegaard, K.L., Ashworth, P.J. and Paola, C., 1992. Secondary flow in coarse-grained braided river confluences. Earth Surface Processes and Landforms, 17, 299– 312.

Best, J.L. and Roy, A.G., 1991. Mixing-layer distortion at the confluence of channels of different depth. Nature, 350, 411–413.

Biron, P., De Serres, B., Roy, A.G., Best, J.L., 1993. Shear layer turbulence at an unequal depth channel confluence. In: Clifford, N.J., French, J.R., Hardisty J. (editors) Turbulence: Perspectives on Flow and Sediment Transport, Wiley, Chichester, 197–213.

Dinehart, R.L. and Burau, J.R., 2005. Averaged indicators of secondary flow in repeated acoustic Doppler current profiler crossings of bends. Water Resources Research, 41, W09405.

Engel, F.L. and Rhoads, B.L., 2016. Three-dimensional flow structure and patterns of bed shear stress in an evolving compound meander bend. Earth Surface Processes and Landforms, 41, 1211–1226.

Gualtieri, C., Ianniruberto, M., Filizola, N., Santos, R. and Endreny, T., 2017. Hydraulic complexity at a large river confluence in the Amazon basin. Ecohydrology, 10, e1863

Gunawan, B., Neary, V.S., McNutt, J.R., 2011. Ornl Adv Post-Processing Guide and Matlab Algorithms for Mhk Site Flow and Turbulence Analysis, Ornl/Tm-2011/404. doi:10.2172/1034377.

Jackson, P.R., Garcia, C.M., Oberg, K.A., Johnson, K.K. and Garcia, M.H., 2008. Density currents in the Chicago River: Characterization, effects on water quality, and potential sources. Science of the Total Environment 401: 130–143.

Kasvi, E., Vaaja, M., Alho, P., Hyyppä, H., Hyyppä, J., Kaartinen, H. and Kukko, A., 2013. Morphological changes on meander point bars associated with flow structure at different discharges. Earth Surface Processes and Landforms, 38, 577-590.

Kasvi, E., Laamanen, L., Lotsari, E. and Alho, P., 2017. Flow Patterns and Morphological Changes in a Sandy Meander Bend during a Flood-Spatially and Temporally Intensive ADCP Measurement Approach. Water, 9, 106.

Knox, R. L. and Latrubesse, E.M., 2017. A geomorphic approach to the analysis of bedload and bed morphology of the Lower Mississippi River near the Old River Control Structure. Geomorphology, 268, 35-47.

Konsoer, K.M. and Rhoads, B.L., 2014. Spatial-temporal structure of mixing interface turbulence at two large river confluences. *Environmental Fluid Dynamics*, 14, 1043-1070.

Kostaschuk, R.A., Shugar, D., Best, J.L., Parsons, D.R., Lane, S.N., Hardy, R.J. and Orfeo, O., 2009. Suspended sediment transport and deposition over a dune: Río Paraná, Argentina. Earth Surface Processes and Landforms, 34, 1605–1611.

Lane, S.N., Parsons, D.R., Best, J.L., Orfeo, O., Kostaschuk, R. a., Hardy, R.J., 2008. Causes of rapid mixing at a junction of two large rivers: Río Paraná and Río Paraguay, Argentina. Journal of Geophysical Research, 113, 1–16. https://doi.org/10.1029/2006JF000745.

Lane, S.N., Bradbrook, K.F., Richards, K.S., Biron, P.M., Roy, a. G., 2000. Secondary circulation cells in river channel confluences : measurement artefacts or coherent flow structures ? Hydrological Processes, 14, 2047–2071. https://doi.org/10.1002/1099-1085(20000815/30)14:11/12<2047::aid-hyp54>3.0.co;2-4.

Local regression [WWW Document], n.d. URL:https://en.wikipedia.org/wiki/Local_regression (accessed 1.22.18).

Lotsari, E., Kasvi, E., Kämäri, M., and Alho, P., 2017. The effects of ice cover on flow characteristics in a subarctic meandering river. Earth Surface Processes and Landforms, 42, 1195–1212.

Marsden, R.F. and Ingram, R.G., 2004. Correcting for beam spread in acoustic Doppler current profiler measurements. Journal of Atmospheric and Oceanice Technology, 21, 1491–1498.

Morlock, S.E., 1996. Evaluation of Acoustic Doppler Current Profiler Measurements of River Discharge. U.S. Geological Survey Water Resources Investigations Report 95-4218.

Muste, M., Yu, K. and Spasojevic M. 2004. Practical aspects of ADCP data use for quantification of mean river flow characteristics: Part I: Moving-vessel measurements. Flow Measurement and Instrumentation, 15, 1–16.

Parsapour-Moghaddam, P. and Rennie, C.D., 2018. Calibration of a 3D Hydrodynamic meandering river model using fully spatially distributed 3D ADCP velocity data. Journal of Hydraulic Engineering, 144, 04018010.

Parsons, D.R., Best, J.L., Orfeo, O., Hardy, R.J., Kostaschuk, R.A. and Lane, S.N., 2005. The morphology and flow fields of three-dimensional dunes, Rio Paraná, Argentina: results from simultaneous multibeam echo sounding and acoustic Doppler current profiling. Journal of Geophysical Research, 110, F04S03.

Parsons, D.R., Best, J.L., Lane, S.N, Orfeo, O., Hardy, R.J. and Kostaschuk, R.A., 2007. Form roughness and the absence of secondary flow in a large confluence-diffluence, Rio Paraná, Argentina. Earth Surface Processes and Landforms, 32, 155–162.

Parsons, D.R., Jackson, P.R., Czuba, J.A., Engel, F.L., Rhoads, B.L., Oberg, K.A., Best, J.L., Mueller, D.S., Johnson, K.K., Riley, J.D., 2013. Velocity Mapping Toolbox (VMT): A processing and visualization suite for moving-vessel ADCP measurements. Earth Surface Processes and Landforms, 38, 1244–1260.

Petrie, J., Diplas, P., Gutierrez, M. and Nam, S., 2013. Combining fixed- and moving-vessel acoustic Doppler current profiler measurements for improved characterization of the mean flow in a natural river. Water Resources Research, 49, 5600–5614.

Rennie, C.D., Millar, R.G. and Church, M.A., 2002. Measurement of bed load velocity using an acoustic Doppler current profiler. Journal of Hydraulic Engineering – ASCE, 128, 473-483.

Rennie, C.D. and Millar, R.G., 2004. Measurement of the spatial distribution of fluvial bedload transport velocity in both sand and gravel. Earth Surface Processes and Landforms, 29, 1173-1193.

Rennie, C.D., Rainville, F., 2006. Case study of precision of GPS differential correction strategies: influence on aDcp Velocity and discharge estimates. Journal of Hydraulic Engineering, 132, 225–234.

Rennie, C. D., and Church, M., 2010. Mapping spatial distributions and uncertainty of water and sediment flux in a large gravel bed river reach using an acoustic Doppler current profiler, Journal of Geophysical Research – Earth Surface, 115.

Rhoads, B.L. and Kenworthy, S.T., 1995. Field measurements of flow structure at a high-angle asymmetrical stream confluence. Geomorphology 11, 273–293.

Rhoads, B.L. and Kenworthy, S.T., 1998. Time-averaged flow structure in the central region of a stream confluence. *Earth Surface Processes and Landforms*, 23, 171-191.

Rhoads, B.L., and Sukhodolov, A.N., 2001. Field investigation of three-dimensional flow structure at stream confluences: 1. Thermal mixing and time-averaged velocities. Water Resources Research, 27, 2393-410.

Rhoads, B.L., and Sukhodolov, A.N., 2004. Spatial and temporal structure of shear layer turbulence at a stream confluence. Water Resources Research, 40, W06304.

Rhoads, B.L., and Sukhodolov, A.N., 2008. Lateral momentum flux and the spatial evolution of flow within a confluence mixing interface. Water Resources Research, 44, W08440.

Riley, J.D. and Rhoads, B.L., 2012. Flow structure and channel morphology at a natural confluent meander bend. Geomorphology, 163, 84-98.

Riley, J.D., Rhoads, B.L., Parsons, D.R. and Johnson K.K., 2015. Influence of junction angle on three-dimensional flow structure and bed morphology at confluent meander bends during different hydrological conditions. Earth Surface Processes and Landforms, 40, 252–271.

Shugar, D.H., Kostaschuk, R., Best, J.L., Parsons, D.R., Lane, S.N., Orfeo, O. and Hardy, R,J., 2010. On the relationship between flow and suspended sediment transport over the crest of a sand dune, Río Paraná, Argentina. Sedimentology 57: 252–272.

SonTek YSI, 2000. Acoustic Doppler Profiler (ADP ®) Principles of Operation.

SonTek YSI, 2010. RiverSurveyor S5/M9 System Manual 115.

Sukhodolov, A.N. and Rhoads, B. L., 2001. Field investigation of three-dimensional flow structure at stream confluences 2. Turbulence. Water Resources Research, 27, 2411-2424.

Sukhodolov, A. N., Krick, J., Sukhodolova, T. A., Cheng, Z., Rhoads, B. L. and Constantinescu, G. S., 2017. Turbulent flow structure at a discordant river confluence: Asymmetric jet dynamics with implications for channel morphology. Journal of Geophysical Research: Earth Surface, 122(6), 1278-1293. https://doi.org/10.1002/2016JF004126.

Szupiany, R.N., Amsler, M.L., Best, J.L. and Parsons, D.R., 2007. Comparison of fixed- and moving vessel measurements with an aDp in a large river. Journal of Hydraulic Engineering, 133, 1299–1309.

Szupiany, R.N., Amsler, M.L., Parsons, D.R. and Best, J.,L., 2009. Morphology, flow structure, and suspended bed sediment transport at two large braid-bar confluences. Water Resources Research, 45, W05415.

Szupiany, R.N., Amsler, M.L., Hernandez, J., Parsons, D.R., Best, J.L., Fornari, E. and Trento, A., 2012. Flow fields, bed shear stresses, and suspended bed sediment dynamics in bifurcations of a large river. Water Resources Research, 48, W11515.

Tomas, G., Bleninger, T., Rennie, C.D., Guarneri, H., 2018. Advanced 3D mapping of hydrodynamic parameters for the analysis of complex flow Motions in a submerged bedrock canyon of the Tocantins River, Brazil. Water (Switzerland) 10, 1–19. https://doi.org/10.3390/w10040367.

Tsubaki, R., Kawahara, Y., Muto, Y. and Fujita, I., 2012. New 3-D flow interpolation method on moving ADCP data. Water Resources Research, 48, 1–15.

Venditti, J.G., Rennie, C.D., Bomhof, J., Bradley, R.W., Little, M., Church, M., 2014. Flow in bedrock canyons. Nature 513, 534–537. https://doi.org/10.1038/nature13779.

Vermeulen, B., Hoitink, A.J.F., van Berkum, S.W. and Hidayat, 2014a. Sharp bends associated with deep scours in a tropical river: The river Mahakam (East Kalimantan, Indonesia). Journal of Geophysical Research, Earth Surface, 119, 1441–1454.

Vermeulen, B., Sassi, M.G. and Hoitink, A.J.F., 2014b. Improved flow velocity estimates from moving-boat ADCP measurements. Water Resources Research, 50, 4186–4196.

Vermeulen, B., Hoitink, A.J.F. and Labeur, R.J., 2015. Flow structure caused by a local cross-sectional area increase and curvature in a sharp river bend. Journal of Geophysical Research, Earth Surface, 120, 1771-1783.

Zhao, J., Chen, Z., and Zhang, H., 2014. A robust method for determining the heading misalignment angle of GPS compass in ADCP measurement. Flow Measurements and Instrumentation, 35, 1–10.

"For the ESPL special issue: Measuring and numerical modelling of hydro-morphological processes in open-water"

Evaluation of aDcp processing options for secondary flow identification at river junctions

Gelare Moradi [1], Bart Vermeulen[3], Colin D. Rennie [2], Romain Cardot [1], Stuart N. Lane[1]

1: University of Lausanne - Institute of Earth Surface Dynamics (UNIL - IDYST)

Université de Lausanne - IDYST Quartier Mouline - Bâtiment Géopolis - Switzerland

2: Civil Engineering Department, University of Ottawa

3: Water Engineering and Management Department, University of Twente, the Netherlands

Abstract

Secondary circulation in river confluences results in a spatial and temporal variation of fluid motion and a relatively high level of morphodynamic change. Acoustic Doppler current profiler (aDcp) vessel-mounted flow measurements are now commonly used to quantify such circulation in shallow water fluvial environments. It is well established that such quantification using vessel-mounted aDcps requires repeated survey of the same cross-section. However, less attention has been given to how to process these data. Most aDcp data processing techniques make the assumption of homogeneity between the measured radial components of velocity. As acoustic beams diverge with distance from the aDcp probe, the volume of the flow that must be assumed to be homogeneous between the beams increases. In the presence of secondary circulation cells, and where there are strong rates of shear in the flow, the homogeneity assumption may not apply,

especially deeper in the water column and close to the bed. To reduce dependence on this assumption, we apply a newly-established method to aDcp data obtained for two medium-sized (~60-80 m wide) gravel-bed river confluences and compare the results with those from more conventional data processing approaches. The comparsion confirms that in the presence of strong shear our method produces different results to more conventional approaches. In the absence of a third set of fully independent data, we cannot demonstrate conclusively which method is best, but our method involves less averaging and so in the presence of strong shear is likely to be more reliable. We conclude that it is wise to apply both our method and more conventional methods to identify where data analysis might be impacted upon by strong shear and where inferences of secondary circulation may need to be made more cautiously.

~~suggests an improvement in secondary flow representation compared to more conventional methods whilst also confirming that repeated transects are required to obtain reliable secondary flow and turbulence measurement. Use of the method resolves two counter-rotating cells in the confluence zone more clearly, with downward velocity in the channel centre. This pattern helps to explain development of confluence scour holes in such streams.~~

Keywords

Acoustic Doppler current profiler

Secondary circulation

River confluences

River junctions

Introduction

Acoustic Doppler current profilers (aDcps) are now used widely to measure river flow in three-dimensions, notably for the quantification of secondary flows. Applications have been made to river bedforms (e.g., Parsons et al., 2005; Kostaschuk et al., 2009; Shugar et al., 2010), bends (e.g., Dinehart and Burau, 2005; Kasvi et al., 2013; Vermeulen et al., 2014a, 2015; Engel and Rhoads, 2016; Knox and Latrubesse, 2016; Kasvi et al., 2017; Lotsari et al., 2017; Parsapour-Moghaddam and Rennie, 2018), junctions (e.g., Parsons et al., 2007; Lane et al., 2008; Szupiany et al., 2009; Riley and Rhoads, 2012; Riley et al., 2015; Gualtieri et al., 2017), bifurcations (e.g., Parsons et al., 2007; Szupiany et al., 2012), canyons (e.g., Alvarez et al., 2017; Tomas et al., 2018; Venditti et al., 2014), deltas (e.g., Czuba et al., 2011) and gravity currents (e.g., Garcia et al., 2007; Garcia et al., 2012). Research has also shown the need to make repeat section measurements (e.g., Szupiany et al., 2007; Jackson et al., 2008) and also to process these data carefully, (Muste et al., 2004; Rennie and Church 2010; Tsubaki et al., 2012; Parsons et al., 2013; Petrie et al., 2013). Such processing must take into account positioning (Rennie and Rainville, 2006) and orientation (Zhao et al., 2014) errors, and the treatment of repeat section measurements (e.g., Szupiany et al., 2007; Jackson et al., 2008).

This paper is concerned with recent observations regarding the inference of secondary flows from aDcp data and concerns regarding the assumption that flow is homogenous in the fluid volumes defined by the acoustic beams emitted from an aDcp and used to calculate any one point estimate (Vermeulen et al., 2014b). Acoustic beams are reflected by suspended particles, which, if moving, cause a Doppler shift in beam frequency, which is then detected at the sensor. This shift is directional so each beam measures the radial velocity, which is the velocity of particle motion parallel to the acoustic path. This can be assumed to be the flow velocity if the particle motion is identical to fluid motion. In order to resolve flow in more than one direction, aDcps require at least three acoustic beams to estimate three Cartesian components of velocity. The radial velocities originating from the beams are traditionally analyzed for a single measurement cycle at a single depth at a time (Vermeulen et al., 2014b). The velocity then applies to the volume of fluid defined by the beams at each depth. Flow within this volume is assumed to be homogeneous. However, as the beams spread from the sensor, depth bins increase in horizontal size (Rennie et al., 2002). This means that: (1) bins further from the sensor are likely to produce less reliable velocities because the bin size is greater and the flow within bins is more likely to be heterogeneous (Gunawan et al., 2011); and (2), even in smaller bins, velocities may be less reliable in zones of strong shear where also the within-bin flow is less likely to be homogeneous. In a river where measurements are made throughout the flow depth, the maximum shear may be close to the bed, where the beam divergence may also be greatest.

One solution to this problem accounts for first order shear within the flow volume (e.g. Marsden and Ingram, 2004) through a Taylor expansion of the coordinate transform used to determine the Cartesian velocity components. Under this solution, flow is allowed to vary linearly within the bin, but the bin's volume becomes potentially larger with distance from the sensor. Vermeulen et al. (2014b) developed and tested a second solution. As explained in detail below, multiple radial (beam) velocity measurements within a single bin are put through a Cartesian transform to obtain a localized within-bin three-dimensional velocity. This method strongly reduces the volume over which homogeneity should be assumed and Vermeulen et al. (2014b) found that this significantly impacted interpretations of secondary velocities in the presence of strong shear. In this paper, we seek to quantify the effects of this method for the measurement of secondary flow in two medium-sized river junctions (c. 60-80 m post-junction channel width). River junctions are associated with very strong shear (e.g. Best and Roy, 1991; Biron et al., 1993, 1996a, 1996b; Sukhodolov and Rhoads, 2001; Rhoads and Sukhodolov, 2004, 2008; Konsoer and Rhoads, 2014; Sukhodolov et al., 2017), as well as well-developed secondary circulation (e.g. Ashmore et al., 1992; Rhoads and Kenworthy, 1995, 1998; Rhoads and Sukhodolov et al., 2001; Lane et al., 2008; Riley and Rhoads, 2012; Riley et al., 2015). Thus, understanding how to process effectively the aDcp data used to describe them is of paramount importance.

Methods for estimating Cartesian velocity components from aDcp data

In this section, we describe the two different methodological approaches used in this study to estimate Cartesian velocity components: (1) M~~m~~ethod A, the Vermeulen et al., (2014b) method; and (2) M~~m~~ethod B, the conventional method. Common to all methods is the assumption that data are available from repeat measurement of the same cross-section, as has been shown to be critical for obtaining reliable estimates of secondary circulation from aDcp data (Szupiany et al., 2007), particularly when single transect measurements are not close enough together.

Method A: based on Vermeulen et al., (2014b)

Application of the Vermeulen et al. (2014b) method requires mapping of radial beam velocity data onto a predefined mesh. This mesh requires both a bottom topography or bathymetric model, and an upper limit just below the water surface. As the measurements were made using several repeat transects for each cross section, the first step is to define a mean cross section for each set of individual transects (boat tracks). The second step is to define a grid mesh for this mean cross section. Third, all measured beam velocities are projected on to this cross section mesh. Finally, the beam velocities within each mesh ~~grid~~ cell are then used to resolve a Cartesian velocity for the mesh~~grid~~ cell. Errors that influence these steps can be estimated.

The first step is estimation of the mesh extremes, both the lower boundary or bathymetry model and the upper boundary near the water surface. To generate the bathymetry model we use depth soundings collected with the aDcp. We recognize that each beam may register a different distance of the stream bed from the sounder, especially as we are dealing with bathymetrically~~largely~~ irregular cross-sections. Specifically, for each bottom track sounding within each transect, we use the UTM coordinates obtained with a coupled differential GPS (dGPS), the range of each bottom track beam return, and the instrument tilt to estimate the bed elevation and horizontal position of each beam impingement point on the bed. These bed positions are combined together to identify an initial mean transect. Provided a point is within a certain distance from the initial mean cross-section, LOWESS interpolation (Appendix A) is applied, which has the effect of defining a bathymetric model that gives most weight to points that appear to be closer to the cross-section. It is important to note that this mean transect is not necessarily orthogonal to the primary flow direction and so will not yield true primary and secondary flow estimates without further correction. We address this below.

Once the initial bathymetric model is defined, we estimate a unique vector using the initial mean transect; that is the principal direction of the scatter cloud of all x and y UTM positions at the bed. This unique vector points in the direction of the largest eigenvector of the covariance matrix of all UTM positions (*t*). We then calculate the mean UTM position (p_{mean}) for each set of individual transects and the difference between each measured beam position (p_b) and the mean position. The dot product of these obtained values and the unique vector is then used to define the projection of each UTM position in the direction of the unique vector. To identify the final mean cross section, we sum up all individual projected vectors and obtain the best fit to all available data (Figure 1).

To define the upper boundary of the mesh, we estimate the elevation of the water surface. As there is a blanking distance at the surface of the water during the measurement, we then remove this blanking distance, taken as 0.30 m. Thus, the mesh has also a blanking distance and the upper part of the cross-section is, strictly, the upper limit of available data, not the water surface.

“Figure1”

The second step uses the defined bathymetric model and available velocity bins within the measured area (not influenced by side lobes, and below the blanking distance) to define a cross-section mesh. The side-lobe interference is caused by the striking of the channel bed by side-lobe energy from each of the acoustic beams. This side-lobe energy has strong reflections from the bed, which result in echoes that overwhelm the signal from scatters near the bed. The thickness of the side-lobe layer is typically 6-7% of the measured depth (Morlock, 1996).

To generate the mesh, the cross section is initially subdivided into vertical slices with equal widths (Δn). For each slice, the simplest definition of mesh cell thicknesses (Δz) divides each vertical equally. These verticals are converted to non-dimensional σ coordinates using following equation:

$$\sigma = 1 - \left(\frac{p_v.\boldsymbol{k} - \eta}{p_b.\boldsymbol{k} - \eta}\right) \quad \text{(Vermeulen et al. 2014b)} \qquad (1)$$

where p_v stands for velocity measurement positions (m), p_b is the corresponding bed position (m) that is found using velocity measurement horizontal positions and applying the bathymetric model, $\boldsymbol{k}$ is the upward pointing unit vector and η are the water surface fluctuations around the mean water level at which z=0.

However, because of beam spreading and differences in the distance of the sounder from the bed, which varies with position of the sounder, this tends to produce a highly heterogeneous number of measurements in each cell within the mesh. The alternative, adopted here, is to allow mesh cell thickness to vary through the water column such that there is a roughly equal number of beam velocities contributing to each mesh cell (see Figure 2 for a typical distribution).

As the river bed form is varying, to follow its shape, each mesh cell is considered to be a cuboid with 6 edges, two on the left side, two in the middle and two on the right side. To define these edges, the first step is to define the middle point of each mesh cell. Once defined, by calculating the slope for each half part of the mesh cell, edges can be obtained.

177 The mesh cell faces are then calculated on the basis of adjacent verticals and the mesh
178 cell upper and lower boundaries.

179 To identify the beams that contribute to each mesh cell, an index for each beam velocity
180 is defined, which shows its associated mesh cell, using the projection of each radial
181 velocity onto the estimated mean cross section (Figure 2).

182 “Figure 2”

183 In the third step, the radial velocities for each beam (**b**) that contribute to each mesh cell
184 (the N beam velocities) have to be transformed into Cartesian velocities (v_x, v_y and v_z)
185 using:

186 $$\begin{pmatrix} b_1 \\ \vdots \\ b_N \end{pmatrix} = \begin{pmatrix} q_1 \\ \vdots \\ q_N \end{pmatrix} . \begin{pmatrix} v_x \\ v_y \\ v_z \end{pmatrix} \leftrightarrow \mathbf{b} = Q.\mathbf{u} \qquad (2)$$

187 where **q** is a unit vector which describes the direction of the acoustic beam.

188 To obtain the raw beam velocities, we use matrix transformations obtained from the raw
189 data to transform measured velocities in XYZ coordinates into beam velocities. The
190 Vermeulen et al., (2014b) method includes in the transformations an explicit treatment of
191 the random errors due to internal and external factors and the bias (systematic errors)
192 caused by the measurement system and the nature of river flow (Tsubaki et al., 2012).
193 Random errors include those that come from sampling a time-varying flow in the presence
194 of strong gradients and represent a form of aliasing. By adding a combined term of errors
195 ε, (2) becomes:

196 $$\mathbf{b} = Q\mathbf{u} + \varepsilon \qquad (3)$$

A least squares solution is fitted to (3) that minimizes the sum of the square of the errors. The optimal estimation ($\hat{\mathbf{u}}$) for ($\mathbf{u}$) is then given by the normal equation:

$$\hat{\mathbf{u}} = Q^{+}\mathbf{b} + \varepsilon \tag{4}$$

where Q^{+} can be defined as:

$$Q^{+} = (Q^{T}Q)^{-1}Q^{T} \tag{5}$$

To solve three Cartesian velocity components, we need at least three equations. Each beam measurement in a mesh cell adds an equation. Where enough beam velocities are collected in a mesh cell and the equations are different from each other (beam velocities are measured from different directions), the velocity can be estimated. To check whether this is the case, the matrix describing the system of equations can be analyzed. In the processing we use the rank which indicates how many unknowns can be solved from the system of equations. When the rank is three, the three Cartesian velocities can be solved. Where the rank of the matrix is one or two, the system cannot be solved. Where the system of equations is overdetermined, the obtained solution is a matrix with more equations (rows) than unknowns (columns). The velocity can be solved using the generalized inverse of the matrix and in such a way that the sum of squared errors is minimized. As this combined term of errors also contains information about the turbulence and accuracy of the measurements, we can obtain the covariance matrix of the velocity components:

$$\hat{\varepsilon} = \mathbf{b} - Q\hat{\mathbf{u}} \tag{6}$$

$$\mathrm{var}(\hat{\mathbf{u}}) = \frac{\hat{\varepsilon}^{T}\hat{\varepsilon}(Q^{T}Q)^{-1}}{N-3} \tag{7}$$

and the variance of the velocity across the section can be then estimated as:

$$\mathrm{var}(\mathbf{u}) = \frac{\mathrm{var}(\hat{\mathbf{u}})}{\mathrm{N}}$$

(8)

Method B: the standard aDcp method

As the Doppler shift is directional, it can only measure radial velocities. With the standard method, to determine Cartesian velocity components, radial velocities then have to be resolved into three orthogonal velocity vectors. To do so, at least three beam velocities pointed in known directions are required. Also, because the beams are measuring different water profiles along their individual slant ranges, the assumption of horizontal homogeneity must be taken into account. Hence, in the standard method, the three dimensional velocity for each depth bin for each ping can be solved for a typical four-beam system using the following equations (Mueller and Wagner, 2009):

$$V_x = \frac{(b_3 - b_1)}{\sqrt{2} \sin\theta} \tag{9}$$

$$V_y = \frac{(b_4 - b_2)}{\sqrt{2} \sin\theta} \tag{10}$$

$$V_z = \frac{-(b_1 + b_3)}{(2\cos\theta)} = \frac{-(b_2 + b_4)}{(2\cos\theta)}$$

(11)

where V_y is the cross stream velocity assuming beam 3 is pointed upstream, V_x is the streamwise velocity, V_z is the vertical velocity, b_1, b_2, b_3 and b_4 are the radial velocities measured in beams 1,2,3 and 4 respectively and θ is the tilt angle of the beams referenced to vertical. These data should then be corrected for pitch and roll angles, obtained from the internal inclinometer and the heading angle from the internal compass. Velocity outputs are already corrected for ship velocities.

To compare results obtained using M~~m~~ethod B with those of M~~m~~ethod A, we use the same mean cross section built for M~~m~~ethod A, as well as the same bathymetric model and the same mesh. Each measured velocity vector is assigned to the appropriate mesh cell by projecting its 3D position (horizontal position and depth) onto the mean cross section mesh. We then average x, y, and z components of all velocities measured within a mesh cell to obtain the mean velocity vector for the mesh cell.

Methodology

This paper is motivated by the need to acquire three-dimensional data from junctions of tributaries with a main river stem, here the River Rhône, western Switzerland, and so the need to identify methods for reliably obtaining Cartesian velocities from aDcp data. The Rhône tributaries typically have very high bedload transport rates for short periods of time, leading to the formation of very large tributary mouth bars downstream of their junctions with the main river. These bars are maintained for weeks or months such that at lower tributary flow, with negligible sediment supply, there is a legacy effect of previous high momentum tributary events upon junction morphology and secondary flow formation.

For this paper, we used a specially-designed rope and pulley system to collect aDcp data from the junction of two tributaries with the Rhône (Figure 3).

“Figure 3”

The Lizerne is a Rhône tributary of almost 20 km length that flows south-westward from the western slopes of the Tête Noire (2451m) or La Fava (2612m), in the Bernese Alps. This river is heavily regulated for hydropower with sediment extracted upstream of the junction. As a result, there is negligible sediment supply and no evidence of point bar formation. It reaches the Rhône between Ardon and Vétroz, forming a 90° junction angle and it has a bed that is nearly concordant with the Rhône.~~.~~

The Grande Eau is a second tributary of the Rhône River which has a length of 26 km and takes its source on the Vaud side of the Les Diablerets and flows into the Rhône River with a 70° confluence angle, near Aigle. The Grande Eau bed is 1.5 m higher than the Rhône such that it is markedly discordant. ~~It has a catchment area of 132 km^2 and the maximum monthly runoff occurs in May with an average of 52.5% of total annual runoff occurring during snowmelt in the four months April–July.~~

In this section, we: (1) describe the aDcp used to collect data; (2) describe how the aDcp was deployed; and (3) outline the analytical approaches used to interpret the results from the different methods. Although the method is valid for any aDcp that has an onboard compass and potential for differential GPS positioning, as is standard with most aDcps, we use a Sontek M9 aDcp in this study.

The Sontek M9 aDcp

The SonTek M9 aDcp is a nine-transducer system with three acoustic frequencies, configured as two sets of four profiling beams (3 MHz and 1 MHz transducers in Janus configurations) and one vertical beam (0.5 MHz Echo sounder) for depth measurements (SonTek YSI, 2010). It uses these two sets of four beams to provide raw radial velocity samples. These beams are equally spaced at 90º azimuth angles and are projected at an angle θ of 25 º off the vertical axis (SonTek YSI, 2000). For the standard configuration, the four beams encompass a sampling diameter of 93% of the distance from the aDcp (7% of side-lobe) (SonTek YSI, 2000).

The output velocities from the SonTek M9 Riversurveyor are either in Cartesian coordinates (XYZ) that are relative to sensor orientation or in Earth coordinates (ENU) for a SonTek system with compass and tilt sensors. These raw velocity data in Earth coordinates or XYZ coordinates are already corrected for the ship motion. To apply M~~m~~ethod A to Sontek output data, as this method is based on radial velocities, it is necessary to transform these output velocities to radial velocities. To do so, we add ship velocities to these output velocities and then apply the inverses of the instrument's matrix coordinate transformations (obtained from MATLAB files output by the SonTek data collection software RiverSurveyor). As the survey is being undertaken using a moving vessel, these radial velocities then have to be corrected again for the boat velocity. There are two key methods for doing this. The first uses the bottom tracking to measure the boat velocity relative to the river bed, under the assumption that the latter is stationary (i.e. there is no bedload transport). The second tracks the boat position using differential GPS (dGPS, e.g. Zhao et al., 2014). In this study, we corrected all raw beam velocities for ship velocities, using dGPS as we could not exclude the possibility of there being bedload transport.

To apply M~~m~~ethod B in this study, we use the raw velocity data in Earth coordinates and we correct it for pitch and roll angles, obtained from internal inclinometer and heading angle data for the internal compass. For SonTek M9 aDcps, pitch is a y-axis rotation and roll an x-axis rotation.

Depending on the water depth and velocity, the Sontek M9 firmware changes the acoustic operating frequency and the water profiling mode on-the-fly, thus the number of ~~measured cells~~sampled points in the vertical varies automatically from one profile to the next. Specifically, when the water is shallower than 0.75 m and the maximum velocity is less than 0.4 ms^{-1}, the M9 reports data acquired with a 3 MHz frequency using the pulse coherent mode to obtain a 2cm depth measurement resolution. For deeper situations, this frequency changes to 1 MHz pulse coherent pings using a 6cm aDcp cell size. If the maximum velocity is greater than 0.4 ms^{-1} then SmartPulse (i.e., broadband) mode is utilized, with the 3 MHz beams if depth is less than 5 m and the 1MHz beams if depth is greater than 5m, with the aDcp cell size optimized based on the current water depth. As a result of these on-the-fly changes, each measured profile has a different number of aDcp cells and different aDcp cell sizes. Hence, to correct the aDcp cell size variability, for both m~~M~~ethods A and B there is the need to define a cross-sectional mesh and to project the measured velocities to this mesh. For Method A we use the beam velocity vertical positions in a non-dimensionalized coordinate system using equation 1, within the predefined mesh explained in section 2.1.

Deployment of the Sontek M9 in the river junctions

The survey work was undertaken in two junctions of the Swiss River Rhône, the Lizerne-Rhône confluence in August 2017 and the Grande Eau-Rhône confluence in May 2018, using a Sontek M9 vessel mounted aDcp and a specially-designed rope-pulley system (Figure 3c). The survey was spatial, monitoring 11 cross-sections from upstream of the junction to its downstream at the Lizerne-Rhône confluence with a Momentum ratio (Mr) of 0.018 (Figure 3a) and 11 cross-sections at the Grande Eau-Rhône confluence with a Mr of 0.022 (Figure 3b). Table 1 shows the general characteristics of these two confluences on the date of the measurements.

“Table 1”

As proposed previously by Dinehart and Burau (2005), Szupiany et al. (2007), Gunawan et al. (2011) and Vermeulen et al., (2014b) at least five repeats are required to have a robust estimation of secondary velocities. Hence, in this paper, data are processed for cross-section 6 at the Lizerne-Rhône confluence (Figure 3a), and for cross section 3 at the Grande Eau-Rhône confluence (Figure 3b). Identification of the minimum number of repeat transects necessary per cross-section was undertaken using cross-section 9 at the Lizerne-Rhône confluence (Figure 3a), which involves 16 repetitions. We noted that after application of Method A, the standard deviation of velocity stabilized with six repetitions, which is the number we adopt for this study.~~Hence, in this paper, data are processed for cross-section 9, which involves 16 repeat transect surveys (Figure 3a) at the Lizerne-Rhône confluence and for cross section 3, which involves 6 repeat transect surveys (Figure 3b) at the Grande Eau-Rhône confluence. The decision to use fewer repeat transects at the Grande Eau-Rhône was based upon the identification of the minimum number of cross-sections needed from the Lizerne-Rhône study.~~

Bin position error determination

Application of M~~m~~ethod A requires estimation of the error terms in (2). The size of the sampling volume in each beam is determined by the size of the bin used. As the SonTek

M9 aDcp uses different bin sizes depending on the water track frequency (section 2.1.3), these volumes could vary. Applying M~~m~~ethod A might improve the velocity estimation for large measurement volumes at depth, as it does not rely on the homogeneity assumption. But as bins with a small number of velocity measurements will have greater error, this method can estimate velocities with error. Also, if the beam velocity distribution within each mesh cell is not linear, as averaging is made in the middle of each mesh cell, it can introduce error in velocity estimation. Thus, it is necessary to calculate a minimum necessary mesh cell size when applying M~~m~~ethod A.

Method B is inherently limited by spatial averaging due to the potential use of divergent beams and the associated homogeneity assumption. In other words, one must assume that the velocity is homogeneous over the horizontal domain defined by beam divergence (Eq.12). Method A has the advantage that velocities are recorded within an individual beam depth bin, thus no spatial averaging between beams is required. However, in order for M~~m~~ethod A to overcome the uncertainty induced by spatial averaging inherent to M~~m~~ethod B, it is essential that the bin location is known explicitly. Error in bin location can be induced by dGPS position and or tilt sensor (pitch and roll) errors. We therefore compare possible bin position errors using M~~m~~ethod A to beam divergence obtained from M~~m~~ethod B to indicate when M~~m~~ethod A should be advantageous over M~~m~~ethod B.

Beam divergence is the spatial separation of the beams due to the Janus configuration of the beams with beam angles of 25°. This divergence determines the sampling volume that must be considered homogeneous for Method B and can be calculated using equation 12:

$$x_b = 2d\tan\theta \qquad (12)$$

where *d* is the depth in *m* and θ is the beam angle which for a SonTek aDcp is 25°. The aDcp dGPS is used to reference the velocity measurements in space and to estimate the ship velocity. If dGPS is used for ship velocity, this introduces errors in measurement of the absolute water velocity (because ship velocity is subtracted from the water velocity measured in the reference frame of the aDcp). This uncertainty introduces error in velocity calculations.

To estimate the errors due to dGPS and the tilt sensors, in this study we assume normally distributed random errors with a standard deviation of ±1° for tilt sensors, based on manufacturer specifications, and a normally distributed displacement error ~~for~~ measured by the dGPS for the dGPS positions (as a function of satellite configuration during measurement), and we apply a Monte Carlo approach which we run 100 times sampling under these uncertainties. Each time we calculate the estimated secondary velocity differences as compared with the original secondary velocities.

To be able to reduce the uncertainty due to velocity estimation using M~~m~~ethod A compared to M~~m~~ethod B, the errors induced in M~~m~~ethod A related to GPS uncertainty and tilt sensors must be less than the errors in M~~m~~ethod B due to beam divergence and the homogeneity assumption. Hence, M~~m~~ethod A can be used if the error associated with a minimum aDcp cell size is in between the error due to beam divergence and the maximum estimated error due to the GPS and tilt sensors. Otherwise using this method introduces more error in velocity estimations than using M~~m~~ethod B.

Data interpretation

Methods A and B, described above, were applied to the Sontek M9 data, to determine Cartesian velocities (v_x, v_y and v_z). As our interest is in process estimation, here we describe the methods we apply to the Cartesian velocities to estimate processes relevant to junction dynamics. In order to distinguish between primary and secondary components of flow, we need to rotate the initial mean transect. Options for doing this are reviewed in Lane et al. (2000) and we do not assess them here, but rather apply~~apply~~ the zero net cross stream discharge definition (Lane et al., 2000). By calculating the mean values of the *x* and *y* velocity components (*U* and *V*), we then calculate the velocity magnitude (*v*). By rotating these velocity components to the direction of the cross-stream velocity, using the unique vector (**σ**), primary velocity vectors ($\boldsymbol{v_p}$) and secondary velocity vectors ($\boldsymbol{v_s}$) then can be estimated.

$$\mathrm{v} = \sqrt{\mathrm{U}^2 + \mathrm{V}^2}$$

(13)

$$\begin{pmatrix}\sigma_x\\ \sigma_y\end{pmatrix} = \begin{pmatrix}U\\ V\end{pmatrix}/v \qquad (14)$$

where σ_x and σ_y are sin and cos of the angle between the section angle and east.

$$\boldsymbol{v}_p = \sigma_x \boldsymbol{v}_x + \sigma_y \boldsymbol{v}_y \qquad (15)$$

$$\boldsymbol{v}_s = -\sigma_y \boldsymbol{v}_x + \sigma_x \boldsymbol{v}_y \qquad (16)$$

However, secondary circulation is all flow that is orthogonal to the primary flow and not just horizontal flow; there should be not net secondary flux in a section; and so correction should also consider vertical velocities. ~~this rotation does not account for the possibility that there is net vertical motion in a section, which is also a component of secondary circulation.~~ Thus, we extend these relationships to include vertical velocities:

413 $$\begin{pmatrix} \sigma_{x,1} & \sigma_{x,2} & \sigma_{x,3} \\ \sigma_{y,1} & \sigma_{y,2} & \sigma_{y,3} \\ \sigma_{z,1} & \sigma_{z,2} & \sigma_{z,3} \end{pmatrix} = \begin{pmatrix} U \\ V \\ W \end{pmatrix} / v \quad (17)$$

414 where: U, V and W are the mean velocities of x, y and z velocity components, respectively

415 and v is the magnitude of the velocity which can be obtained using:

416 $$v = \sqrt{U^2 + V^2 + W^2} \quad (18)$$

417 $$\boldsymbol{v}_p = \sigma_{x,1}\boldsymbol{v}_x + \sigma_{x,2}\boldsymbol{v}_y + \sigma_{x,3}\boldsymbol{v}_z$$

418 (19)

419 $$\boldsymbol{v}_s = \sigma_{y,1}\boldsymbol{v}_x + \sigma_{y,2}\boldsymbol{v}_y + \sigma_{y,3}\boldsymbol{v}_z$$

420 (20)

421 $$\boldsymbol{v}_v = \sigma_{z,1}\boldsymbol{v}_x + \sigma_{z,2}\boldsymbol{v}_y + \sigma_{z,3}\boldsymbol{v}_z$$

422 (21)

423 To estimate velocity gradients, and to correct for weak curvature with the survey method

424 at the edges of each transect line (e.g. Figure 3), ~~solve the curvature of cross sections,~~ all

425 data have been transformed into row and column coordinates (η and ζ) using the following

426 transformation:

427 $$\begin{pmatrix} \frac{\partial}{\partial n} \\ \frac{\partial}{\partial z} \end{pmatrix} = \begin{pmatrix} \frac{\partial \eta}{\partial n} & \frac{\partial \zeta}{\partial n} \\ \frac{\partial \eta}{\partial z} & \frac{\partial \zeta}{\partial z} \end{pmatrix} \begin{pmatrix} \frac{\partial}{\partial \eta} \\ \frac{\partial}{\partial \zeta} \end{pmatrix} \quad (22)$$

428 where n and z are horizontal and vertical coordinates on the section plane, respectively

429 (Vermeulen et al., 2014b).

Results

Primary and secondary velocities

Primary and secondary velocities estimated using m~~m~~ethods A and B for the Lizerne-Rhône confluence appear to be similar at cross-section 6 (Figures 4a and 4b) and the differences in estimated secondary flows are minor. The differences are most pronounced b~~B~~etween -~~-~~10 and -5 m, in the middle of the main channel.~~, the differences in secondary velocity vectors are more pronounced.~~

These primary and secondary velocity patterns show higher differences at cross-section 3 of the confluence of Grande Eau-Rhône (Figures 4c and 4d) despite it having a similar momentum ratio to the Lizerne during measurement. Primary velocities differ significantly between m~~m~~ethods A and B: (1) at greater distance from the aDcp because the bins contain larger volumes of water assumed to be homogenous; and (2) at the edges of the cross-section where there are more beam velocity measurements (contours in Figures 4c and 4d). Secondary velocity vectors estimated using M~~m~~ethod A indicate flow convergence at the surface and flow descending towards the riverbed throughout the centre of the channel (Figure 4c). This is due to a high degree of bed discordance between the Grande Eau and the Rhône, which increases the penetration of the tributary flow into the main channel ~~above~~ over the junction, ~~which~~ and which forms a zone of high lateral and vertical shear, on the one hand, and main channel narrowing because of penetration of the tributary ~~point~~ mouth bar on the other hand. The secondary velocity vectors estimated by M~~m~~ethod B show a weaker penetration of the tributary flow into the main channel, which results in a reverse flow towards the bank on the ~~inner~~ tributary ~~bank~~ side of the channel at the surface of the mixing interface (Figure 4d). In this case, the core of the secondary circulation is located in the middle of the main channel and closer to the inner bank.

“Figure 4”

Figure 5 and Figure 6 quantify the differences in primary and secondary velocity patterns estimated using m~~m~~ethods A and B, for the Lizerne-Rhône confluence. Figures 5a and 5c and Figures 6a show that almost 4% of mesh cells have a relative difference in primary velocities between m~~m~~ethods A and B of more than 10%. These differences can exceed 0.2 ms^{-1} and so they are relatively small. Velocity differences are more pronounced in estimated secondary velocities, with almost 82% of mesh cells having a difference of more than 10%, and almost 37% of mesh cells having a difference of more than 50% (Figure 5b, 5d and 6b).

“Figure 5”

“Figure 6”

At the Grande Eau-Rhône confluence, these differences are greater as compared with those of the Lizerne-Rhône confluence. Figures 7a, 7c and 8a show that these differences for primary velocities exceed 0.4 ms^{-1} in the zone of high vertical and lateral shear and near the inner bank. Almost 20% of the mesh cells have a relative difference in primary velocities between m~~m~~ethods A and B of more than 10%. The secondary velocity differences are more pronounced between these two methods. Figures 7b and 7d show differences with a magnitude of 0.4 ms^{-1} near the edges and near the bed. Almost all the mesh cells have a difference in estimated secondary velocities between two methods. Figure 8b shows that almost 93% of the mesh cells have a relative difference of 10%

between m~~m~~ethods A and B. although this value decreases to 55% for a relative difference of 90% between these two methods.

“Figure 7”

“Figure 8”

Velocity gradients

As Figure 9 shows, there is a strong relationship between lateral gradient in secondary velocities and differences between the secondary velocities estimated using methods A and B for both the Lizerne-Rhône and the Grande Eau-Rhône confluences. This is because a stronger velocity gradient increases the probability that the assumption of flow homogeneity within a bin is likely to fail. Indeed, the marked differences between methods A and B at the Grande Eau confluence (Figure 7) ~~in the true right secondary circulation cell describe above~~ are~~is~~ also in a zone of strong lateral shear.

“Figure 9”

Number of repeat transects

One way to reduce data fluctuations due to random errors and turbulence, during the measurement using moving vessel aDcps, is to average by using several repeat transects together in one cross section. As each estimated velocity measurement is a single sample in time, adding in a repeat section adds in an additional estimated velocity measurement. Under [8], this should cause the variance to increase, despite the number of measurements used in its estimation increasing, until the point at which there are enough repeats to capture the effects the range of scales of variation in turbulence impacting the measurement. Then, this variance will become stable. At this stage we can consider the number of repeats as the minimum number required to have a robust estimation of secondary velocity vectors that is to have reached estimates of velocity that are asymptotic on this stable state.

Here we apply both methods A and B to the survey of 16 repeats at cross-section 9 in Figure 3a at the Lizerne-Rhône confluence. To allow a reasonable comparison, three mesh cells in the middle of the cross section, and at three different depths (near the surface, middle depth and near the bed) have been chosen (Figure 11). Results show that by using M~~m~~ethod A, after six repeats, a stable variance of the velocity estimator is obtained at the Lizerne-Rhône confluence (Figure 11a). Many more repeats are needed using M~~m~~ethod B (Figure 11b) and this is likely because Method B uses fewer measurements per mesh cell. These results also show a higher standard deviation of the velocity estimation near the surface, using M~~m~~ethod A and before achieving the stable situation. This can be explained by the fact that near the surface M~~m~~ethod A is more sensitive to errors caused by positioning, while near the bed, hence with distance from the sounder, as the beam spread increases, the improvement obtained using M~~m~~ethod A is more pronounced (Figure 11a).

“Figure 10”

“Figure 11”

DGPS and tilt sensor uncertainty analysis

As explained above a normally distributed random error has been applied 100 times to both dGPS positioning (by adding a random offset) and tilt sensors (by changing pitch and roll angles randomly) and the secondary velocities have been estimated using M~~m~~ethod A for each perturbed dataset. As Figure 12 shows, the magnitude of errors related to dGPS accuracy are higher than those related to tilt sensor accuracy, for both confluences. These values can reach ±0.03 ms^{-1} and confirms the earlier finding of Rennie and Rainville (2006) which showed that GPS corrections can have average errors of about ±0.03 ms^{-1} (Figures 12a and 12c). These magnitudes are also higher near the surface and near the bed for the Lizerne-Rhône confluence (Figure 12a). Near the surface, as there ~~is a greater random error due to ship movements~~fewer measurements that can contribute to the estimation of aDcp position and tilt, uncertainties in dGPS data will have a ~~larger~~ greater effect ~~on a bad velocity estimation~~. Near the bed, as the velocity gradient is higher, errors will be greater as well. Figure 12c shows higher magnitudes near the surface at cross-section 3 in Figure 3b for the Grande Eau-Rhône confluence.

Errors related to tilt sensor uncertainty are higher where there is a higher velocity gradient. This is related to the fact that within the mesh cells with higher velocity gradients, as the velocity distribution is not linear, and as averaging is made in the middle of the mesh cell, it is more probable that the velocity will be affected by sensor inaccuracies of bin positioning, and so be in error (Figures 12b and 12d).

“Figure 12”

Homogeneity assumption analysis

Figure13 shows the maximum inhomogeneity allowance, using M~~m~~ethod B for both case studies. These results are obtained by dividing the velocity gradient obtained from equation 22 by the divergence of the beams from equation 12. They confirm that, for the homogeneity assumption to be valid and thus error to be minimized using M~~m~~ethod B, the maximum ~~c~~mesh cell size, which can be used is as small as 5cm near the bed. Clearly, this is impossible as the configuration of the beams using aDcps always results in beam divergence greater than 5cm.

“Figure 13”

Primary and secondary flow patterns

In this section, we compared estimated primary and secondary velocities using methods A and B for other cross sections in Figure 3 for both river confluences.

Figure 14 shows the results for cross sections 4, 5 and 7 (in Figure 3a) at the Lizerne-Rhône confluence. These cross sections also show similar results in primary and secondary velocity patterns for both methods A and B. Figure15 shows different patterns in primary and secondary velocities estimation using M~~m~~ethod A and B for cross sections 4,6 and 8 in Figure 3b at the Grande Eau-Rhône confluence. Method A ~~produces~~ leads to the identification of a stronger and more coherent tributary penetration at cross-section 4 and weaker upwelling mid-channel, giving the impression of less intense secondary circulation (Figure 15). At section 6, flow towards the true left across the shallow top of the tributary ~~point~~ mouth bar ~~top~~ is ~~maintained~~ identified and is coherent with M~~m~~ethod A. At the channel-scale there is general flow convergence reflecting channel narrowing (Figure 15). When using~~ith~~ M~~m~~ethod B, these patterns are less coherent and flow is towards the true right in the vicinity of the ~~point~~ tributary mouth bar. These patterns are repeated for section 8 (Figure 15).

“Figure 14”

“Figure 15”

Discussion

In this paper we used data collected with boat-mounted aDcp technology at two confluences of the Swiss river Rhône, both with similar and very low momentum ratios (0.018, 0.022) and analysed these using two different methods, A and B, to estimate Cartesian velocity components. Method A is based on a methodological approach developed by Vermeulen et al. (2014b). It differs by treating explicitly each individual beam velocity based on its position within a predefined mesh. Results show that this method reduces the volume over which the flow must be assumed to be homogenous (Fig 13). It can, but not necessarily does, result in differences in estimated primary and secondary velocities as compared with the more traditional method (B in this study), that involves determining velocities by averaging data from the spreading beams. Our results show that these differences are more pronounced in estimated secondary velocities than primary velocities and are higher where there is a greater lateral velocity gradient (Figure 9). The comparison between the two case studies shows that even though both confluences have a very low momentum ratio, as the confluence of the Grande Eau-Rhône has a more ~~intense~~ complex ~~lateral~~ shear zone, likely due to the effects of bed discordance, and there are more significant differences in the estimation of primary and secondary velocities. This is related to the extent to which spreading of the aDcp measurement beams influences the secondary velocities, particularly in relation to lateral gradients in flow conditions. More standard methods (M~~m~~ethod B in this study) are valid if the flow is completely homogenous over the diameter of the fluid column that the beams spread. This diameter varies over depth and is largest near the bed. In the case of the Grande Eau-Rhône confluence where stronger lateral velocity gradients exist in the flow, individual beams will not be measuring homogenous conditions, particularly near the bed and in the zone of high shear near the inner bank, because the spread of the beams may be greater in diameter than the width of the zone of lateral velocity variation. In this case, as M~~m~~ethod A involves less spatial-averaging than M~~m~~ethod B, it may ~~can~~ provide more accurate information on the flow behavior, but such a conclusion really needs a third and independent method to confirm it. At the Lizerne-Rhône confluence, even though the momentum ratio is similar to Grande Eau-Rhône confluence, there is only more localized ~~lateral~~ shear in the flow and a simplified shear zone~~,~~ (Figure 9). In such a situation, ~~and~~ using M~~m~~ethod B to detect the large scale patterns of secondary flow may be more advantageous, because it involves more spatial averaging.

The above discussion suggests that whether or not high rates of later shear influence the ~~need to adopt~~potential importance of Method A depends on distance from the aDcp: with more divergence at greater depths, lower levels of lateral shear are likely to be acceptable. Figures 16a and 16b quantifies the relationship between lateral velocity gradient, depth and the magnitude of the relative differences in secondary velocities estimated using methods A and B for the cross-section 6 of the Lizerne-Rhône and cross-section 3 of the Grande Eau-Rhône confluences, respectively. At the Lizerne-Rhône confluence, as the zone of high lateral shear is absent, even though there is a strong relationship between the magnitude of the relative differences in secondary velocities estimated using methods A and B and the depth (Figure 16a), their relationship with the lateral velocity gradients is poor. In contrast, ~~not as clear as~~for the case of the Grande Eau-Rhône confluence (Figure 16b), where increasing the lateral velocity gradient and depth results in higher relative differences in secondary velocities. Thus, the need to use M~~m~~ethod A will depend on the case being used and the extent to which there is lateral shear at greater distances from the aDcp. This is why whilst it may be tempting to introduce some kind of shear or velocity gradient threshold to identify when Method A might be preferable, to do so would be misleading as the threshold will also depend on the distance of the shear from the aDcp.

“Figure 16”

Results also confirm that several repeat transects are indispensable to provide a robust estimation of secondary circulation and to reduce the effect of spatial inhomogeneity and temporal variations. Although M~~m~~ethod A reduces the minimum number of repeat transects needed to estimate the secondary velocities, a larger number of these minimum repeat transects (6 or more repeats for Lizerne-Rhône confluence) appeared to be required. This is higher than in the~~, compared to~~ earlier findings of Szupiany et al. (2007) and Vermeulen et al., (2014b) who argue that 5 repeats are enough to have a robust estimation of the turbulence averaged velocity. We also note that an even number of repeats may be important to avoid directional bias in dGPS positions.

~~As aDcp data obtained from multiple transects are notoriously noisy, another approach to averaging involves post-processing that takes binned data estimated from multiple transects, and averaging these data through spatial smoothing. This is adopted in the Velocity Mapping Toolbox (VMT) (Parsons et al., 2013). The VMT maps ensembles onto the mean straight cross-section and interpolates each one of these grid nodes using linear interpolation. The bed profile is estimated using the mean of the four beams. These projected and interpolated velocity data from each set of transects are averaged using a simple arithmetic averaging, at every grid node, to provide a composite representation of the velocity field. Once the averaging is complete for all the nodes, a coordinate~~

~~transformation is applied to transform Earth velocity components into velocity components in the plane of the cross section (U, V and W) (Parsons et al., 2013). The VMT can also use a smoothing window which is a moving average and it averages every velocity vector with its nearest neighbor. The user can define the horizontal and vertical smoothing window size.~~

~~It was not the aim of this paper to evaluate the specific VMT method, but to put our comparison of Methods A and B into context, Figure 17a shows results obtained for primary and secondary velocities for the VMT, at cross section 6 in Figure 3a at the Lizerne- Rhône confluence, that is comparable with Figures 4a and 4b for our Methods A and B. The pattern of primary and secondary velocities are similar to each other for all three methods (Figures 17a, 4a and 4b). Although the VMT results have been obtained using a horizontal and vertical smoothing window sizes of 2, they are not as coherent as the results obtained using methods A and B, suggesting that using the VMT requires more repeat transects or more repeat stationary measurements.~~

~~Figure 17b shows primary and secondary velocities estimated using the VMT for cross-section 3 in Figure 3b at the Grande Eau-Rhône confluence. Again, as the VMT uses a straight mean cross section, estimated velocities are not as coherent as those of method A and B (Figures 4c and 4d).~~

~~"Figure 17"~~

Since M~~m~~ethod A is based on the position of beams, if the bin position errors related to d~~D~~GPS accuracy as well as sensor tilt are greater than homogeneity errors associated with beam divergence, standard M~~m~~ethod B is more reliable. This is likely to be the case particularly ~~the case~~ in rivers ~~smaller~~ shallower than those studied here ~~rivers~~ and where high resolution is required due to large velocity gradients. In ~~big~~ rivers of the scale studied here, and deeper, by increasing the mesh cell size, we can still have sufficient data to estimate velocity vectors, and the ~~errors related to~~effects dGPS and tilt sensor errors have a minor effect. ~~-~~This confirms the earlier findings by Vermeulen et al., (2014b), which showed that M~~m~~ethod A provides the greatest improvement where the aDcp cell size is much smaller than the beam spread. We are not yet in a position to identify the depth at which Method A becomes preferable to Method B, and again this will depend on other parameters such as the intensity of shear and so may not be readily generalizable between confluences.

The difficulty of identifying the depths of rivers and intensities of shear that make one method preferable over another precludes adoption of simple quantitative guidance on which method to use when. As both methods have some disadvantages, we argue that both methods should be applied. If they give similar results, then there should be confidence in both. If and where they differ, analysis should be undertaken to identify why, and hence which method is likely to be preferable. Association of the differences in primary and secondary velocities inferred between the two methods with estimates of shear intensity and with estimated tilt and positioning errors should then help decide whether Method A or Method B is preferable in a particular case. This preference may vary between confluences but also through time at a confluence, if shear or flow depth changes significantly between survey dates.

Finally, we wish to emphasise that the impact of averaging is only one element that must be considered in obtaining reliable primary and secondary clow estimates in river confluences. Other issues, such as the rotation method needed to distinguish primary and secondary circulation, remain important and should be considered routinely.

Conclusions

This paper shows the advantage of working with the radial (beam) velocity measurements of an aDcp within each bin prior to averaging them across a given volume of fluid (M~~m~~ethod A) as opposed to identify volumes of fluid and assuming bend homogeneity within them (M~~m~~ethod B). Such a treatment is important where there are strong velocity gradients in the flow as with river channel confluences. In the first of our case-study confluences, the Lizerne-Rhône, a very small tributary joined the main river, and the pattern of primary and secondary velocities obtained with methods A and B were relatively similar, more so for primary velocities. But for a second confluence, the Grande Eau-Rhône, with a similar momentum ratio, there were much larger differences. We attributed this to the formation of much stronger shear at this confluence. Method A also appeared to reduce the number of repeat transects needed to estimate secondary velocities reliably. The main downside is that M~~m~~ethod A is more sensitive to errors related to positioning. Thus, good dGPS accuracy and precision are required to perform a robust estimation of velocity.

In smaller/shallower rivers, Method B may be acceptable indeed preferable as it is less sensitive to GPS errors. In larger rivers, Method A may be necessary, especially in the presence of strong shear at the confluence. Choice between these m~~M~~ethods should be based upon an initial screening of the extent to which there is strong shear in the flow as well as the extent to which bins further from the aDcp are influenced by beam divergence.

Appendix A

The LOWESS model is a locally weighted polynomial regression, which at each point and in the range of dataset, a low degree polynomial is fitted to a subset of the data, using weighted least squares. This polynomial fit gives more weight to points closer to the point whose response is being estimated. The value of the regression function for the point is then obtained by evaluating the local polynomial using the explanatory variable values for that data point. The LOWESS fit is complete after regression function values have been computed for each of the *n* data points. Many of the details of this method, such as the degree of the polynomial model and the weights, are flexible ("Local regression," n.d.).

Acknowledgements

This paper benefited from constructive and detailed suggestions from two anonymous reviewers and Editor Mike Kirkby. The work was supported by Swiss National Science Foundation Grant 200021_160020. The codes used may be obtained upon request to Gelare Moradi.

References

Alvarez, L. V., Schmeeckle, M.W., Grams, P.E., 2017. A detached eddy simulation model for the study of lateral separation zones along a large canyon-bound river. J. Geophys. Res. Earth Surf. 122, 25–49. https://doi.org/10.1002/2016JF003895.

Ashmore, P.E., Ferguson, R.I., Prestegaard, K.L., Ashworth, P.J. and Paola, C., 1992. Secondary flow in coarse-grained braided river confluences. Earth Surface Processes and Landforms, 17, 299– 312.

Best, J.L. and Roy, A.G., 1991. Mixing-layer distortion at the confluence of channels of different depth. Nature, 350, 411–413.

Biron, P., De Serres, B., Roy, A.G., Best, J.L., 1993. Shear layer turbulence at an unequal depth channel confluence. In: Clifford, N.J., French, J.R., Hardisty J. (editors) Turbulence: Perspectives on Flow and Sediment Transport, Wiley, Chichester, 197–213.

Dinehart, R.L. and Burau, J.R., 2005. Averaged indicators of secondary flow in repeated acoustic Doppler current profiler crossings of bends. Water Resources Research, 41, W09405.

Engel, F.L. and Rhoads, B.L., 2016. Three-dimensional flow structure and patterns of bed shear stress in an evolving compound meander bend. Earth Surface Processes and Landforms, 41, 1211–1226.

Gualtieri, C., Ianniruberto, M., Filizola, N., Santos, R. and Endreny, T., 2017. Hydraulic complexity at a large river confluence in the Amazon basin. Ecohydrology, 10, e1863

Gunawan, B., Neary, V.S., McNutt, J.R., 2011. Ornl Adv Post-Processing Guide and Matlab Algorithms for Mhk Site Flow and Turbulence Analysis, Ornl/Tm-2011/404. doi:10.2172/1034377.

Jackson, P.R., Garcia, C.M., Oberg, K.A., Johnson, K.K. and Garcia, M.H., 2008. Density currents in the Chicago River: Characterization, effects on water quality, and potential sources. Science of the Total Environment 401: 130–143.

Kasvi, E., Vaaja, M., Alho, P., Hyyppä, H., Hyyppä, J., Kaartinen, H. and Kukko, A., 2013. Morphological changes on meander point bars associated with flow structure at different discharges. Earth Surface Processes and Landforms, 38, 577-590.

Kasvi, E., Laamanen, L., Lotsari, E. and Alho, P., 2017. Flow Patterns and Morphological Changes in a Sandy Meander Bend during a Flood-Spatially and Temporally Intensive ADCP Measurement Approach. Water, 9, 106.

Knox, R. L. and Latrubesse, E.M., 2017. A geomorphic approach to the analysis of bedload and bed morphology of the Lower Mississippi River near the Old River Control Structure. Geomorphology, 268, 35-47.

Konsoer, K.M. and Rhoads, B.L., 2014. Spatial-temporal structure of mixing interface turbulence at two large river confluences. *Environmental Fluid Dynamics*, 14, 1043-1070.

Kostaschuk, R.A., Shugar, D., Best, J.L., Parsons, D.R., Lane, S.N., Hardy, R.J. and Orfeo, O., 2009. Suspended sediment transport and deposition over a dune: Río Paraná, Argentina. Earth Surface Processes and Landforms, 34, 1605–1611.

Lane, S.N., Parsons, D.R., Best, J.L., Orfeo, O., Kostaschuk, R. a., Hardy, R.J., 2008. Causes of rapid mixing at a junction of two large rivers: Río Paraná and Río Paraguay, Argentina. Journal of Geophysical Research, 113, 1–16. https://doi.org/10.1029/2006JF000745.

Lane, S.N., Bradbrook, K.F., Richards, K.S., Biron, P.M., Roy, a. G., 2000. Secondary circulation cells in river channel confluences : measurement artefacts or coherent flow structures ? Hydrological Processes, 14, 2047–2071. https://doi.org/10.1002/1099-1085(20000815/30)14:11/12<2047::aid-hyp54>3.0.co;2-4.

Local regression [WWW Document], n.d. URL:https://en.wikipedia.org/wiki/Local_regression (accessed 1.22.18).

Lotsari, E., Kasvi, E., Kämäri, M., and Alho, P., 2017. The effects of ice cover on flow characteristics in a subarctic meandering river. Earth Surface Processes and Landforms, 42, 1195–1212.

Marsden, R.F. and Ingram, R.G., 2004. Correcting for beam spread in acoustic Doppler current profiler measurements. Journal of Atmospheric and Oceanice Technology, 21, 1491–1498.

Morlock, S.E., 1996. Evaluation of Acoustic Doppler Current Profiler Measurements of River Discharge. U.S. Geological Survey Water Resources Investigations Report 95-4218.

Muste, M., Yu, K. and Spasojevic M. 2004. Practical aspects of ADCP data use for quantification of mean river flow characteristics: Part I: Moving-vessel measurements. Flow Measurement and Instrumentation, 15, 1–16.

Parsapour-Moghaddam, P. and Rennie, C.D., 2018. Calibration of a 3D Hydrodynamic meandering river model using fully spatially distributed 3D ADCP velocity data. Journal of Hydraulic Engineering, 144, 04018010.

Parsons, D.R., Best, J.L., Orfeo, O., Hardy, R.J., Kostaschuk, R.A. and Lane, S.N., 2005. The morphology and flow fields of three-dimensional dunes, Rio Paraná, Argentina:

results from simultaneous multibeam echo sounding and acoustic Doppler current profiling. Journal of Geophysical Research, 110, F04S03.

Parsons, D.R., Best, J.L., Lane, S.N, Orfeo, O., Hardy, R.J. and Kostaschuk, R.A., 2007. Form roughness and the absence of secondary flow in a large confluence-diffluence, Rio Paraná, Argentina. Earth Surface Processes and Landforms, 32, 155–162.

Parsons, D.R., Jackson, P.R., Czuba, J.A., Engel, F.L., Rhoads, B.L., Oberg, K.A., Best, J.L., Mueller, D.S., Johnson, K.K., Riley, J.D., 2013. Velocity Mapping Toolbox (VMT): A processing and visualization suite for moving-vessel ADCP measurements. Earth Surface Processes and Landforms, 38, 1244–1260.

Petrie, J., Diplas, P., Gutierrez, M. and Nam, S., 2013. Combining fixed- and moving-vessel acoustic Doppler current profiler measurements for improved characterization of the mean flow in a natural river. Water Resources Research, 49, 5600–5614.

Rennie, C.D., Millar, R.G. and Church, M.A., 2002. Measurement of bed load velocity using an acoustic Doppler current profiler. Journal of Hydraulic Engineering – ASCE, 128, 473-483.

Rennie, C.D. and Millar, R.G., 2004. Measurement of the spatial distribution of fluvial bedload transport velocity in both sand and gravel. Earth Surface Processes and Landforms, 29, 1173-1193.

Rennie, C.D., Rainville, F., 2006. Case study of precision of GPS differential correction strategies: influence on aDcp Velocity and discharge estimates. Journal of Hydraulic Engineering, 132, 225–234.

Rennie, C. D., and Church, M., 2010. Mapping spatial distributions and uncertainty of water and sediment flux in a large gravel bed river reach using an acoustic Doppler current profiler, Journal of Geophysical Research – Earth Surface, 115.

Rhoads, B.L. and Kenworthy, S.T., 1995. Field measurements of flow structure at a high-angle asymmetrical stream confluence. Geomorphology 11, 273–293.

Rhoads, B.L. and Kenworthy, S.T., 1998. Time-averaged flow structure in the central region of a stream confluence. *Earth Surface Processes and Landforms*, 23, 171-191.

Rhoads, B.L., and Sukhodolov, A.N., 2001. Field investigation of three-dimensional flow structure at stream confluences: 1. Thermal mixing and time-averaged velocities. Water Resources Research, 27, 2393-410.

Rhoads, B.L., and Sukhodolov, A.N., 2004. Spatial and temporal structure of shear layer turbulence at a stream confluence. Water Resources Research, 40, W06304.

Rhoads, B.L., and Sukhodolov, A.N., 2008. Lateral momentum flux and the spatial evolution of flow within a confluence mixing interface. Water Resources Research, 44, W08440.

Riley, J.D. and Rhoads, B.L., 2012. Flow structure and channel morphology at a natural confluent meander bend. Geomorphology, 163, 84-98.

Riley, J.D., Rhoads, B.L., Parsons, D.R. and Johnson K.K., 2015. Influence of junction angle on three-dimensional flow structure and bed morphology at confluent meander bends during different hydrological conditions. Earth Surface Processes and Landforms, 40, 252–271.

Shugar, D.H., Kostaschuk, R., Best, J.L., Parsons, D.R., Lane, S.N., Orfeo, O. and Hardy, R,J., 2010. On the relationship between flow and suspended sediment transport over the crest of a sand dune, Río Paraná, Argentina. Sedimentology 57: 252–272.

SonTek YSI, 2000. Acoustic Doppler Profiler (ADP ®) Principles of Operation.

SonTek YSI, 2010. RiverSurveyor S5/M9 System Manual 115.

Sukhodolov, A.N. and Rhoads, B. L., 2001. Field investigation of three-dimensional flow structure at stream confluences 2. Turbulence. Water Resources Research, 27, 2411-2424.

Sukhodolov, A. N., Krick, J., Sukhodolova, T. A., Cheng, Z., Rhoads, B. L. and Constantinescu, G. S., 2017. Turbulent flow structure at a discordant river confluence: Asymmetric jet dynamics with implications for channel morphology. Journal of Geophysical Research: Earth Surface, 122(6), 1278-1293. https://doi.org/10.1002/2016JF004126.

Szupiany, R.N., Amsler, M.L., Best, J.L. and Parsons, D.R., 2007. Comparison of fixed- and moving vessel measurements with an aDp in a large river. Journal of Hydraulic Engineering, 133, 1299–1309.

Szupiany, R.N., Amsler, M.L., Parsons, D.R. and Best, J.,L., 2009. Morphology, flow structure, and suspended bed sediment transport at two large braid-bar confluences. Water Resources Research, 45, W05415.

Szupiany, R.N., Amsler, M.L., Hernandez, J., Parsons, D.R., Best, J.L., Fornari, E. and Trento, A., 2012. Flow fields, bed shear stresses, and suspended bed sediment dynamics in bifurcations of a large river. Water Resources Research, 48, W11515.

Tomas, G., Bleninger, T., Rennie, C.D., Guarneri, H., 2018. Advanced 3D mapping of hydrodynamic parameters for the analysis of complex flow Motions in a submerged bedrock canyon of the Tocantins River, Brazil. Water (Switzerland) 10, 1–19. https://doi.org/10.3390/w10040367.

Tsubaki, R., Kawahara, Y., Muto, Y. and Fujita, I., 2012. New 3-D flow interpolation method on moving ADCP data. Water Resources Research, 48, 1–15.

Venditti, J.G., Rennie, C.D., Bomhof, J., Bradley, R.W., Little, M., Church, M., 2014. Flow in bedrock canyons. Nature 513, 534–537. https://doi.org/10.1038/nature13779.

Vermeulen, B., Hoitink, A.J.F., van Berkum, S.W. and Hidayat, 2014a. Sharp bends associated with deep scours in a tropical river: The river Mahakam (East Kalimantan, Indonesia). Journal of Geophysical Research, Earth Surface, 119, 1441–1454.

Vermeulen, B., Sassi, M.G. and Hoitink, A.J.F., 2014b. Improved flow velocity estimates from moving-boat ADCP measurements. Water Resources Research, 50, 4186–4196.

Vermeulen, B., Hoitink, A.J.F. and Labeur, R.J., 2015. Flow structure caused by a local cross-sectional area increase and curvature in a sharp river bend. Journal of Geophysical Research, Earth Surface, 120, 1771-1783.

Zhao, J., Chen, Z., and Zhang, H., 2014. A robust method for determining the heading misalignment angle of GPS compass in ADCP measurement. Flow Measurements and Instrumentation, 35, 1–10.

Sites	Lizerne	Grande eau
Tributary upslope contributing area (km^2)	64.8	132
Main stem upslope contributing area (km^2)	3401	5088
Basin area ratio	1.89%	2.59%
Tributary width (m)	6.5	16.5
Main stem width upstream of junction (m)	46	58
Width ratio	0.15	0.28
Junction angle (°)	80	70
Tributary Froude number	0.32	0.05
Bed slope of the tributaries upstream of the confluence (%)	~0.5	0.5-1
Main stem slope upstream of the confluence (%)	2	2.2
Tributary slope (°)	33.1	26.6
Rhône discharge during measurement (m^3s^{-1})	182	300
Tributary discharge during measurement (m^3s^{-1})	4	8.13
Discharge ratio during measurement	0.022	0.027
Momentum ratio (Mr) during measurement	0.018	0.022

Table 1: Selected upper Rhône tributaries with their typical characteristics

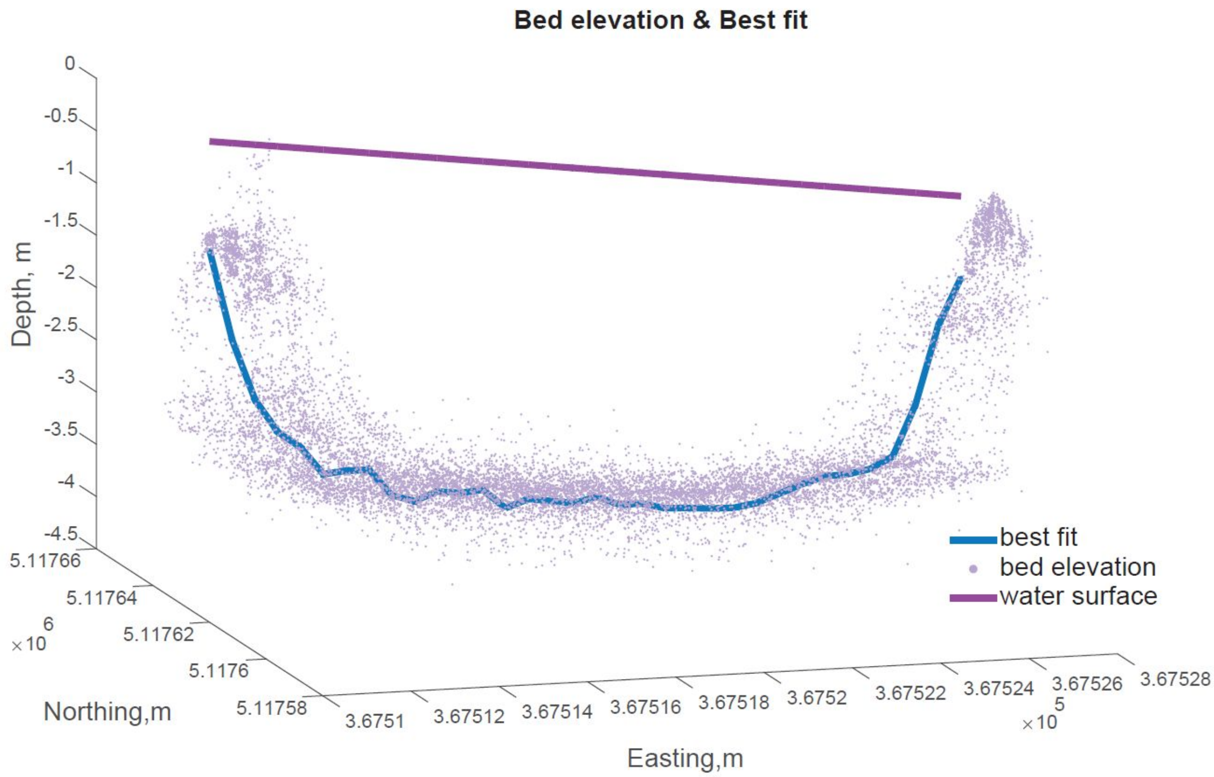

Figure 1: Bed elevations, the best fit to those elevations and the water level representation

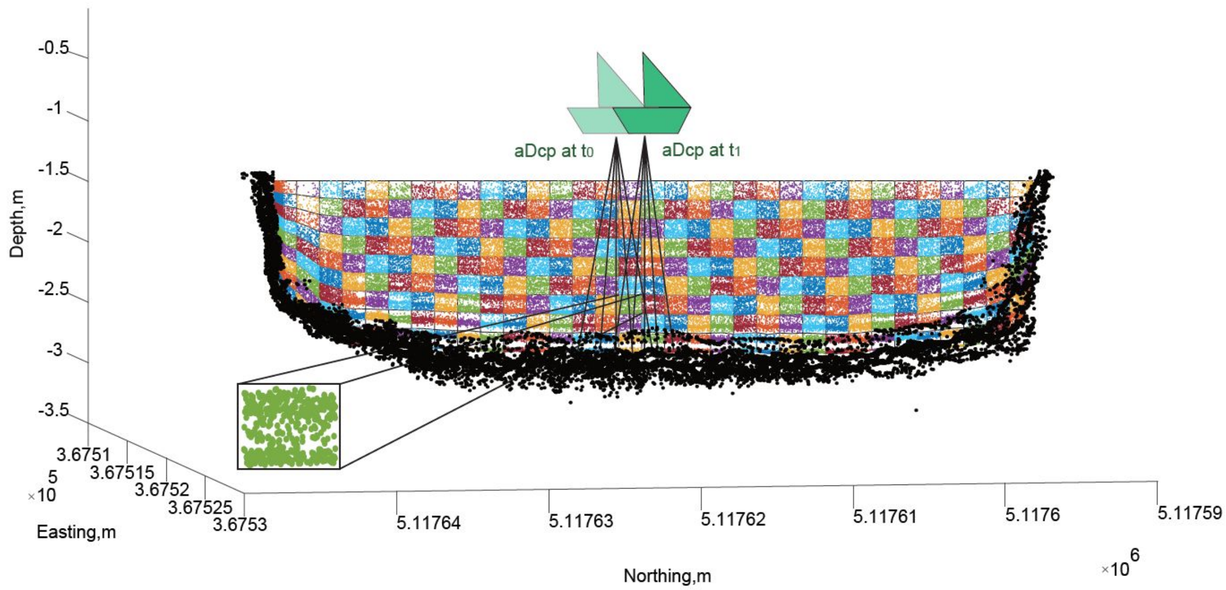

Figure 2: An example of beam velocity positioning within each mesh cell, using M~~m~~ethod A, dots show beam velocities and color is an automatic Matlab function to distinguish between different mesh cells

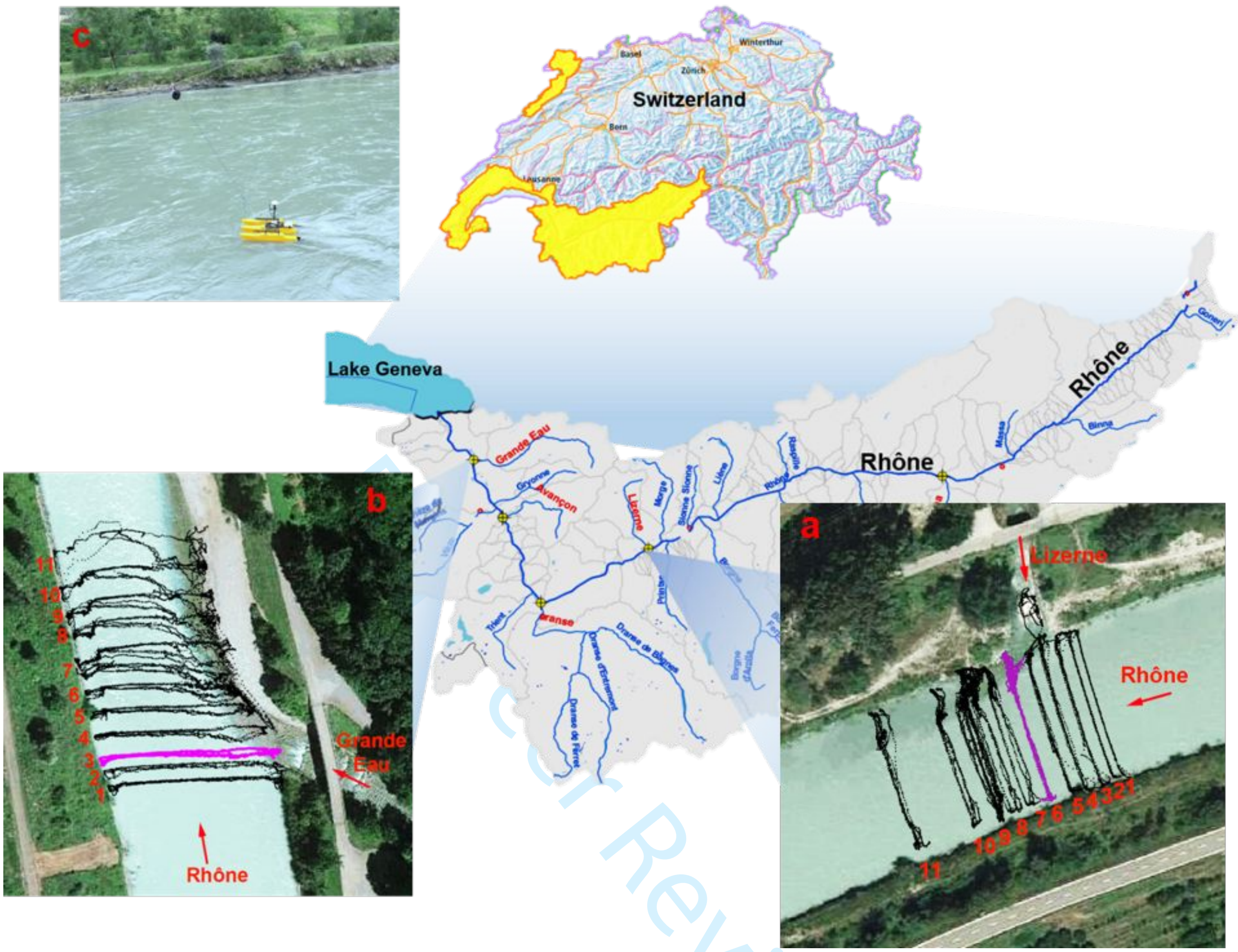

Figure 3: Tracks navigated by SonTek aDcp moving boat system at a) Lizerne-Rhône confluence near Vétroz, at 07/07/2017 and b) Grande Eau-Rhône confluence near Aigle at 23/05/2018. The repeated transect data assessed in this paper are from cross-section 6 at the Lizerne-Rhône confluence a and cross-section 3 at the Grande Eau-Rhône confluence and c) Rope-Pulley system

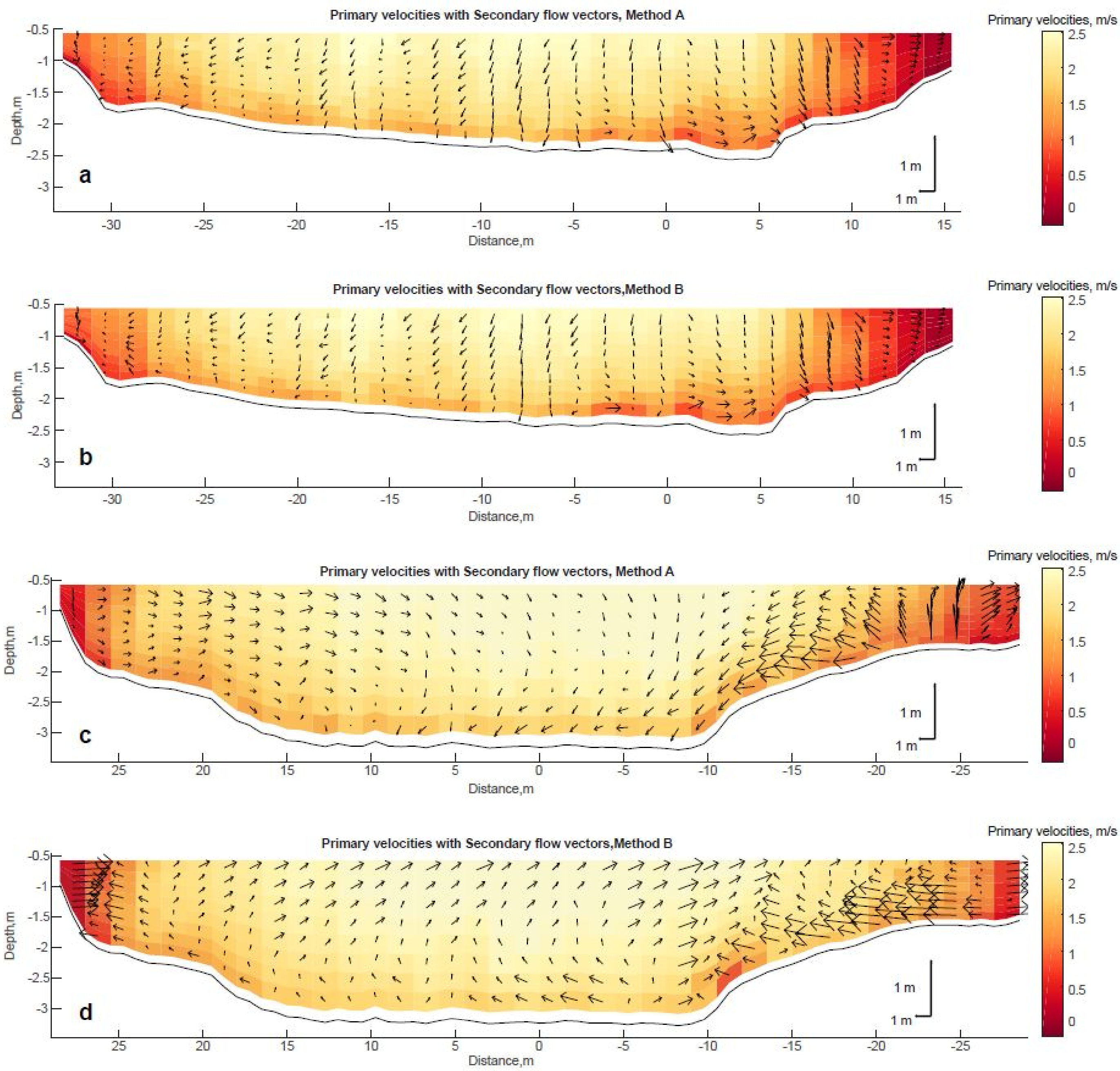

Figure 4: Primary and secondary velocities estimated ~~with method A at a)~~ for the Lizerne-Rhône Method A (a) and Method B (b) and the ~~, cross-section 9 and b) Grande Eau-Rhône, cross-section 3, confluences and method B at c) Lizerne-Rhône, cross-section 9, and d)~~ Grande Eau-Rhône Method A (c) and Method B (d); view is looking downstream.~~, cross-section 3, confluences~~

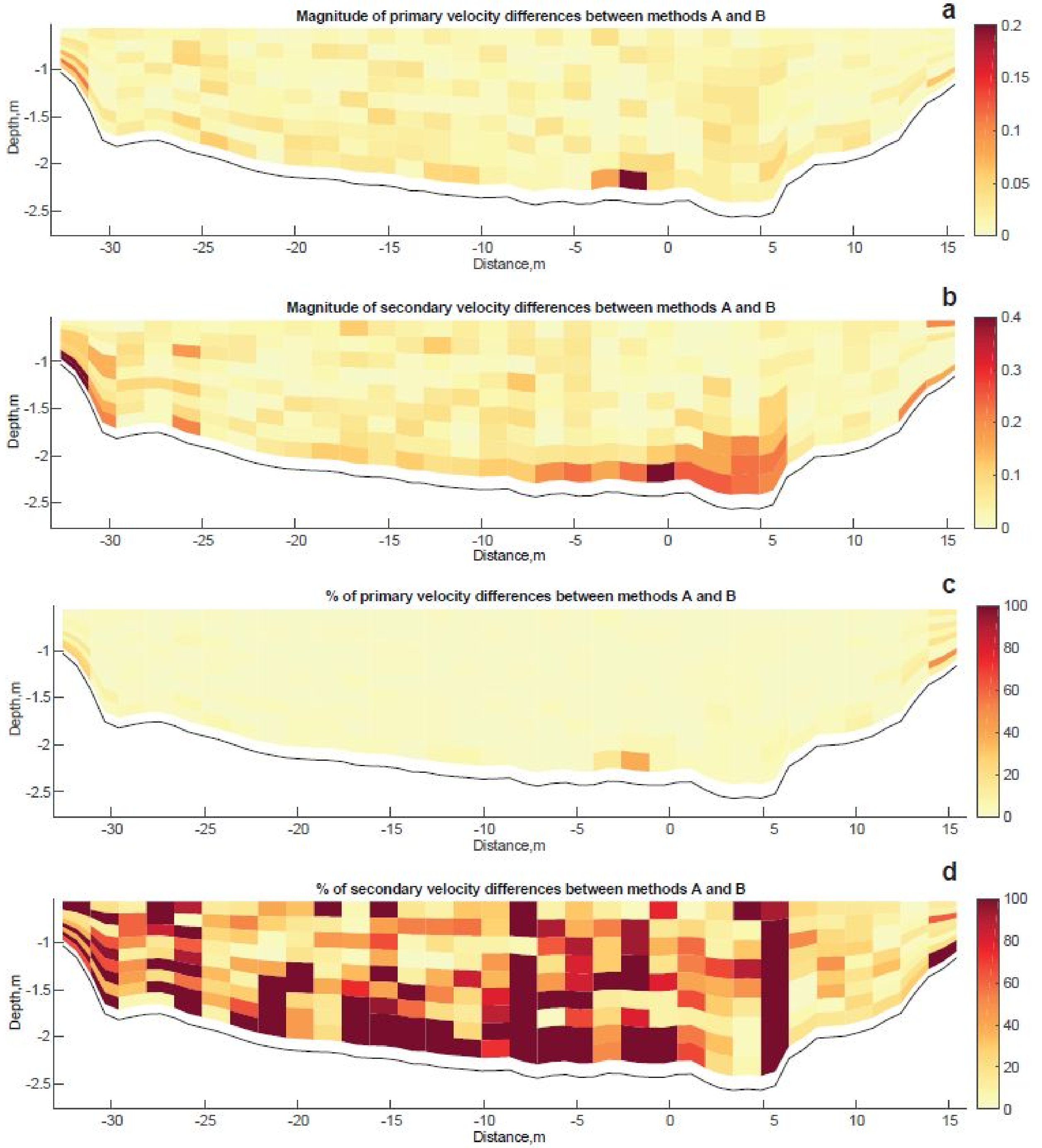

Figure 5: Differences between magnitude of primary and secondary velocities (m/s) between methods A and B (a and b) and the percentages of their difference (m/s) (c and d), at the Lizerne-Rhône confluence, for cross-section 9; view is looking downstream.

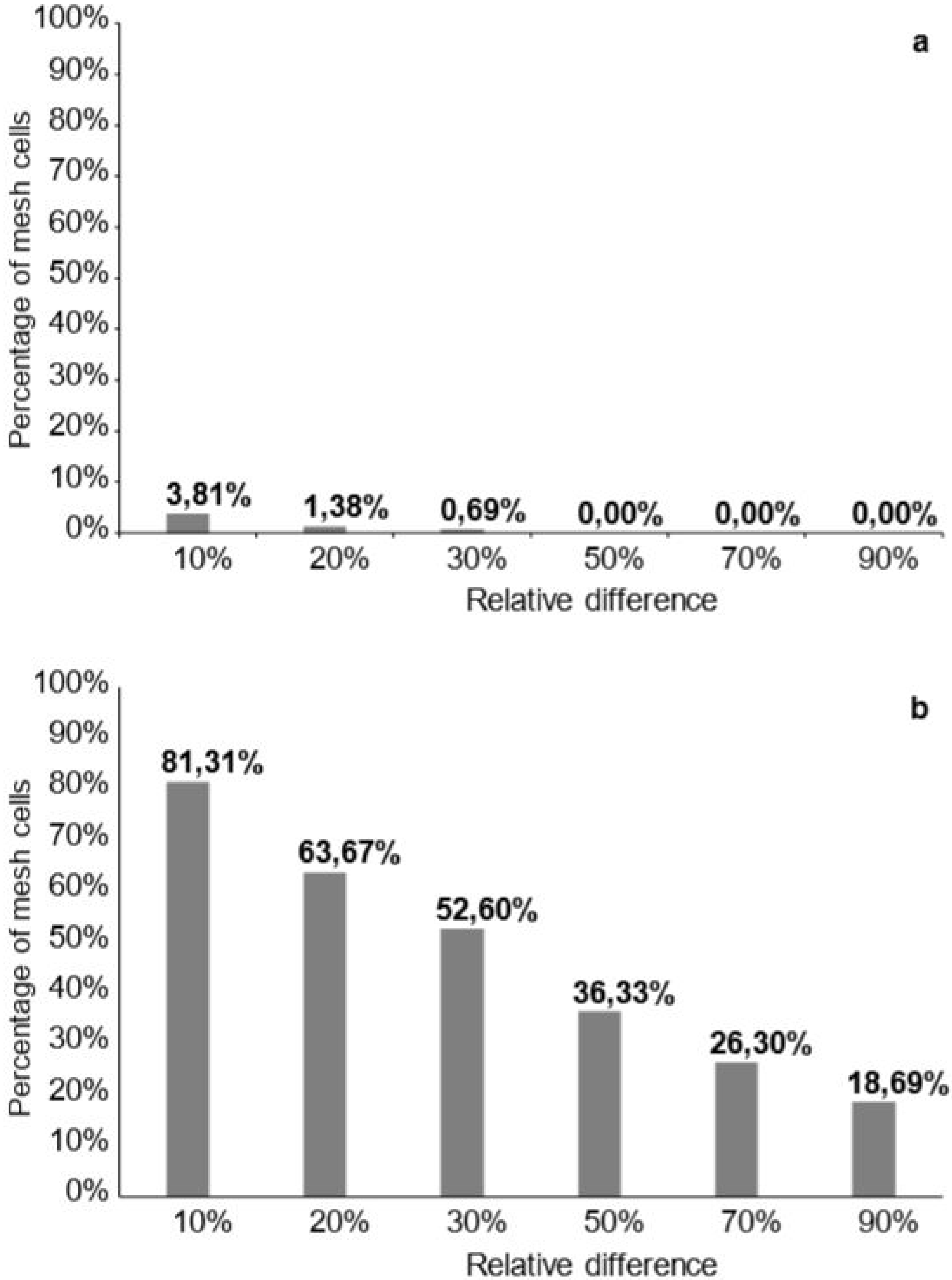

Figure 6: Relative differences in a) primary velocity magnitudes and b) secondary velocity magnitudes, between methods A and B, at the Lizerne-Rhône confluence, for corss-section 9

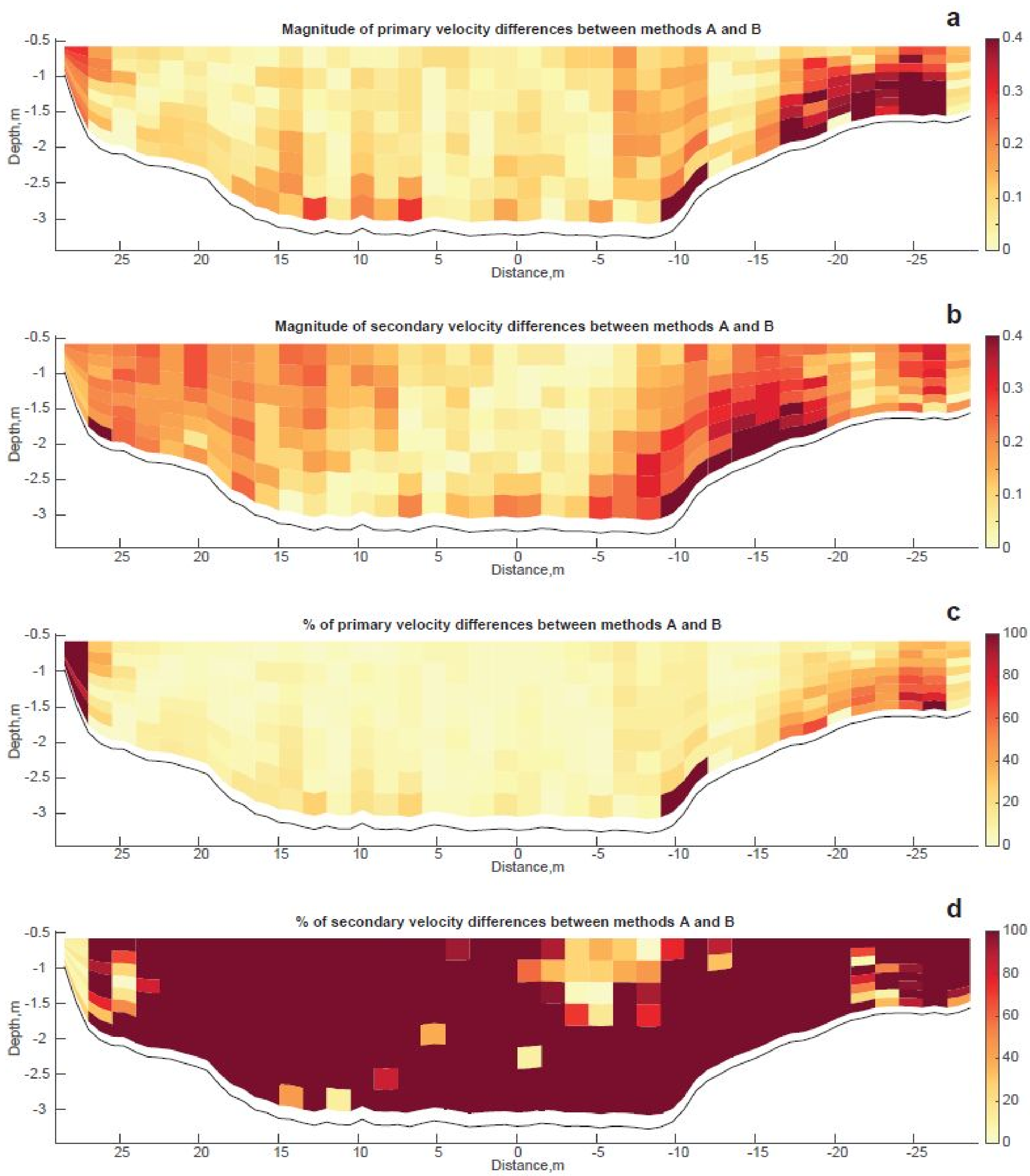

Figure 7: Differences between magnitude of primary and secondary velocities (m/s) between methods A and B (a and b) and the percentages of their difference (m/s) (c and d), at the Grande Eau-Rhône confluence, for cross-section 3; view is looking downstream.

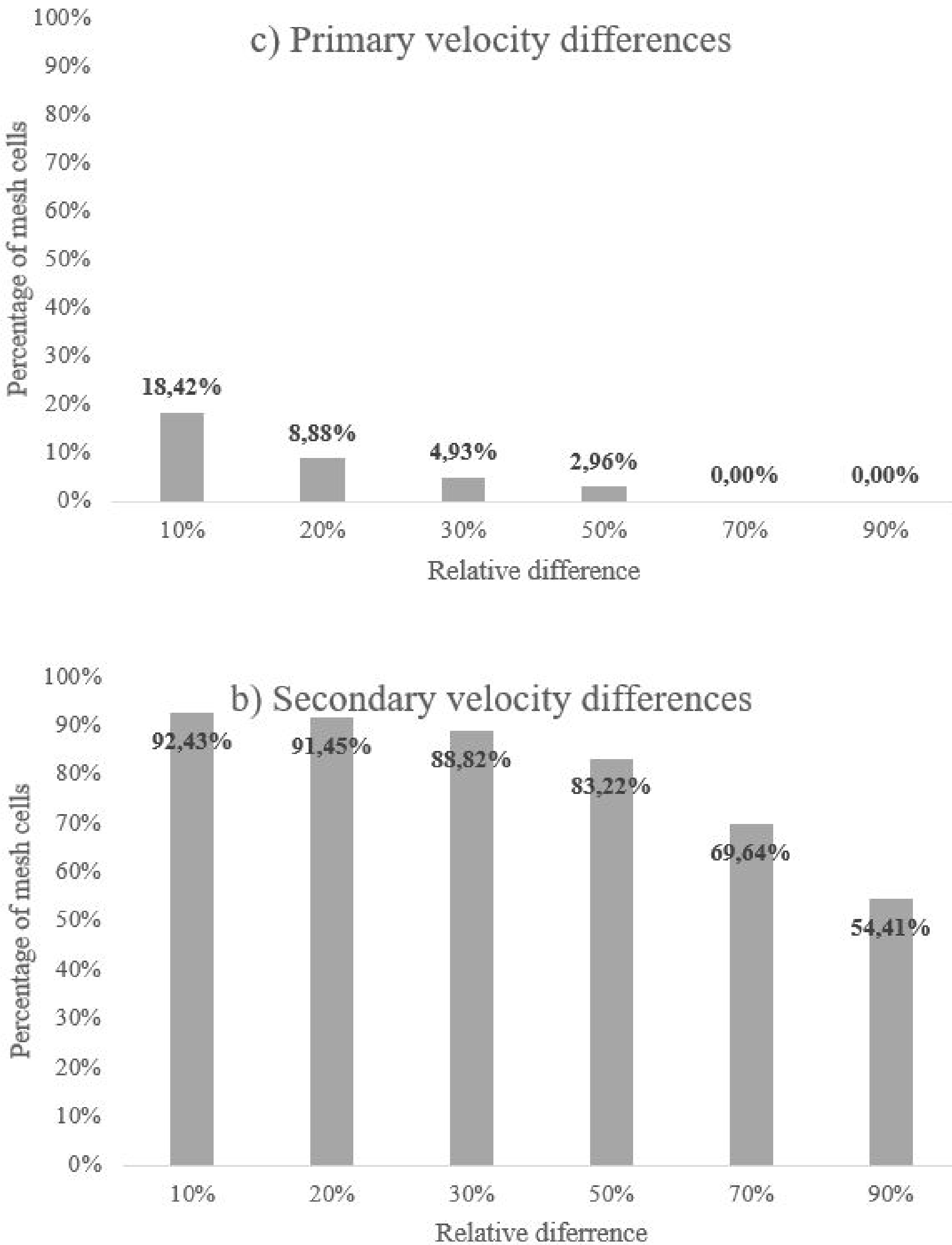

Figure 8: Relative differences in a) primary velocity magnitudes and b) secondary velocity magnitudes, between methods A and B, at the Grande Eau-Rhône confluence, for cross-section 3; view is looking downstream.

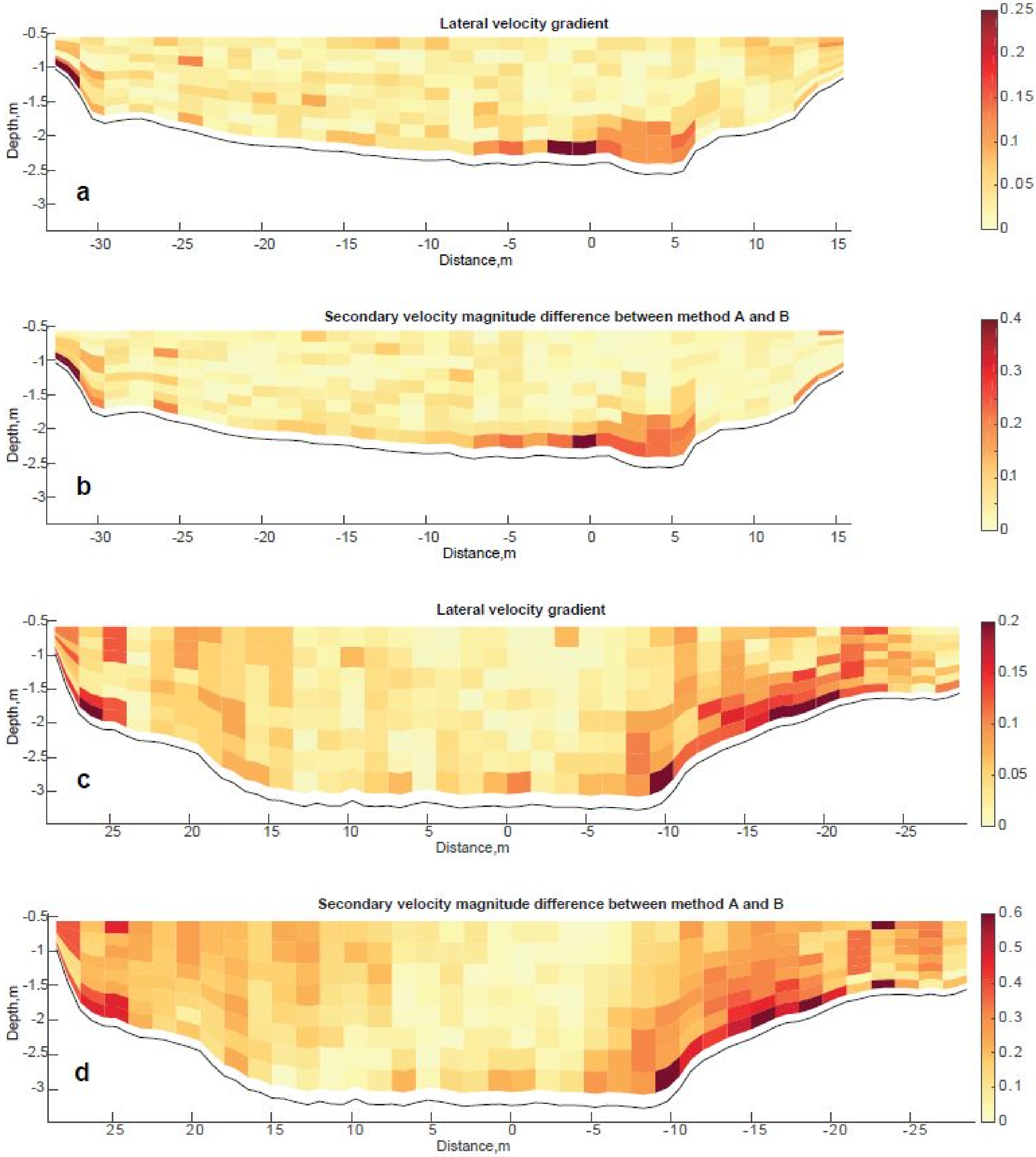

Figure 9: Lateral velocity gradients (a, c) and differences in the secondary velocity magnitudes (b, d) at the Lizerne-Rhône cross-section 9 (a,b) and the Grande Eau-Rhône cross-section 3 (c,d) confluences; view is looking downstream.

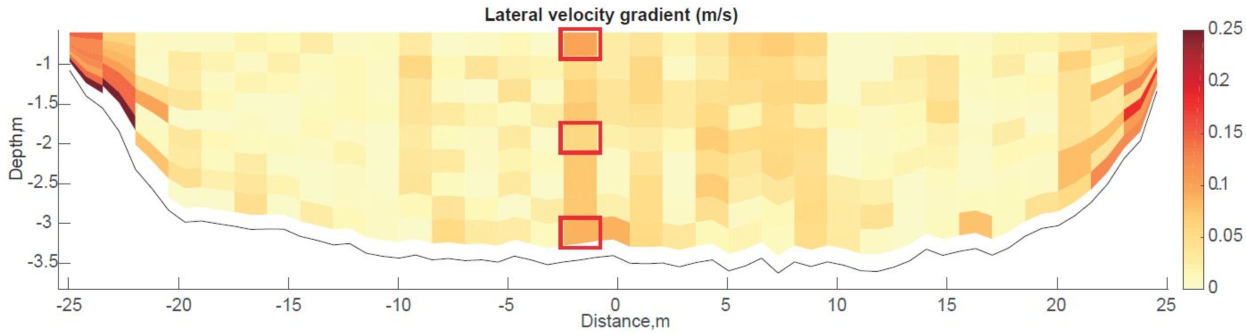

Figure 10: Water column and mesh cells for cross section 9 in Figure 3a at the Lizerne-Rhône confluence, in which standard deviation of the estimated velocities have been calculated; view is looking downstream.

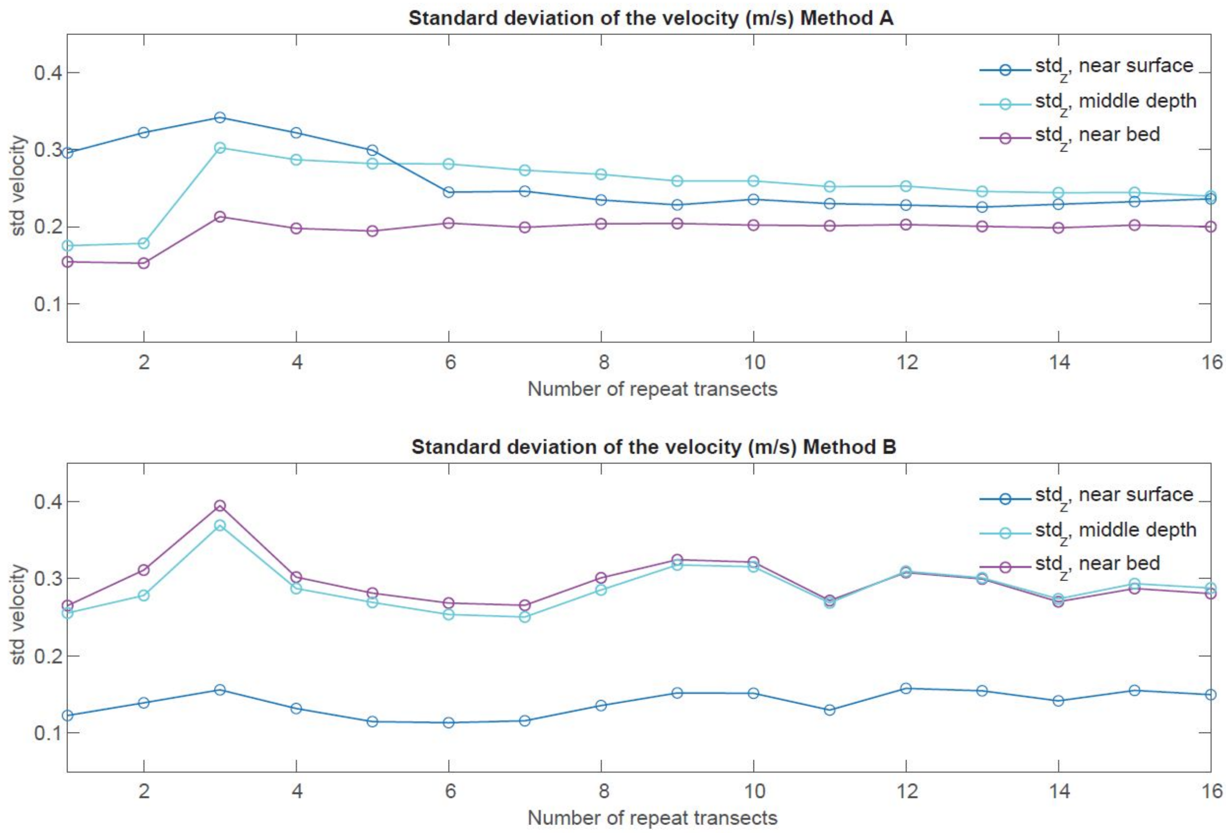

Figure 11: Standard deviation of the velocity estimated using methods A and B for 16 repeats at the Lizerne-Rhône confluence cross-section 9

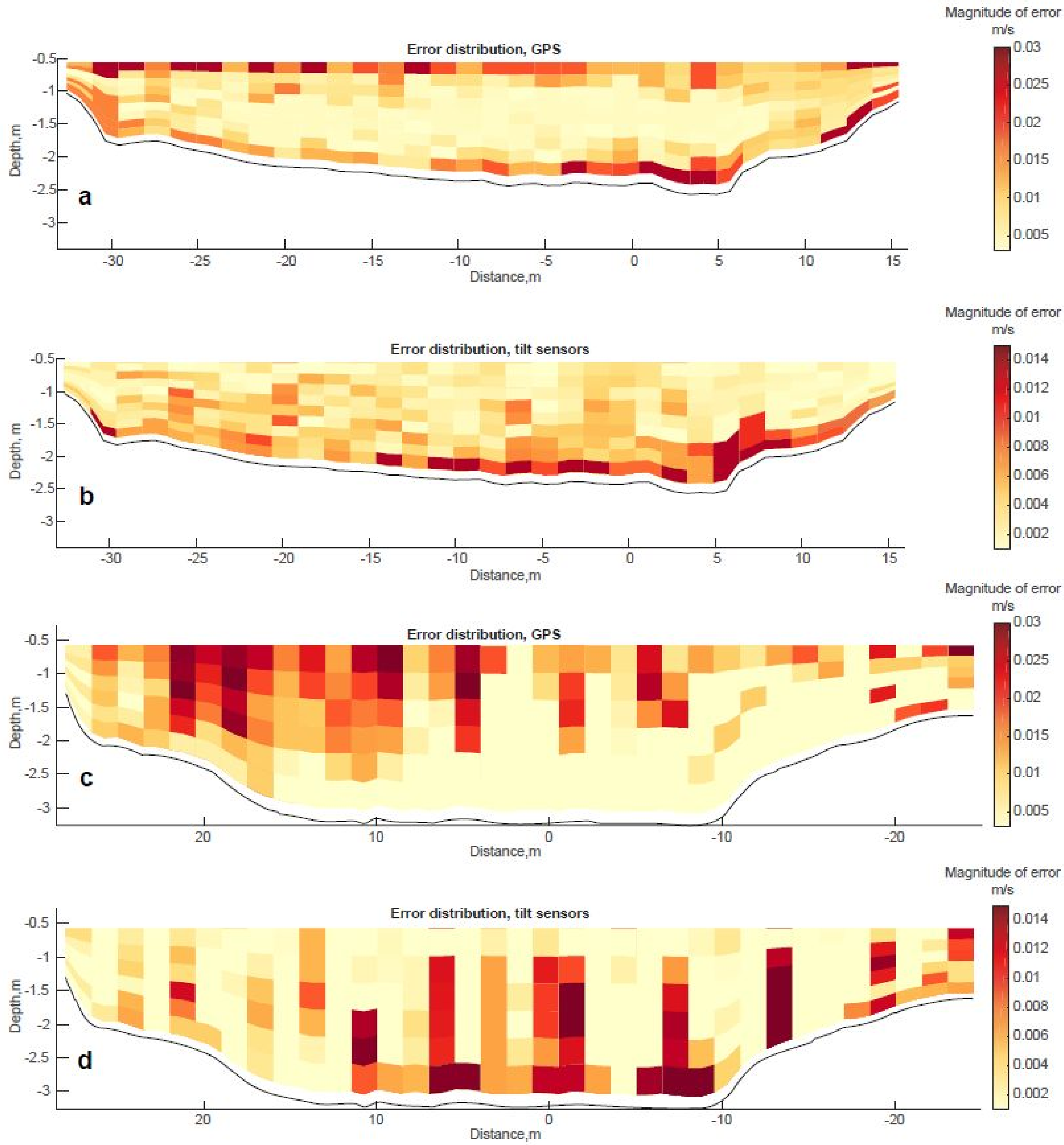

Figure 12: Error distributions related to GPS for a) Lizerne-Rhône confluence and c) Grande Eau- Rhône confluence, and sensors accuracies for b) Lizerne-Rhône confluence and d) Grande Eau-Rhône confluence, in estimating the secondary velocities using M~~m~~ethod A; view is looking downstream.

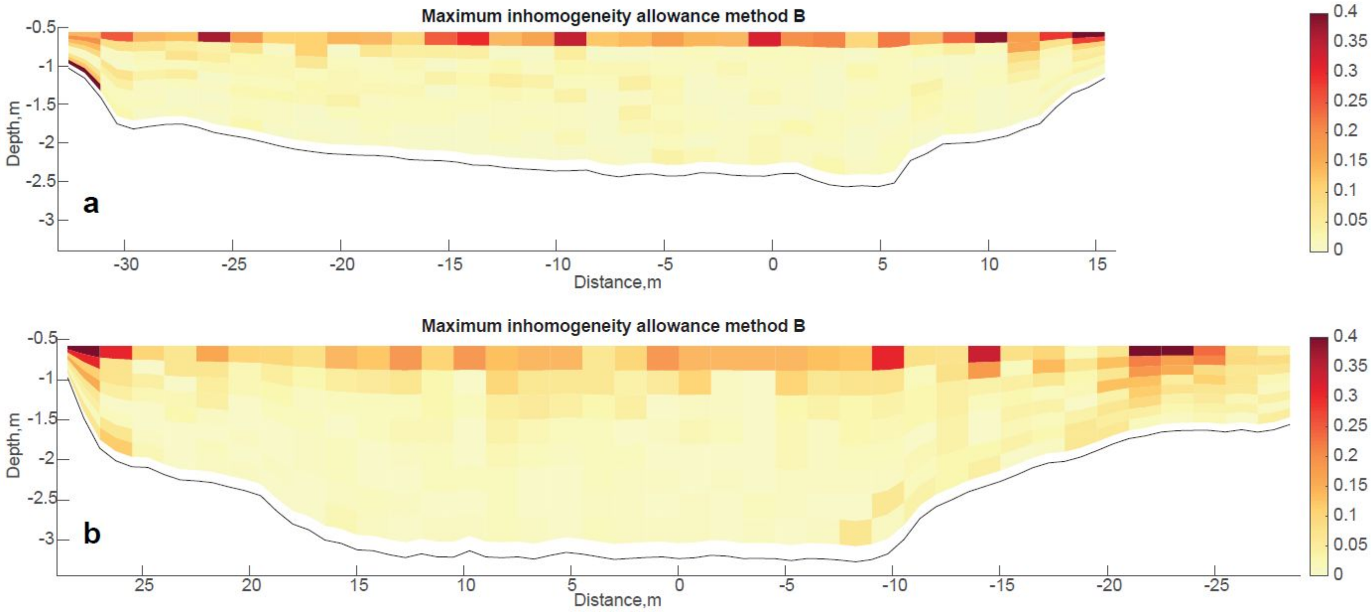

Figure 13: Maximum inhomogeneity allowance (m) using M~~m~~ethod B for a) Lizerne-Rhône and b) Grande Eau-Rhône confluences; view is looking downstream.

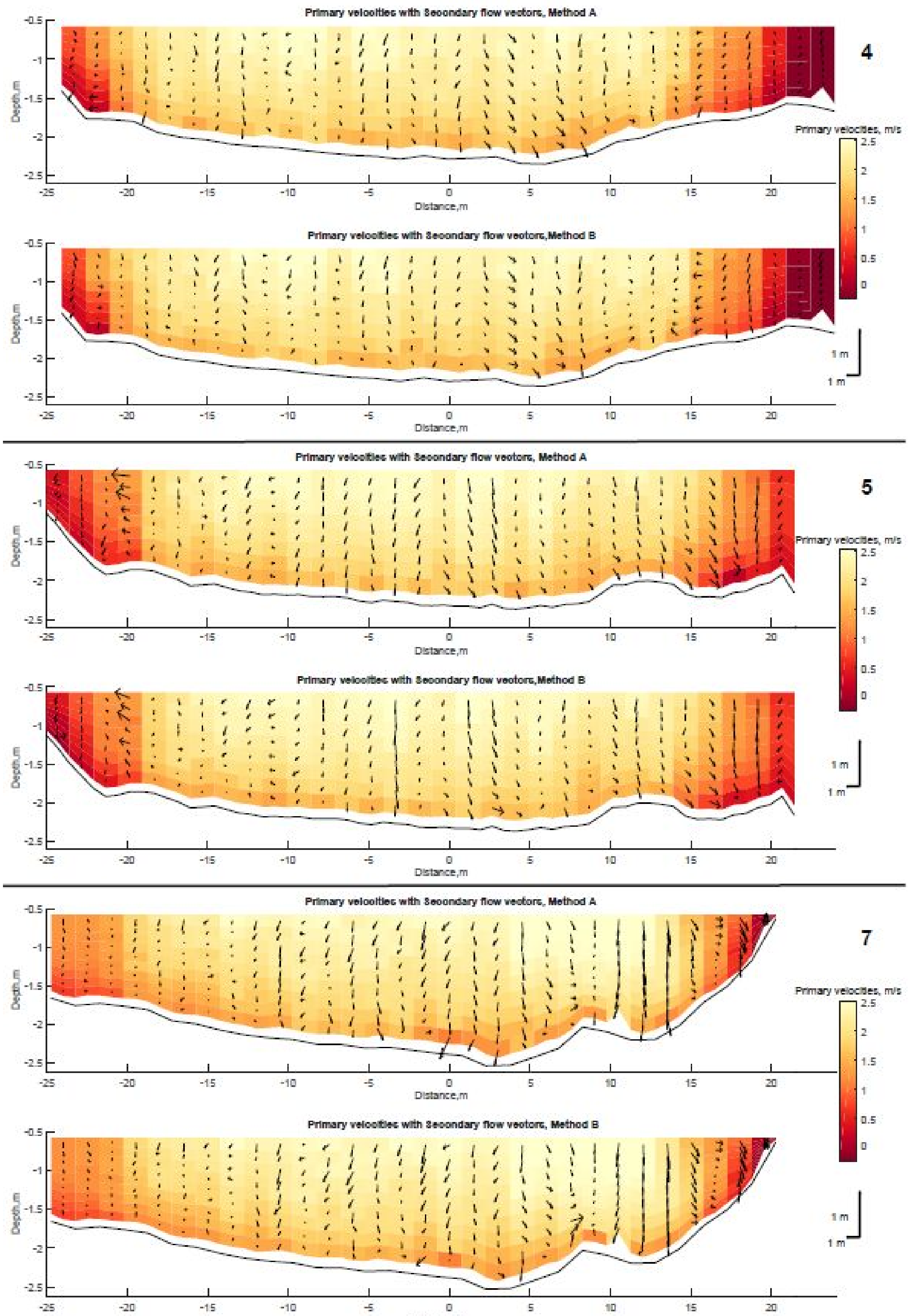

Figure 14: Primary velocities (contours) with secondary velocity vectors estimated using methods A and B at cross sections 4,5 and 7 in Figure 3a at the Lizerne-Rhône confluence; view is looking downstream.

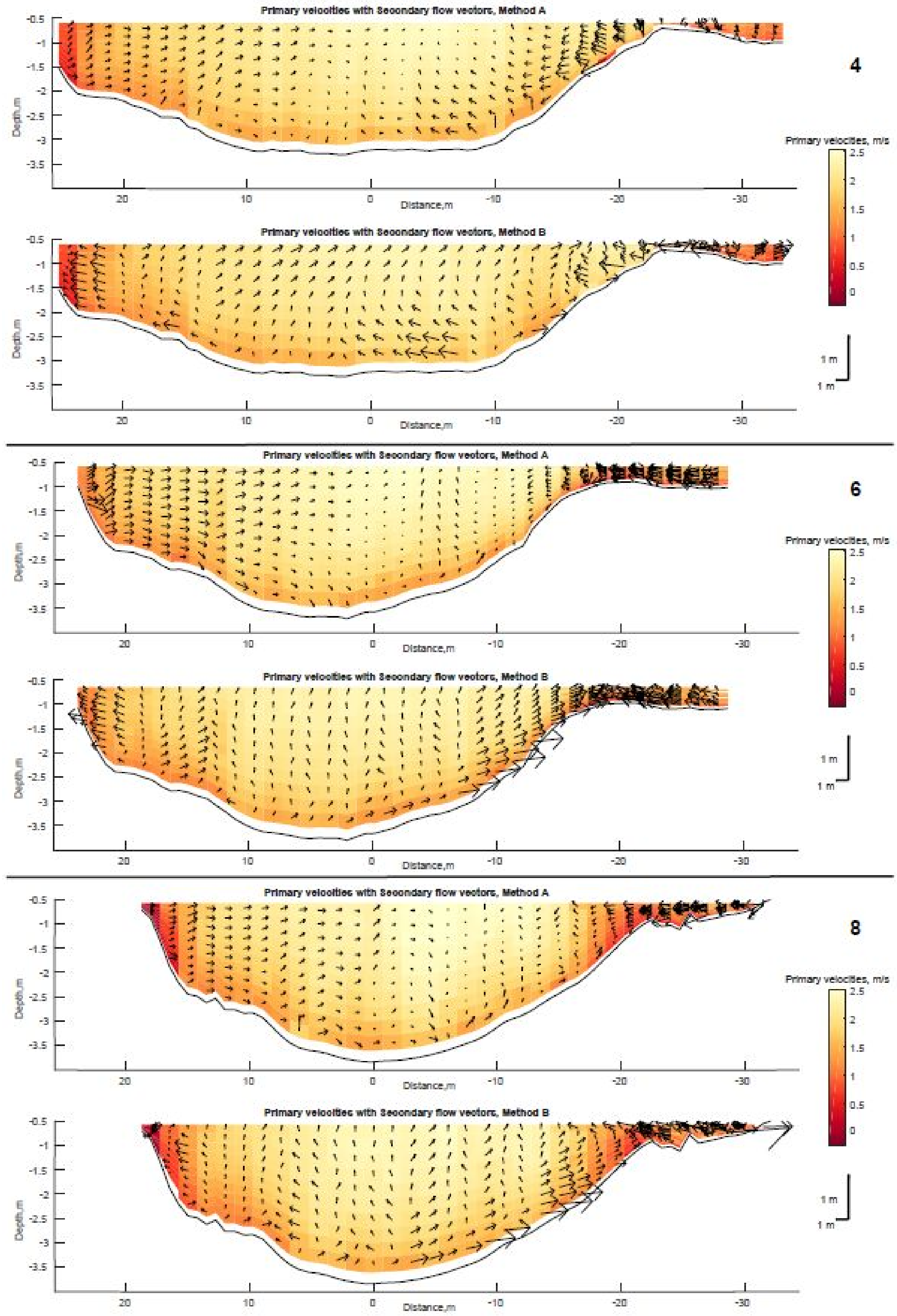

Figure 15: Primary velocities (contours) with secondary velocity vectors estimated using methods A and B at cross sections 4,6 and 8 in Figure 3b at the Grande Eau-Rhône confluence; view is looking downstream.

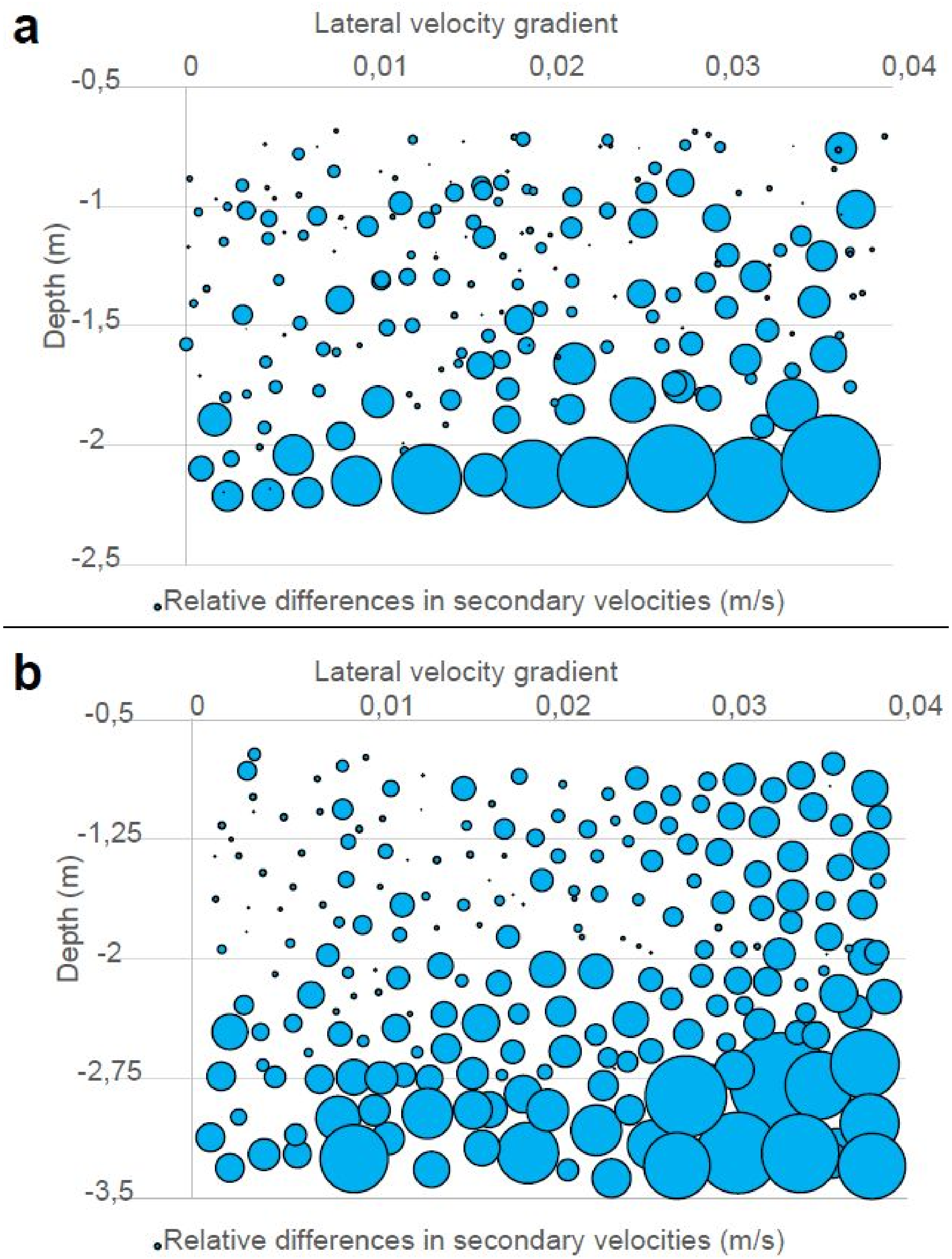

Figure 16: Relationship between lateral velocity gradient, depth and relative differences in secondary velocities for a) the Lizerne-Rhône confluence and b) the Grande Eau-Rhône confluence

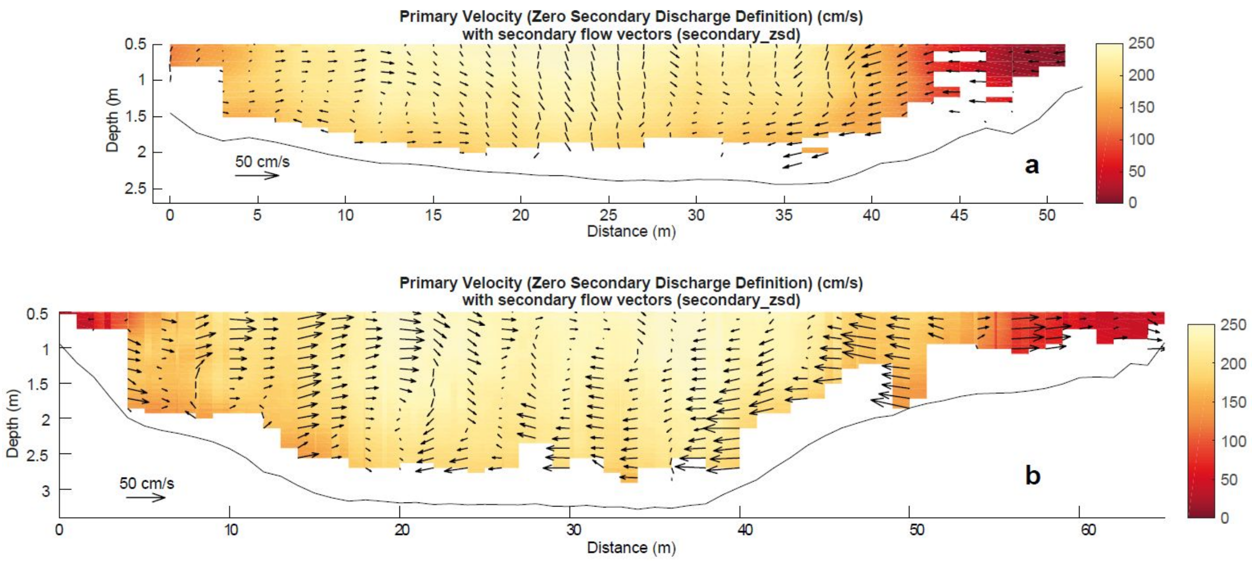

~~Figure 17: Primary velocities (contours) with secondary velocity vectors estimated using the VMT at cross section 6 in Figure 3a at the Lizerne-Rhône confluence and at cross section 3 in Figure 3b at the Grande Eau-Rhône confluence. These are comparable with results in Figure 4a/4b for the Lizerne-Rhône and 4c/4d for the Grande Eau-Rhône confluences~~

Dear Professor Kirkby,

Thank you for the decision of moderate revision on our paper ESP-19-0030.R1. We have now been able to undertake the requested changes (marked below in black). We detail our response below (marked below in blue) and we have also supplied a manuscript with changes tracked.

With best wishes
Gelare Moradi for the authors

ASSOCIATE EDITORS COMMENTS

Thank you for your careful revision which has greatly improved the manuscript. However reviewers have identified a number of points that require some further revision or clarification before acceptance.
Thank you for this positive assessment. We explain our response to these revision requests below.

Reviewer: 1

The revised version of this paper is much improved and the modified analysis presented in the paper focusing on flow within two confluences, rather than downstream of a single confluence, provides a refined basis for comparison of the two different methods (A and B) for evaluating flow structure at confluences using ADCP data. The authors are to be commended for undertaking this substantial revision and addressing most of the issues raised in my previous review.
We thank the reviewer for this positive assessment.

The paper now represents an important contribution, but still needs moderate revision to be of publishable quality.
We explain the changes made below.

1) Abstract lines 26-29 The blanket statement here that method A is an improvement over Method B (implied) is somewhat at odds with the conclusion that the two methods have advantages and disadvantages and that both can in the absence of strong shear produce similar results. Also, the extent to which Method A is more accurate than Method B cannot be determined conclusively from a comparison using the two different methods to process the same ADCP data. Some independent measure of the flow using information that is known to accurately represent local flow conditions (such as a dense array of ADV measurements) would be needed to determine whether ADCP data from either method are accurately capturing the flow structure. What seems most appropriate is to indicate that the two methods can, in the presence of strong shear, produce different results, and, given the averaging inherent to method B, it is reasonable to assume that Method A should provide more accurate results under these conditions than Method B. In other words, a more tempered statement would seem appropriate given what is accomplished in the study.
This is a very fair point. We have now replaced the end of the abstract with "*The comparison confirms that in the presence of strong shear our method produces*

different results to more conventional approaches. In the absence of a third set of fully independent data, we cannot demonstrate conclusively which method is best, but our method involves less averaging and so in the presence of strong shear is likely to be more reliable."

2) Abstract lines 29-32 This statement about counter-rotating cells and scour is not consistent with results presented in the paper. No clear identification of counter-rotating cells using method A is presented in the results, nor is a comparison made between counter-rotating cells by methods A versus B. These cells also are not related to scour. This statement should be dropped from the abstract and perhaps replaced with a statement that the use of both methods, along with consideration of the factors that influence each method, is valuable for evaluating flow structure at confluences (see point 30 below).
We agree. This has been removed and replaced with "*We conclude that it is wise to apply both our method and more conventional methods to identify where data analysis might be impacted upon by strong shear and where inferences of secondary circulation may need to be made more cautiously.*"

3) Line 118 – irregular cross-sections. I assume this is referring to the irregularity of the bathmetry at cross sections, rather than an irregular alignment of the cross section. This should be made clear.
Agreed – we have inserted "*bathymetrically*" before "*irregular*"

4) Lines 126 to 134 If I understand it correctly, given the way the processing calculates the mean cross section, the orientation of any cross section relative to the alignment of the river channel can vary from cross section to cross section along the river. In many fluvial applications the desire is to have cross sections perpendicular to the local channel alignment. For a relatively straight channel, such as the Rhone in this study, that would also imply that cross sections are parallel to one another. The extent to which this condition is achieved seems to depend on the boat tracks and the clouds of bathymetric points produced by these tracks. To what extent did the resulting cross sections for analysis differ from one another and from the alignment of the river?
To some extent this issue is rendered moot by the use of the zero net secondary discharge to analyze the flow structure, but that method also involves rotation of the cross sections. It might be good to show the alignment of the cross sections derived from the processing method and the alignment of the zero net secondary discharge cross sections on figure 3. Cross section alignment can influence the interpretation of secondary flow (see point 7 below).
The reviewer is right to note here that there are two controls on the analysis relating to cross-section orientation: the first is the orientation of data collection which defines the initial mean transect, and this is easier when the main channel is straighter; but this does not necessarily lead to the correct identification of secondary circulation, for which rotation is then needed. To respond to this revision request, we have made two changes.

1. We have added the following at before former line 126 "I*t is important to note that this mean transect is not necessarily orthogonal to the primary flow direction and so will not yield true primary and secondary flow estimates without further correction. We address this below.*"; and just after reminded the reader that the initial bathymetric model is the initial mean transect. This

makes the relationship between the transect definition during data collection and the identification of primary/secondary circulation clearer.

2. In response to point 7 below, we mention more clearly the importance of secondary flow correction, and that we do not assess this in this study.

5) Lines 326-329 The decision to use six cross sections seems to be based on the analysis of standard deviation of the velocity data. Although this is presented in the results, this basis should at least be mentioned here.

Agreed – we have added "*Hence, in this paper, data are processed for cross-section 6 at the Lizerne-Rhône confluence (Figure 3a), and for cross section 3 at the Grande Eau-Rhône confluence (Figure 3b). Identification of the minimum number of repeat transects necessary per cross-section was undertaken using cross-section 9 at the Lizerne-Rhône confluence (Figure 3a), which involves 16 repetitions. We noted that after application of Method A, the standard deviation of velocity stabilized with six repetitions, which is the number we adopt for this study*."

6) Lines 363-368 why was a standard deviation of plus or minus 1 degree chosen as a reasonable value for tilt sensor error? Also what was the standard deviation of the displacement error distribution? How was this determined?

We have added "*based on manufacturer specifications*" for the tilt error; and "*measured by the dGPS for the dGPS positions (as a function of satellite configuration during measurement)*" for the positions.

7) Lines 380-381 The zero net secondary discharge method was used to determine secondary flow. This choice can have an influence on the depiction of secondary flow compared to other secondary-flow depiction methods (e.g. cross-stream perpendicular to the local channel alignment, Rozovskii method, maintenance of flow continuity of between cross sections). This issue should at least be mentioned in the discussion or conclusion (i.e. that this aspect of data processing, not just the ADCP operation, is a relevant one for producing differences in secondary flow patterns, but is not considered in this study).

This is correct. We use the zero net secondary discharge method as work two decades (Lane et al., 2000) showed that other methods (e.g. Rozovskii) are not correct (Rozovskii, for example, means that the primary flow direction changes within an individual cross-section). To make this clear, we have made two changes

1. In the methods section we now write "*In order to distinguish between primary and secondary components of flow, we need to rotate the initial mean transect. Options for doing this are reviewed in Lane et al. (2000) and we do not assess them here, but rather apply the zero net cross stream discharge definition (Lane et al., 2000).*"
2. We have added at the end of the Discussion "*Finally, we wish to emphasise that the impact of averaging is only one element that must be considered in obtaining reliable primary and secondary clow estimates in river confluences. Other issues, such as the rotation method needed to distinguish primary and secondary circulation, remain important and should be considered routinely.*"

8) Lines 391 to 400 It is not clear why angular rotations are needed for vertical velocities. A rotation should not be necessary if the cross section is a plane aligned from the flow surface to the bed.

No – we disagree here. Secondary velocity is defined as that component of velocity that is orthogonal to the primary flow direction and this includes components that will be both predominantly lateral and vertical. The next flux associated with both lateral and vertical fluxes should be zero for true definition of the primary velocity, which is why this rotation is needed. We have made this clear by adding "*secondary circulation is all flow that is orthogonal to the primary flow and not just horizontal flow; there should be not net secondary flux in a section; and so correction should also consider vertical velocities*".

9) Line 401 What does curvature of cross-sections refer to here?? How are the cross-sections curved?
We have clarified this by adding "*correct for weak curvature with the survey method at the edges of each transect line (e.g. Figure 3),*".

10) Lines 410-411 this statement about differences is not put into any context and seems to contradict the previous sentence that the velocities are similar for the two methods
Agreed – modified to "*and the differences in estimated secondary flows are minor. The differences are most pronounced between -10 and 5 m, in the middle of the main channel*".

11) Figure 4 - the caption for this figure appears to be incorrect. The top two frames (a and b) are for one confluence and the bottom two (c and d) are for the other. The caption is confusing as written.
Corrected to "*Figure 4: Primary and secondary velocities estimated for the Lizerne-Rhône Method A (a) and Method B (b) and the Grande Eau-Rhône Method A (c) and Method B (d)*"

12) Table 1 It would be good to include the velocity ratio (ratio of mean velocities) in this table as this should provide the most direct information on the difference in the magnitude of lateral fluid shear between the two flows. Based on the arguments in the text this ratio should be much larger for Grand Eau than for Lizerne.
This may be correct if the two tributaries had beds at the same altitudes, but there is also a very marked difference in tributary elevations and hence depth ratios. This means that the velocity ratio is not a useful parameter to report. This was not clear in our previous version of the paper and so we have now made this clear through the following changes:

1. Where we introduce the Lizerne, we have modified the description of the junction angle to: "*It reaches the Rhône between Ardon and Vétroz, forming a 90° junction angle and it has a bed that is nearly concordant with the Rhône*." – and where we introduce the Grande Eau, we now write: "*The Grande Eau bed is c. 1.5 m higher than the Rhône such that it is markedly discordant*".
2. In the results, we now mention the importance of bed discordance with the relevant sentence modified to: "*This is due to a high degree of bed discordance between the Grande Eau and the Rhône, which increases the penetration of the tributary flow into the main channel over the junction, and which forms a zone of high lateral and vertical shear, on the one hand, and main channel narrowing because of penetration of the tributary point bar on the other hand.*"

3. When we now discuss Figure 7 we have added in reference to vertical and lateral shear.

13) Line 415 reference figures 4 c and d here
Added

14) Line 421 and 422 above the junction? Flow enters at the junction. This phrase can be deleted.
Clarified – it was meant to be vertical. We now use "*over*" rather than "*above*".

15) Line 423 tributary point bar should be change to tributary mouth bar. Point bars occur in meandering rivers
Changed

16) Line 427 inner bank? Not clear which bank this is. Assume the left bank but it should be specificied as there is no clear inner and outer bank
Changed to "*bank on the tributary side of the channel*".

17) Line 456 to to 459 It is not entirely clear what cell is being referred to here as the "described above" is disconnected by many lines of intervening text. Recommend it be explicitly reidentified here.
We have rewritten the sentence as "*Indeed, the marked differences between methods A and B at the Grande Eau confluence (Figure 7) are also in a zone of strong lateral shear*." to make reference back to Figure 7.
Also the use of the term cell for secondary flow and cell for the mesh can be confusing at places. May want to consider using mesh cell and secondary cell rather than just the term cell.
This is an excellent point – there are actually 3 cells: the aDcp, the mesh (numerical, that we use for the analysis) and secondary circulation. For all mentions of cell we now distinguish between these.

18) Line 475 -478 the stabilization of the variance is likely a product of the number of measurements contained within the each mesh cell. Do methods A and B produce different numbers of measurement points within each mesh cell? It seems likely they would given that method A should produce many more individual velocity readings than method B. This might be an important factor in stabilizing variance.
This is right and we have clarified it – adding, "and this is likely because method B uses fewer measurements per mesh cell."

19) Line 527 mouth bar
Modified

20) Line 521-523 careful with language here. Method A cannot produce stronger penetration or weaker upwelling of the flow. It indicates that secondary velocity components differ from those depicted by Method B, which has implications for the strength of penetration and upwelling.
Yes – and so we have modified the text in 6 places to make sure we mean identification rather than production.

21) Line 546 would be good to present velocity ratio in table 1 to confirm this. Also information from the primary velocity data on the maximum lateral shear gradients for the shear layers in each confluence would also be useful.
This is a useful point and did need some clarification. As noted above, the issue is more that the GE-R has a more complex shear zone (with lateral and vertical shear) rather than necessarily a more intense lateral shear zone. To capture this point, we have rewritten the section as "*the Grande Eau-Rhône has a more complex shear zone, likely due to the effects of bed discordance, and there are more significant differences in the estimation of primary and secondary velocities*"

22) Line 557 As mentioned with the abstract, this statement should be qualified. One can reasonably assume it should provide more accurate information on the secondary velocities, but this cannot be conclusively confirmed without independent corroborating evidence.
Yes – this is a very fair point and to follow our changes to the abstract, ee have modified the sentence to: "*In this case, as method A involves less spatial-averaging than method B, it may provide more accurate information on the flow behavior, but such a conclusion really needs a third and independent method to confirm this conclusion*."

23) Line 564 low levels of lateral shear acceptable for using method B??
Given our response to point 21, we have modified this sentence to: "*At the Lizerne-Rhône confluence, even though the momentum ratio is similar to Grande Eau-Rhône confluence, there is only more localized shear in the flow and a simplified shear zone (Figure 9). In such a situation, using method B to detect the large scale patterns of secondary flow may be more advantageous, because it involves more spatial averaging.*"

24) Line 569 velocity ratio and max values of lateral velocity would help confirm the absence of lateral shear.
See above – lateral shear is not, in our view, the only issue (it is already shown also in Figure 9 – it is more the complexity of the shear zone arising from both lateral and vertical shear. We hesitate in adding more quantitative data because it might lead to others applying an overly simplified rule when the magnitude of shear likely to lead to method A being needed also varies with the distance of the shear zone from the sensor. We now make this point explicitly by adding "*It may be tempting to introduce some kind of shear or velocity gradient threshold to identify when Method A might be preferable. To do so could be misleading as this value will also depend on the distance of the shear from the aDcp*."

25) Line 568-573 run-on sentence need to revise this by at least splitting it into two sentences.
Sentence split into two

26) Line 579-584 Again a rather long sentence. Also it is best to use an even number of transects to avoid potential directional bias in GPS signals
The sentence is now split and we have added "*We also note that an even number of repeats may be important to avoid directional bias in dGPS positions*."

27) Line 599-611 This section on VMT is underdeveloped and gives the impression of material that has been inserted into the paper as an afterthought. The comparison is only for a single cross section and generalizations should not be drawn on the basis of this comparison, even suggestively, especially given that VMT has provided high-quality depictions of secondary flow at confluences in many instances. It is also not clear why the results of the VMT analysis include larger areas near the bed without data. Moreover, the statement about VMT using a straight mean cross-section is confusing. Don't methods A and B also use straight mean cross-sections? It seems best that this rather superficial comparison with VMT be deleted from the paper. Doing so will not detract from its main message of the paper. Generally VMT results should be consistent with Method B, although the level of spatial detail may be greater in VMT depending on the size of the cells in relation to bin size.
We agree and so have removed completely this text, including Figure 17.

28) Lines 615-618 can some indication be provided here about what constitutes a small river versus a large river (would avoid the use of the term "big" since that term is often associated with mega rivers such as the Amazon and Congo)? Use of small versus large is rather subjective and it would be helpful to have at least some metrics associated with these terms.
This is a good point and needed three changes to be made. First, we are now explicit that what we think matters here is depth (and hence shallower versus deeper). Second, we don't have enough cases to specify what this depth is and so we simply state relative to our studied confluences in the modified text.
These two changes are now included in this statement: "*This is likely to be the case particularly in rivers shallower than those studied here and where high resolution is required due to large velocity gradients. In rivers of the scale studied here, and deeper, by increasing the mesh cell size, we can still have sufficient data to estimate velocity vectors, and the effects dGPS and tilt sensor errors have a minor effect."*
The third change relates to the point that we don't have enough data either to identify specifically what we mean by big and small but also to urge caution, following the difficulty if identifying critical values of shear. What is big (so Method A) and small (so method B) will also depend on shear. To capture this point we have added: "*We are not yet in a position to identify the depth at which Method A becomes preferable to Method B, and again this will depend on other parameters such as the intensity of shear and so may not be readily generalizable between confluences.*"

29) Line 631 again velocity data would be useful for evaluating shear
See arguments made above.

30) It might be appropriate to recommend that it can be useful to use both methods to analyze flow structure at confluences, as this paper has done, to see how they differ. If they do not differ greatly this provides reinforcement that the depicted patterns are probably accurate. If they differ, consideration should be given to the factors that can produce differences between the two methods, and a preference for one depiction over another weighted according to the prevalence of these factors.
This is an excellent suggestion and conforms with our Conclusion. Our response to point 24 partly makes this conclusion.
We have added the following to capture this argument:

"*We are not yet in a position to identify the depth at which Method A becomes preferable to Method B, and again this will depend on other parameters such as the intensity of shear and so may not be readily generalizable between confluences.*
The difficulty of identifying the depths of rivers and intensities of shear that make one method preferable over another precludes adoption of simple quantitative guidance on which method to use when. As both methods have some disadvantages, we argue that both methods should be applied. If they give similar results, then there should be confidence in both. If and where they differ, analysis should be undertaken to identify why, and hence which method is likely to be preferable. Association of the differences in primary and secondary velocities inferred between the two methods with estimates of shear intensity and with estimated tilt and positioning errors should then help decide whether Method A or Method B is preferable in a particular case. This preference may vary between confluences but also through time at a confluence, if shear or flow depth changes significantly between survey dates."

Reviewer: 2

Comments to the Author
General comments

The reviewer appreciates all the answers and effort made by the authors to address all suggestions and comments made by reviewers in the new manuscript submission, which has significantly improved the manuscript.
We thank the reviewer for this positive assessment.

Before publication, I suggest the authors clarify some specific questions detailed below.

Note: As a suggestion, in order to the proposed methodology is easily apply by ADCP users, I strongly recommend the development of an open source code. To include these methods into the widely used VMT software will be an excellent tool for ADCP users interested on flow structures estimation at complex hydrodynamics zone such as confluence, bifurcation, bends, etc…
We think the best way to achieve this is to integrate the method into the VMT and we are currently in discussion with the VMT developers to do this. We can also make our own code available upon request and have added this to the acknowledgements.

Specific Comments:

Table 1: discharge from Rhone and tributary rivers are not provided.
Added

Figure 4: caption references do not agree with figures and text.
Corrected in response to Reviewer 1.

Figure 4: I suppose sections are looking downstream. Clarify in caption.
Clarified, and in all other captions

Line 411-412: there are other verticals with similar differences. Could the authors justified in more details?

Typo: -5m should be 5 m – corrected; this then deals with this concern

Line 416-417: It was confuse to me that this affirmation is valid for primary velocities but secondary component look opposite (i.e. at shorter distance from ADCP). Could you clarify?
We don't make this affirmation for secondary velocities. This difference, though, is partly explained because it depends on the magnitude of primary velocity relative to secondary velocity. We don't think this needs to be explained as we don't discuss secondary velocities in this way.

Line 421-428: the sentence is very confused. Could the authors rewrite this sentence?
Clarified in response to the request from reviewer 1 (point 14)
Moreover, Grande Eau-Rhône streams have difference densities that could explain the penetration of Grande Eau river into Rhone near bed? It will be useful for reader to have this information to understand the non-common secondary pattern processes presented at this confluence.
We don't believe this is an issue as the differences in suspended sediment load and temperature were negligible during measurement. We prefer not to get into this issue as it would detract from the paper.

Figure 4 and 7: I cannot see an agreement between Figure 4c,d and Figure 7b,d. For example, a clear differences in secondary velocities intensity is presented near water surface at distance between 0 to -10 and lower discrepancy between distance 20 to 10. However, Figure 7 shows the opposite behavior.
This is simply a color scale effect – Figure 7 plots magnitudes of difference whereas Figure 4 c/d show absolute values. The zone described above suggests differences of around 0.1 m/s in Figure 7 which scales with the differences shown in the same zone by comparing vector lengths Figures 4c and 4d. No changes made.

Figure 6: add legend in figure 6a.
We have deleted the figure 6b legend

Line 495-497: This sentence is not clear to me. Why the relation between ship movements and uncertainties in dGPS data produce a large error near surface and not in all water columns?
This was unclear – and so we have rewritten it as "*Near the surface, as there fewer measurements that can contribute to the estimation of aDcp position and tilt, uncertainties in dGPS data will have a greater effect*."

Line 608-612: it is surprising to me the big difference between Method A and B with VMT (similar that is doing by methods B). How many transects were used to obtain figure 17b using VMT? In order to compare the methods should be the same amount than Figure 4. Clarify.
The VMT comparison has been removed.

Table 1: Selected upper Rhône tributaries with their typical characteristics

Sites	**Lizerne**	**Grande eau**
Tributary upslope contributing area (km^2)	64.8	132
Main stem upslope contributing area (km^2)	3401	5088
Basin area ratio	1.89%	2.59%
Tributary width (m)	6.5	16.5
Main stem width upstream of junction (m)	46	58
Width ratio	0.15	0.28
Junction angle (º)	80	70
Tributary Froude number	0.32	0.05
Bed slope of the tributaries upstream of the confluence (%)	~0.5	0.5-1
Main stem slope upstream of the confluence (%)	2	2.2
Tributary slope (°)	33.1	26.6
Rhône discharge during measurement (m^3s^{-1})	182	300
Tributary discharge during measurement (m^3s^{-1})	4	8.13
Discharge ratio during measurement	0.022	0.027
Momentum ratio (Mr) during measurement	0.018	0.022

Figure 1: Bed elevations, the best fit to those elevations and the water level representation

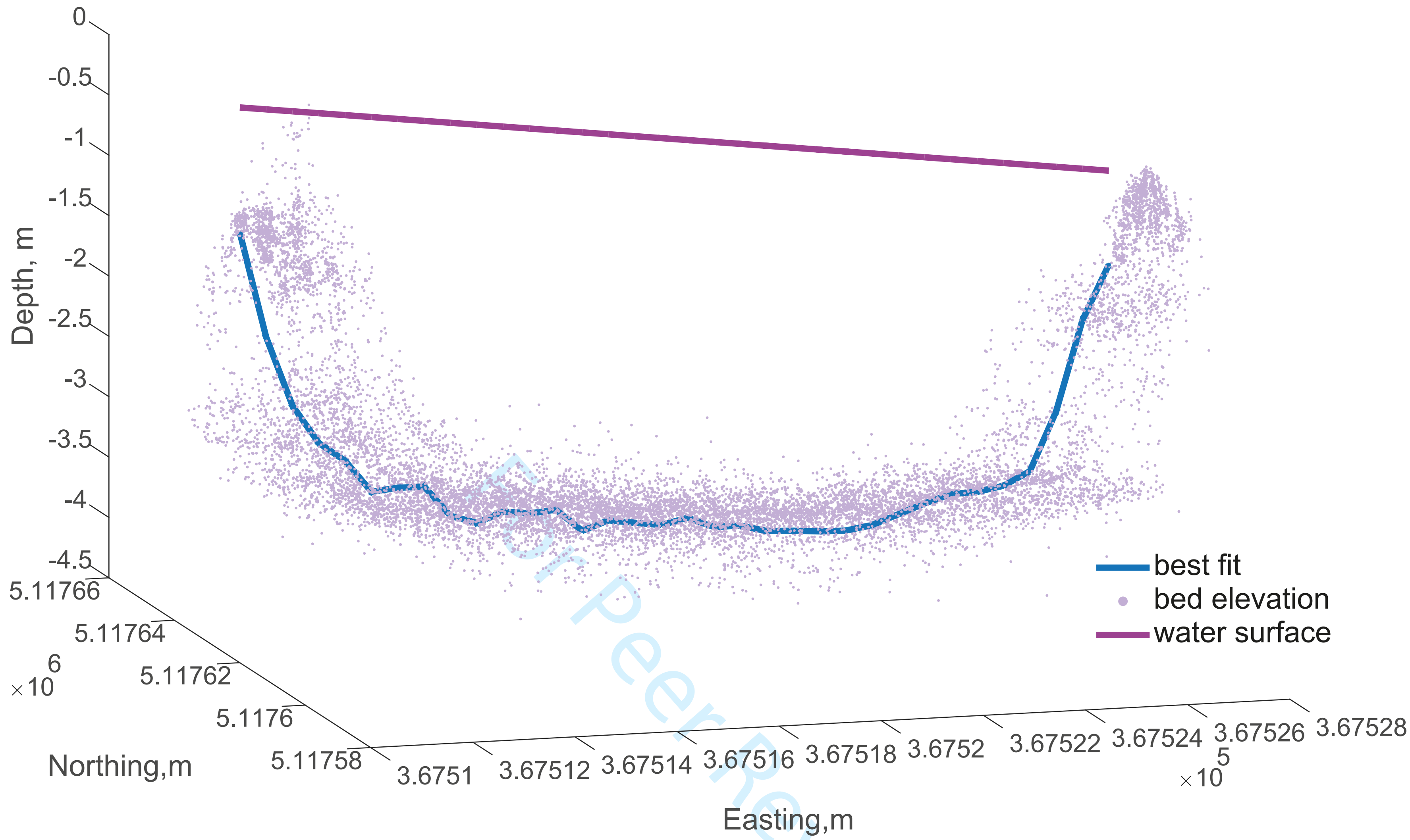

Figure 2: An example of beam velocity positioning within each mesh cell, using method A, Dots show beam velocities and color is an automatic Matlab function to distinguish between different cells

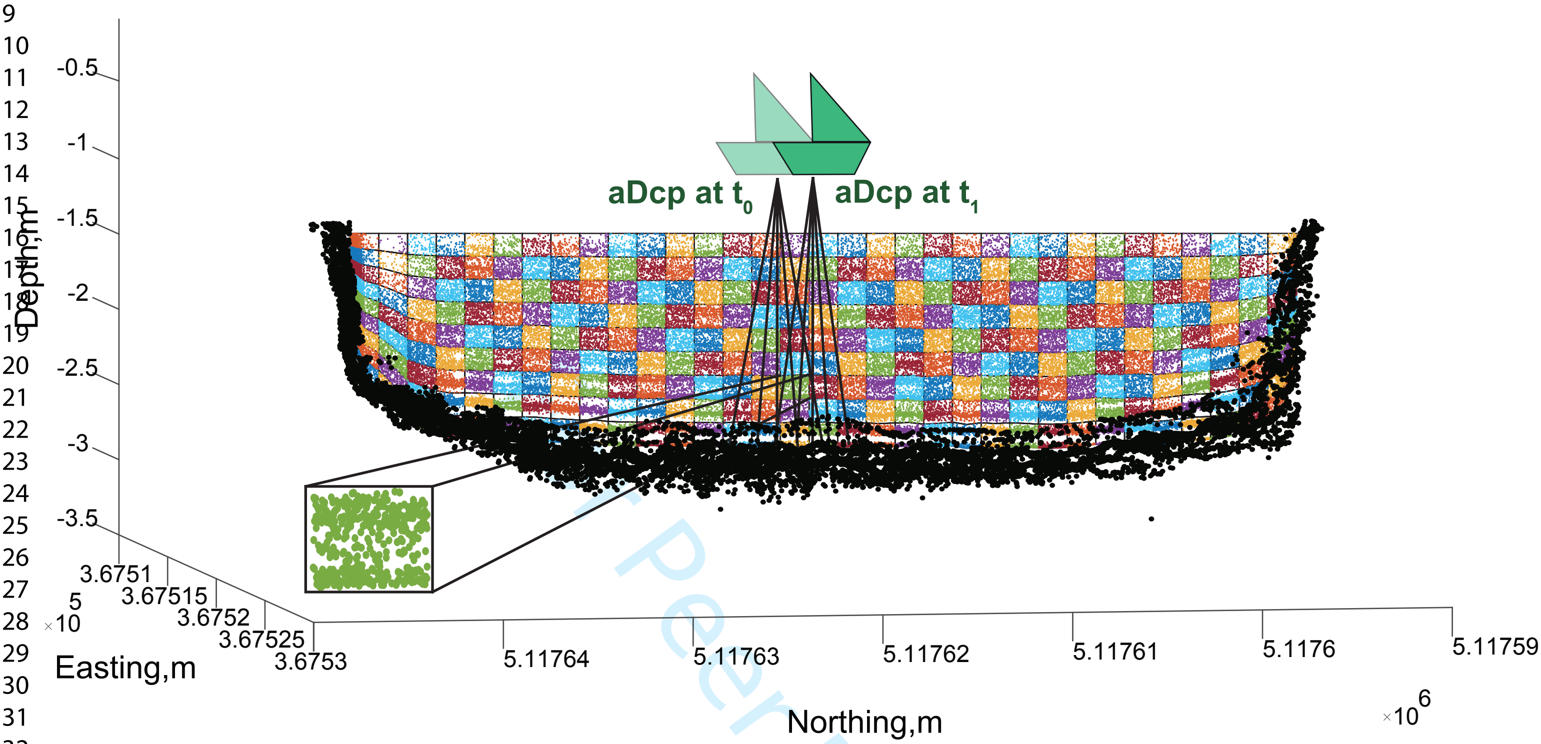

Figure 3: Tracks navigated by SonTek aDcp moving boat system at a) Lizerne-Rhône confluence near Vétroz, at 07/07/2017 and b) Grande Eau-Rhône confluence near Aigle at 23/05/2018. The repeated transect data assessed in this paper are from cross-section 6 at the Lizerne-Rhône confluence and cross-section 3 at the Grande Eau-Rhône confluence and c) Rope-Pulley system

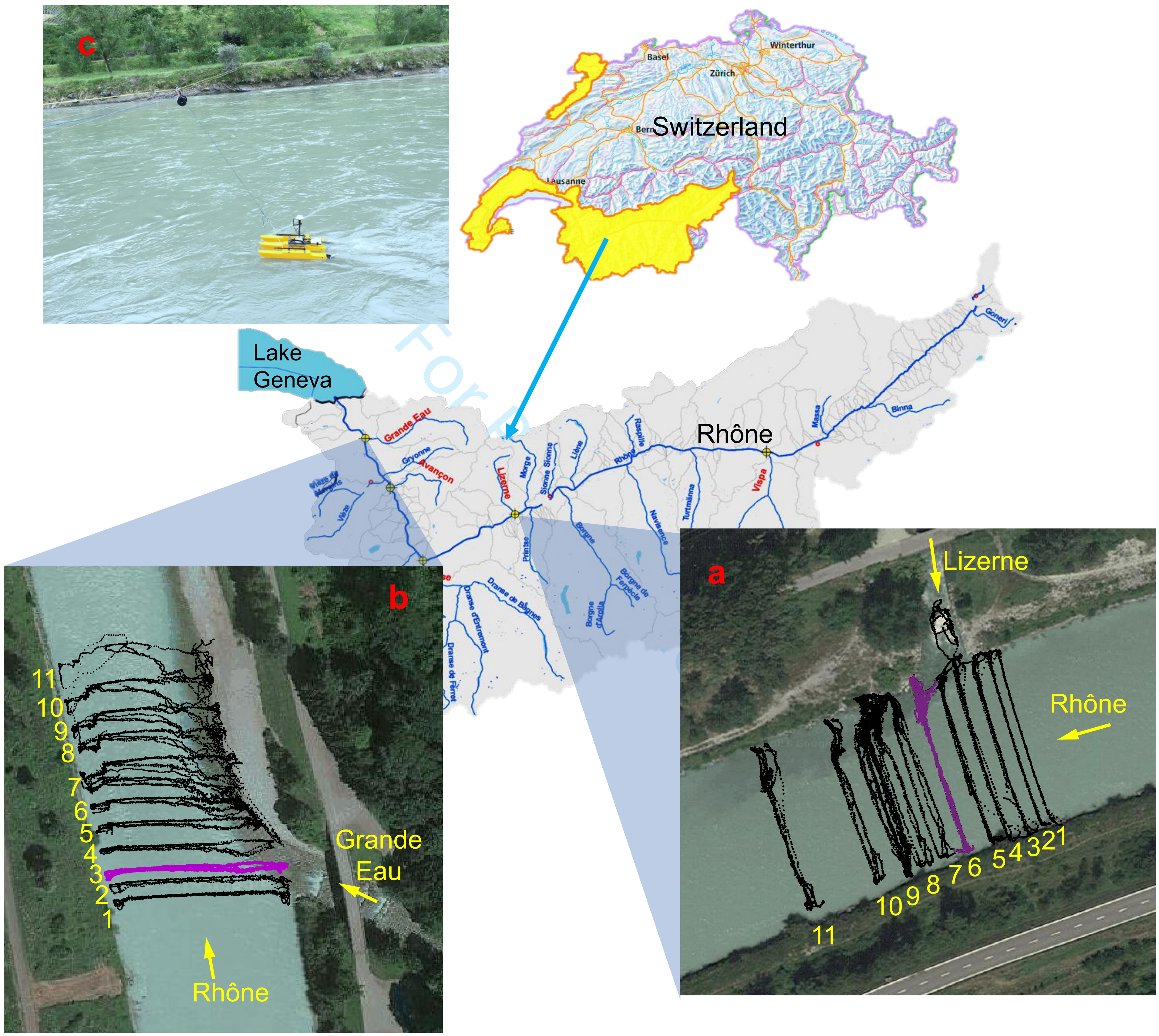

Figure 4: Primary and secondary velocities estimated for the Lizerne-Rhône Method A (a) and Method B (b) and the Grande Eau-Rhône Method A (c) and Method B (d); view is looking downstream.

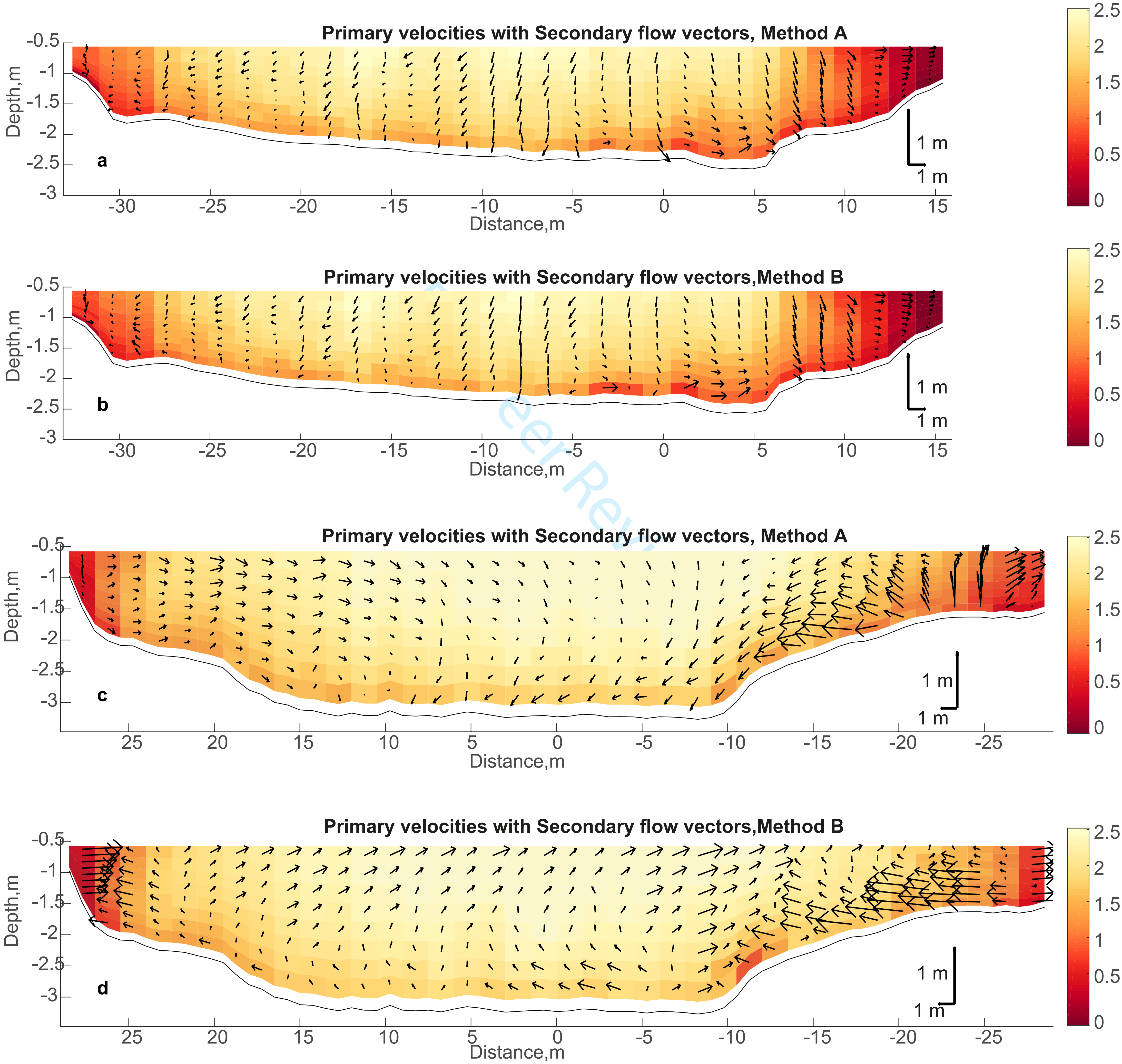

Figure 5: Differences between magnitude of primary and secondary velocities (m/s) between methods A and B (a and b) and the percentages of their difference (m/s) (c and d), at the Lizerne-Rhône confluence, for cross-section 9; view is looking downstream.

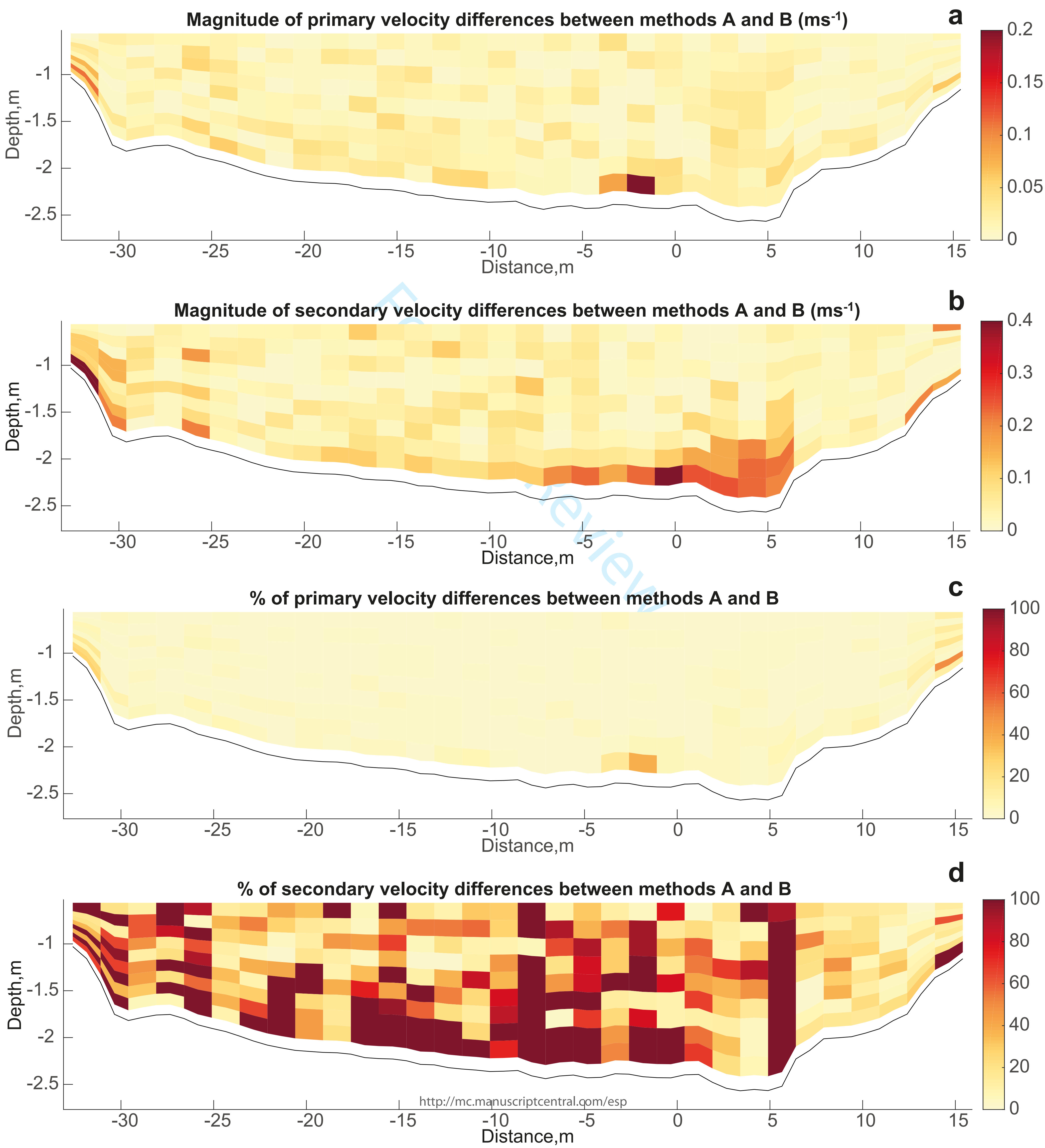

Figure 6: Relative differences in a) primary velocity magnitudes and b) secondary velocity magnitudes, between methods A and B, at the Lizerne-Rhône confluence, for cross-section 6

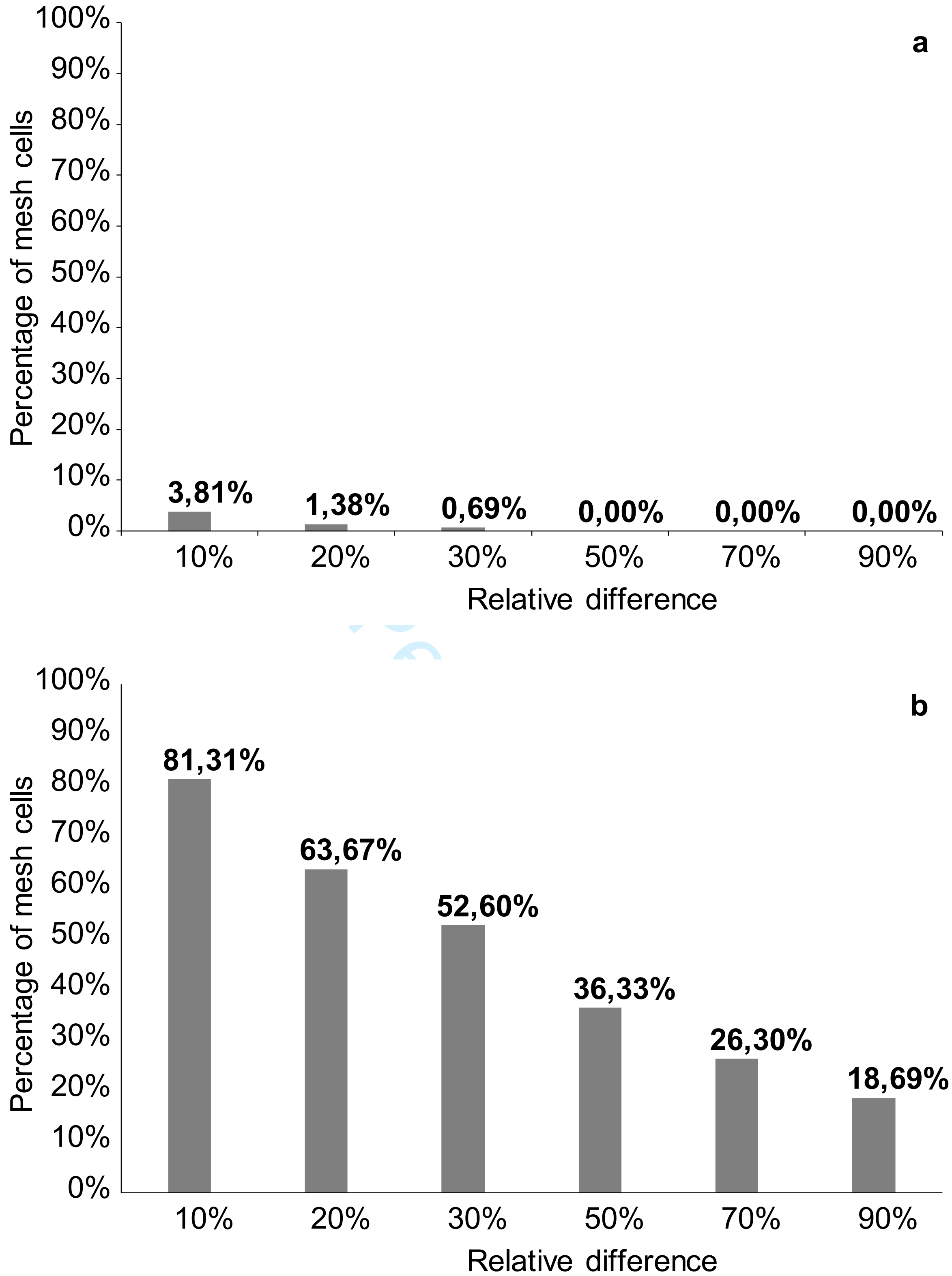

Figure 7: Differences between magnitude of primary and secondary velocities (ms^{-1}) between methods A and B (a and b) and the percentages of their difference (c and d), at the Grande Eau-Rhône confluence, for cross-section 3. view is looking downstream.

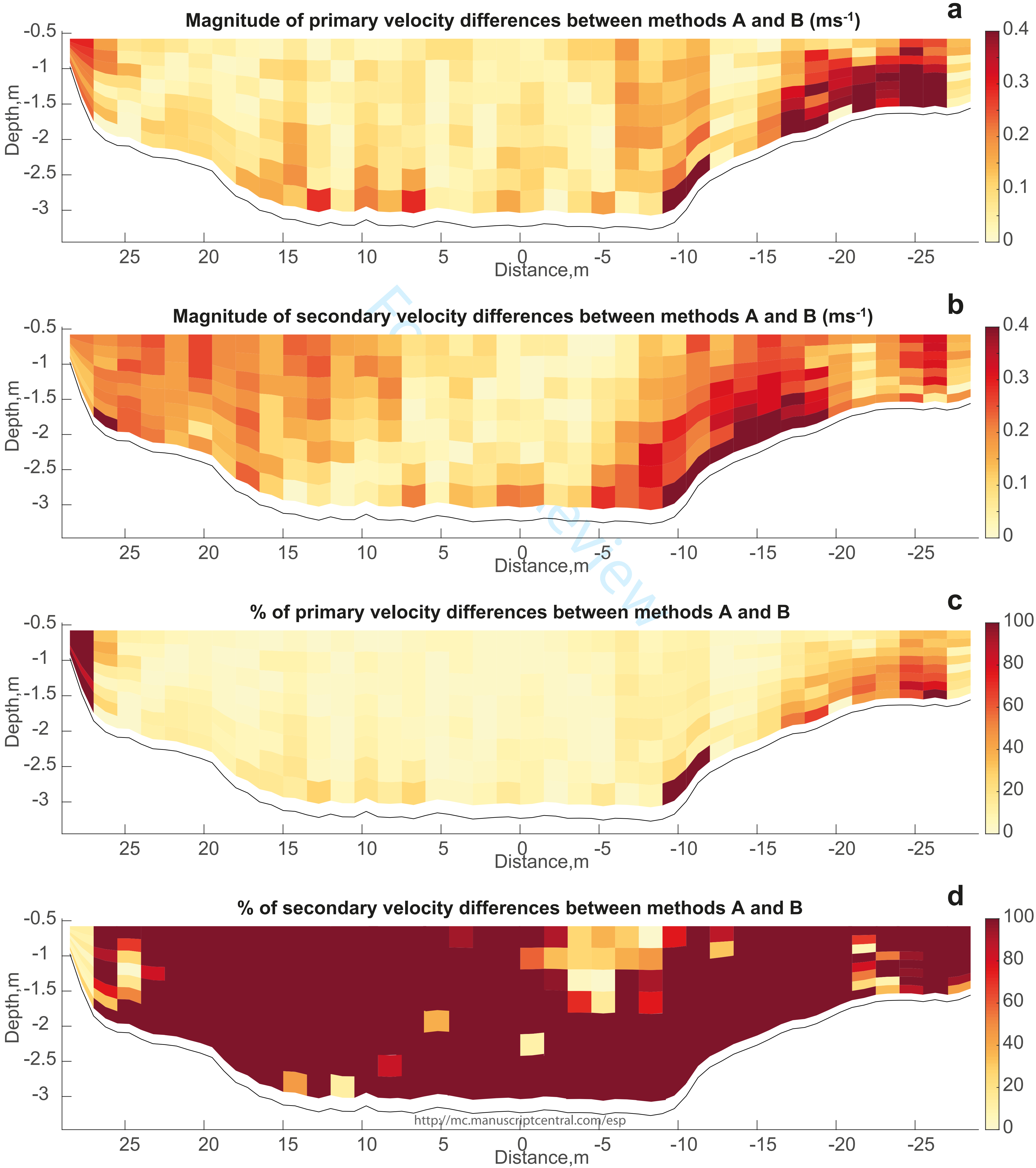

Figure 8: Relative differences in a) primary velocity magnitudes and b) secondary velocity magnitudes, between methods A and B, at the Grande Eau-Rhône confluence, for cross-section 3, view is looking downstream.

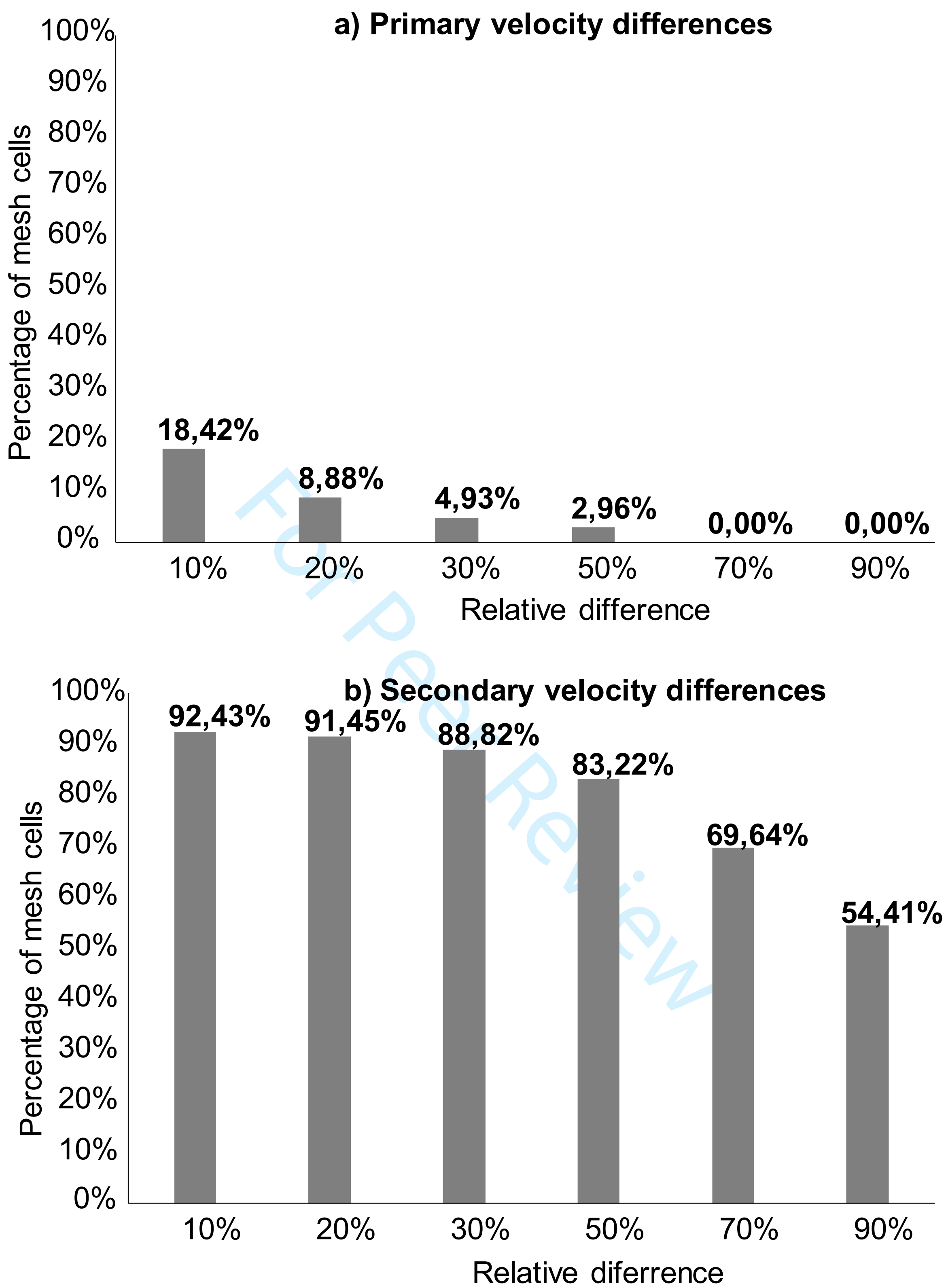

Figure 9: Lateral velocity gradients (s^{-1}) (a, c) and differences in the secondary velocity magnitudes (ms^{-1}) (b, d) at the Lizerne-Rhône cross-section 6 (a,b) and the Grande Eau-Rhône cross-section 3 (c,d) confluences. view is looking downstream.

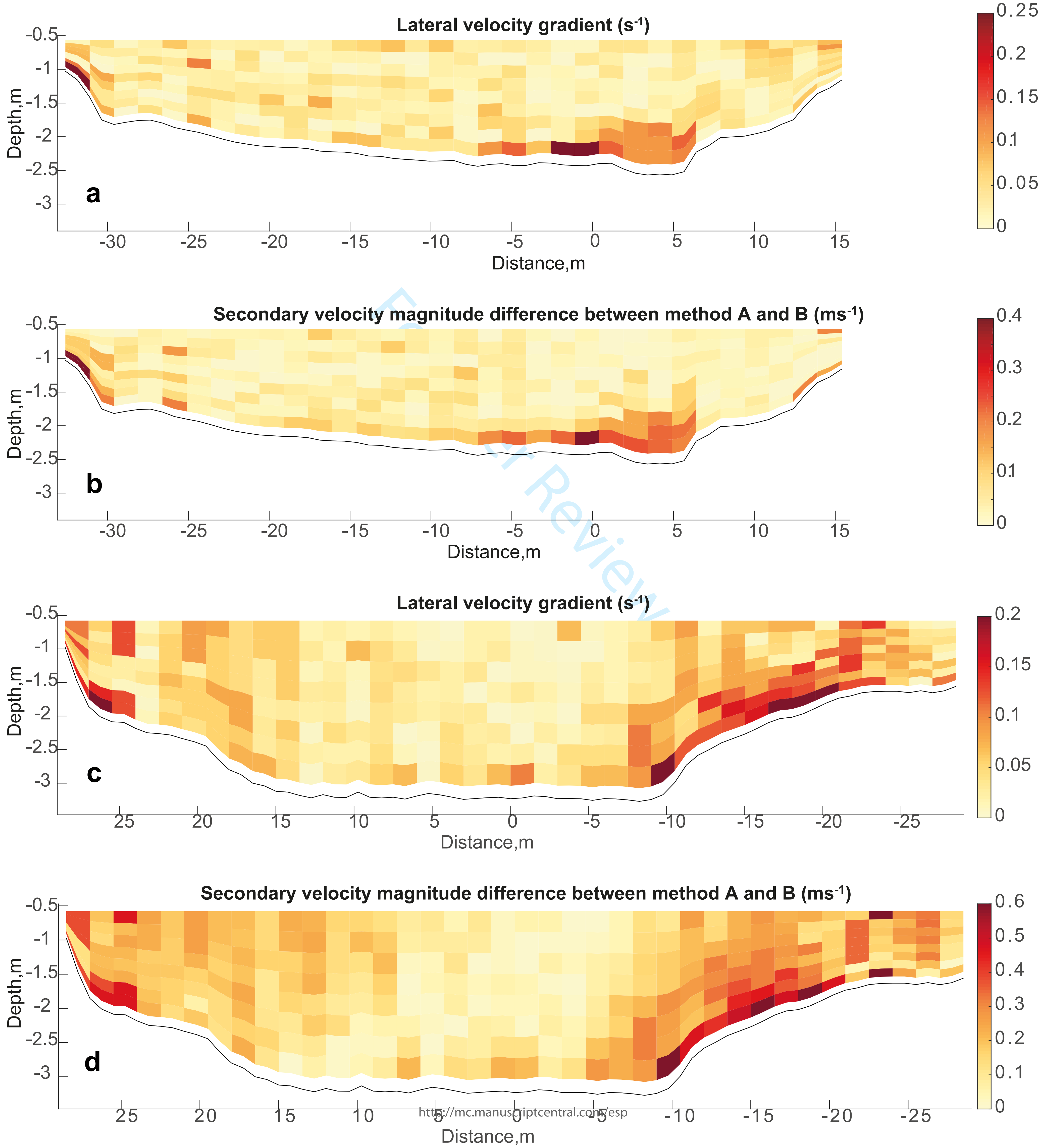

Figure 10: Water column and mesh cells for cross section 9 in Figure 3a at the Lizerne-Rhône confluence, in which standard deviation of the esti-mated velocities have been calculated. view is looking downstream.

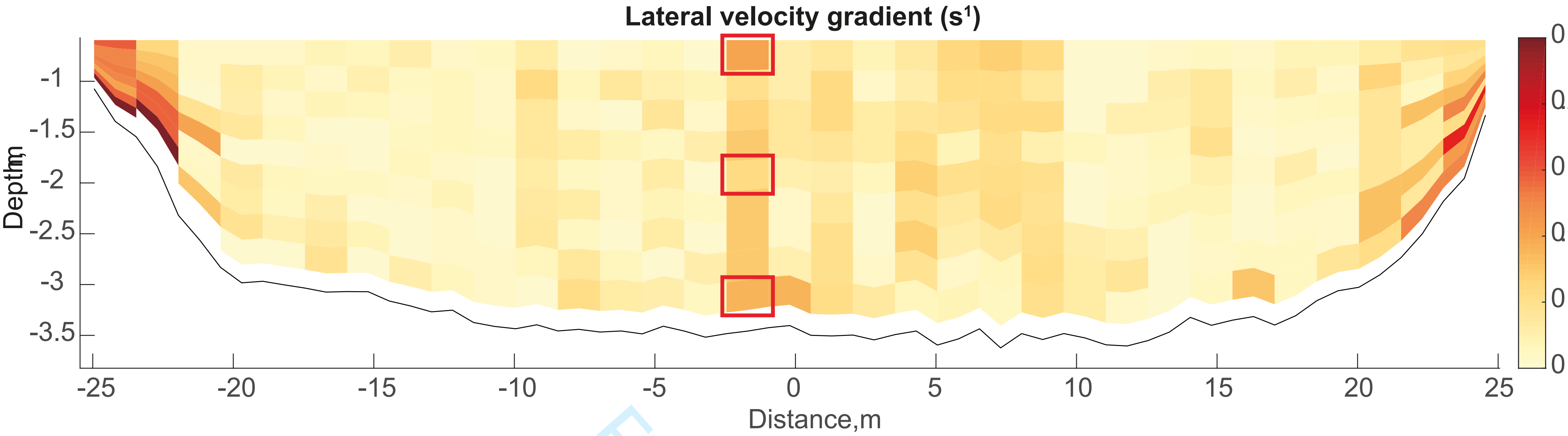

Figure 11: Standard deviation of the velocity estimated using methods A and B for 16 repeats at the Lizerne-Rhône confluence cross-section 9

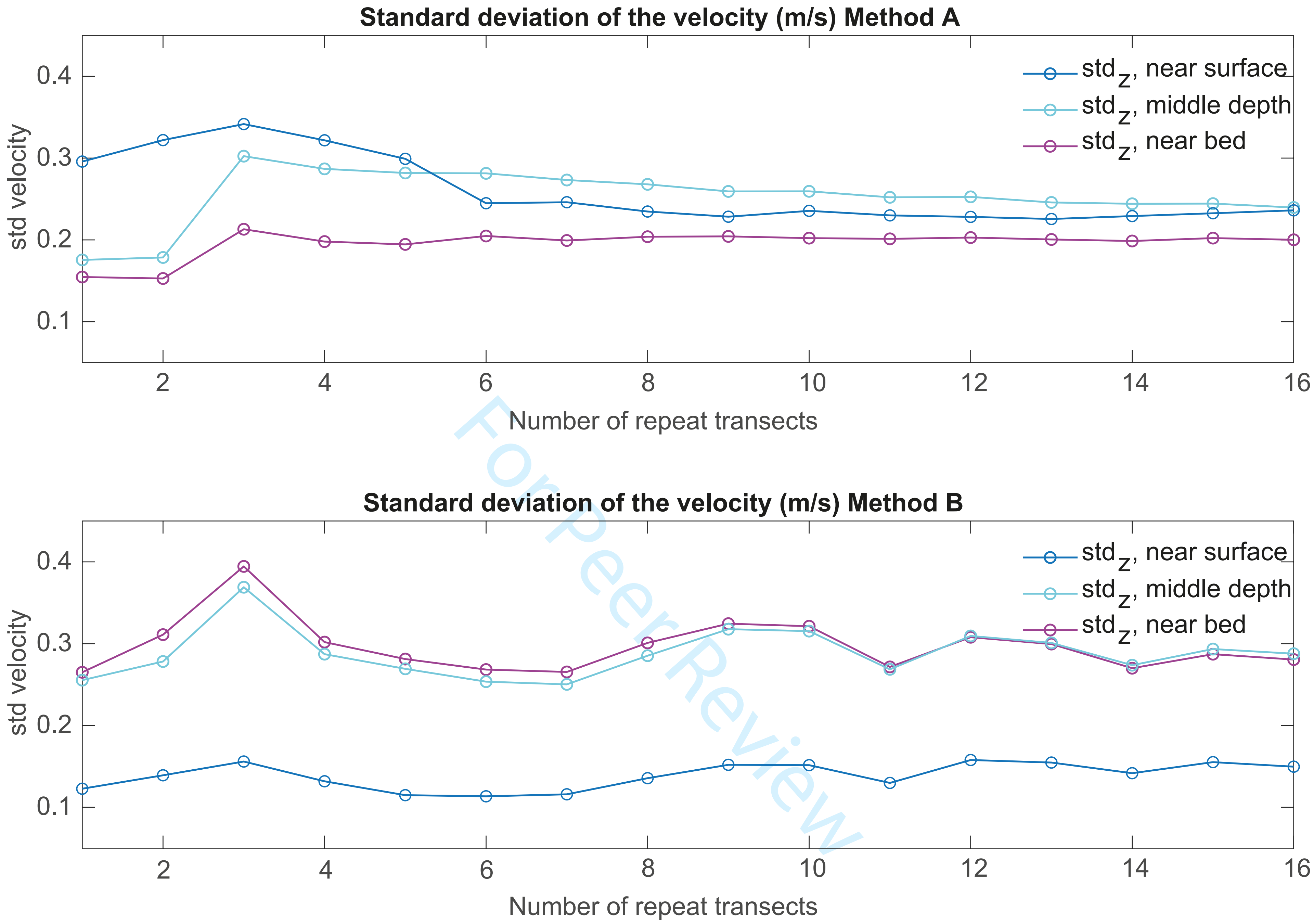

Figure 12: Error distributions related to GPS for a) Lizerne-Rhône confluence (cross-section 6) and c) Grande Eau- Rhône confluence (cross-section 3), and sensors accuracies for b) Lizerne-Rhône confluence (cross-section 6) and d) Grande Eau-Rhône confluence (cross-section 3), in estimating the secondary velocities using method A. view is looking downstream.

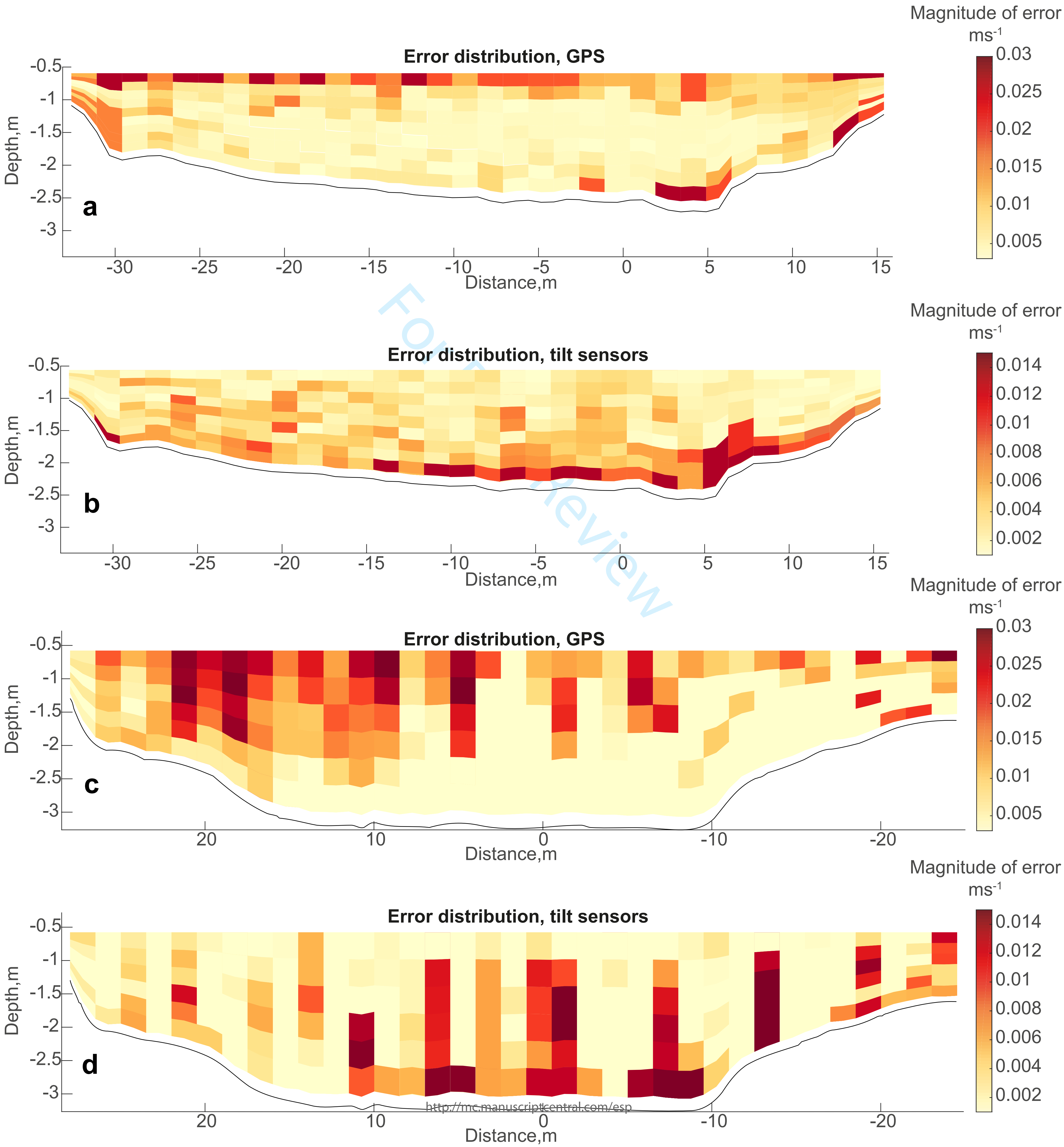

Figure 13: Maximum inhomogeneity allowance (m) using method B for a) Lizerne-Rhône confluence at cross-section 6 and b) Grande Eau-Rhône confluence at cross-section 3. view is looking downstream.

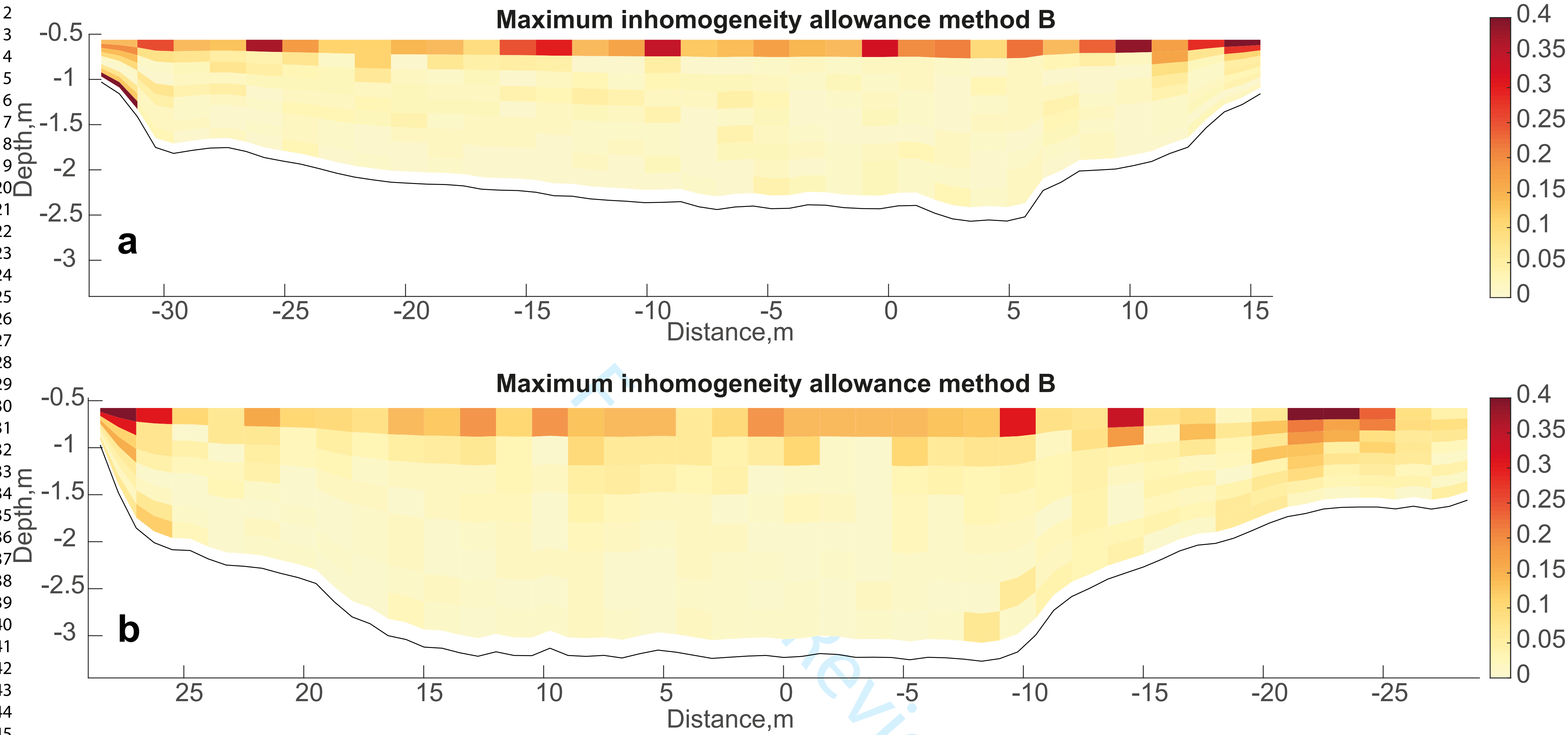

Figure 14: Primary velocities (contours) with secondary velocity vectors estimated using method A and B at cross sections 4,5 and 7 in Figure 3a at the Lizerne-Rhône confluence. view is looking downstream.

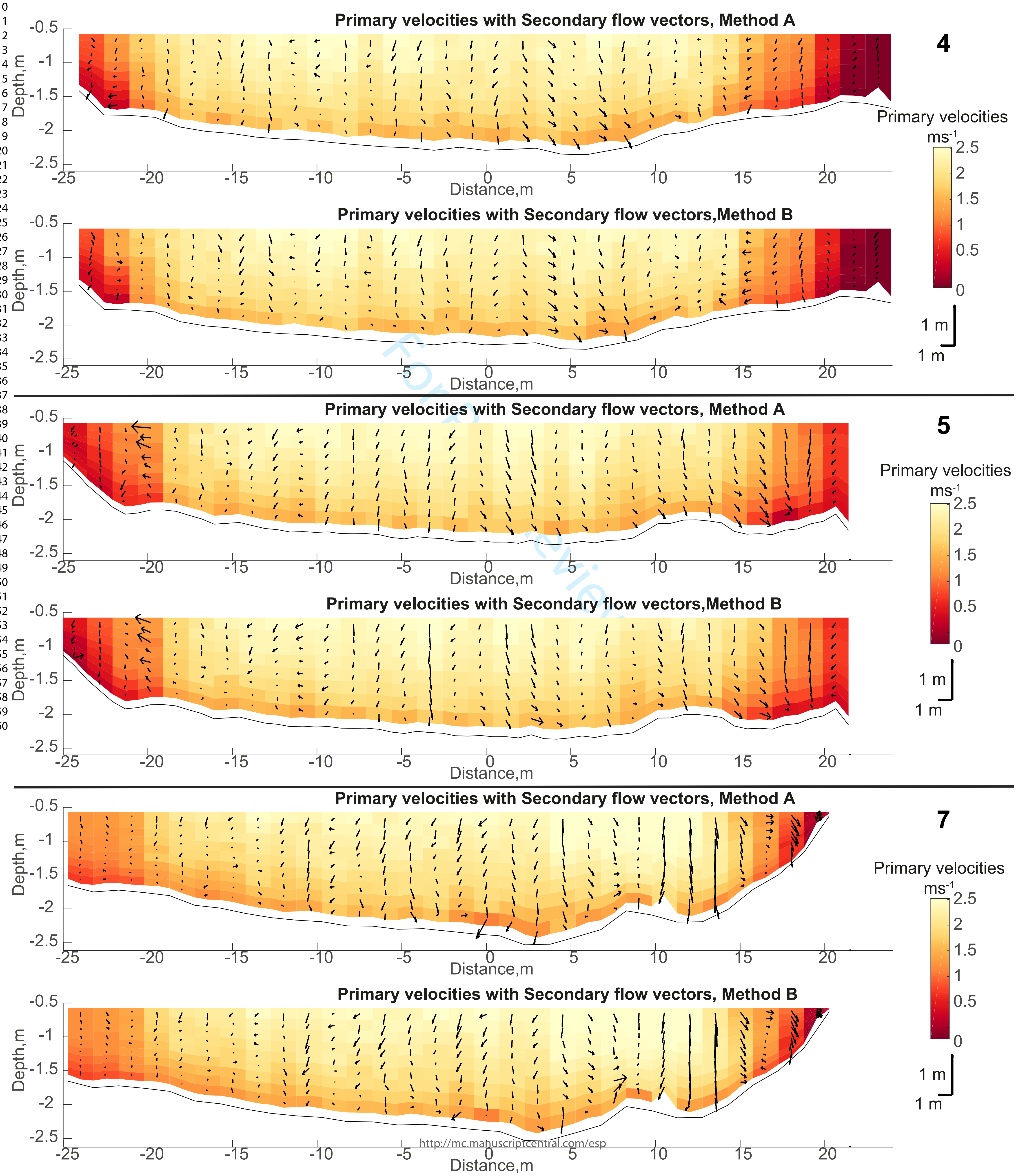

Figure 15: Primary velocities (contours) with secondary velocity vectors estimated using method A and B at cross sections 4,6 and 8 in Figure 3b at the Grande Eau-Rhône confluence. view is looking downstream.

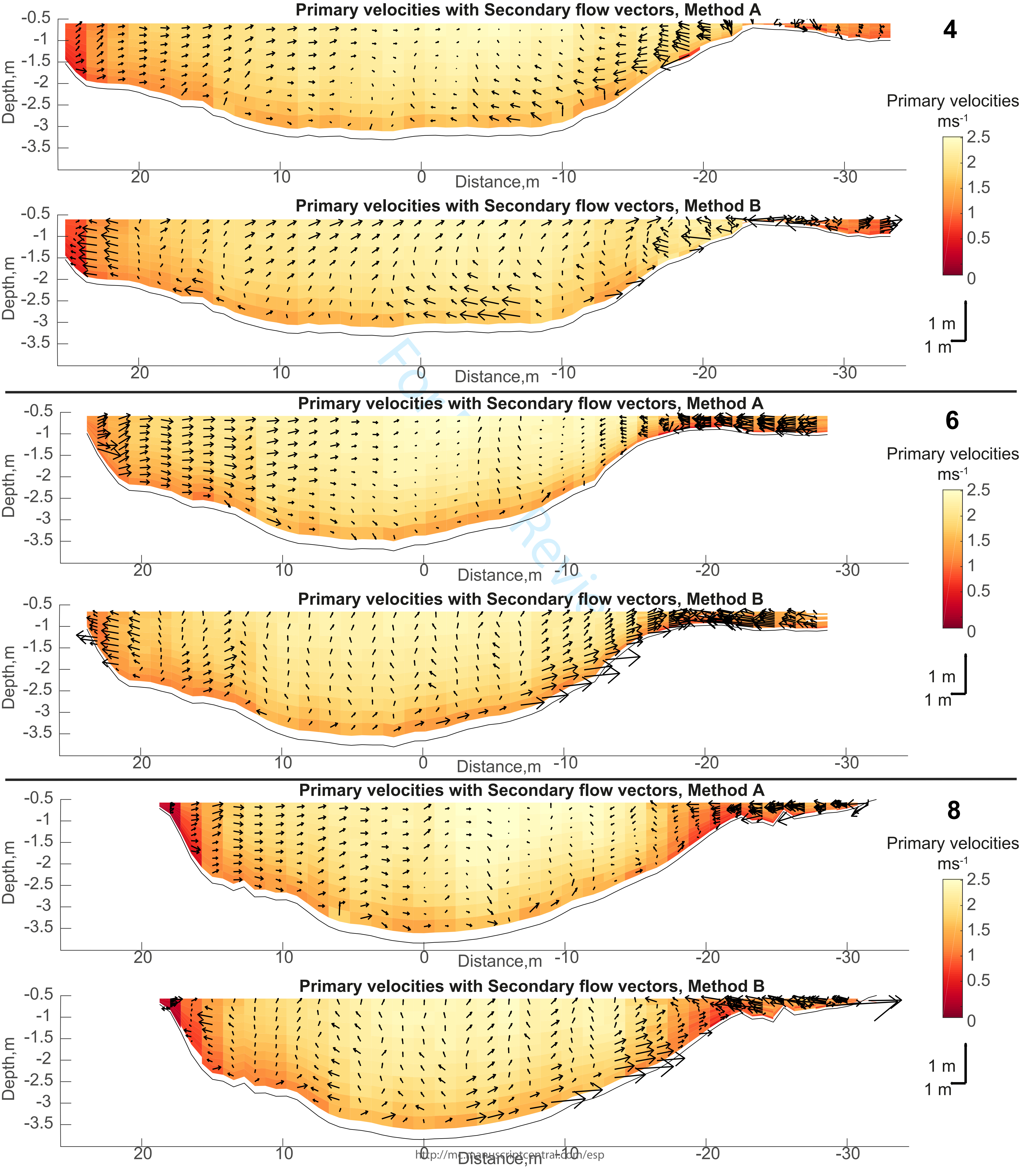

Figure 16: Relationship between lateral velocity gradient, depth and relative differences in secondary velocities for a) the Lizerne-Rhône confluence at cross-section 6 and b) the Grande Eau-Rhône confluence at cross-section 3

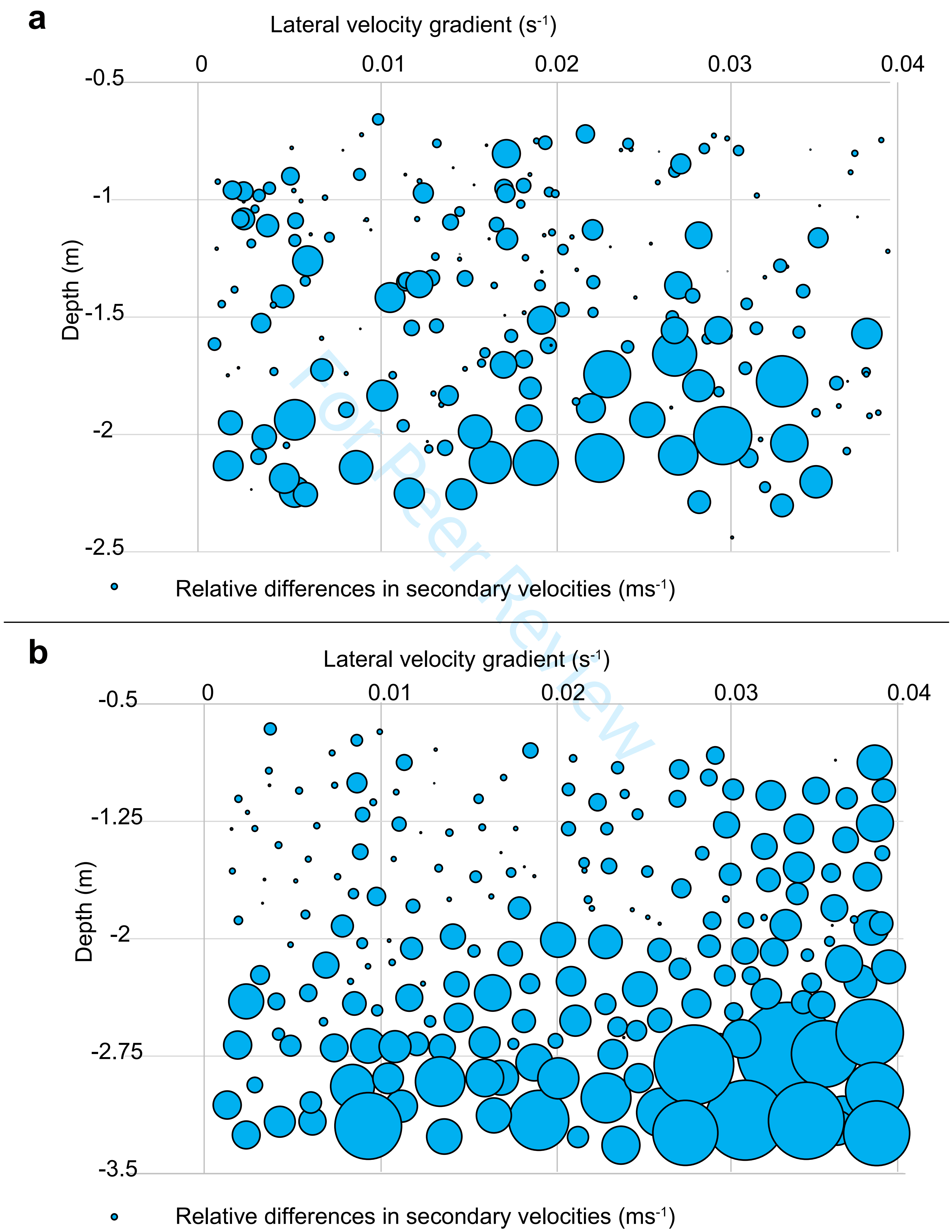

"For the ESPL special issue: Measuring and numerical modelling of hydro-morphological processes in open-water"

Evaluation of aDcp processing options for secondary flow identification at river junctions

Gelare Moradi [1], Bart Vermeulen[3], Colin D. Rennie [2], Romain Cardot [1], Stuart N. Lane[1]

1: University of Lausanne - Institute of Earth Surface Dynamics (UNIL - IDYST)

Université de Lausanne - IDYST Quartier Mouline - Bâtiment Géopolis - Switzerland

2: Civil Engineering Department, University of Ottawa

3: Water Engineering and Management Department, University of Twente, the Netherlands

Abstract

Secondary circulation in river confluences results in a spatial and temporal variation of fluid motion and a relatively high level of morphodynamic change. Acoustic Doppler current profiler (aDcp) vessel-mounted flow measurements are now commonly used to quantify such circulation in shallow water fluvial environments. It is well established that such quantification using vessel-mounted aDcps requires repeated survey of the same cross-section. However, less attention has been given to how to process these data. Most aDcp data processing techniques make the assumption of homogeneity between the measured radial components of velocity. As acoustic beams diverge with distance from the aDcp probe, the volume of the flow that must be assumed to be homogeneous between the beams increases. In the presence of secondary circulation cells, and where there are strong rates of shear in the flow, the homogeneity assumption may not apply,

especially deeper in the water column and close to the bed. To reduce dependence on this assumption, we apply a newly-established method to aDcp data obtained for two medium-sized (~60-80 m wide) gravel-bed river confluences and compare the results with those from more conventional data processing approaches. The comparsion confirms that in the presence of strong shear our method produces different results to more conventional approaches. In the absence of a third set of fully independent data, we cannot demonstrate conclusively which method is best, but our method involves less averaging and so in the presence of strong shear is likely to be more reliable. We conclude that it is wise to apply both our method and more conventional methods to identify where data analysis might be impacted upon by strong shear and where inferences of secondary circulation may need to be made more cautiously.

Keywords

Acoustic Doppler current profiler

Secondary circulation

River confluences

River junctions

Introduction

Acoustic Doppler current profilers (aDcps) are now used widely to measure river flow in three-dimensions, notably for the quantification of secondary flows. Applications have been made to river bedforms (e.g., Parsons et al., 2005; Kostaschuk et al., 2009; Shugar et al., 2010), bends (e.g., Dinehart and Burau, 2005; Kasvi et al., 2013; Vermeulen et al., 2014a, 2015; Engel and Rhoads, 2016; Knox and Latrubesse, 2016; Kasvi et al., 2017; Lotsari et al., 2017; Parsapour-Moghaddam and Rennie, 2018), junctions (e.g., Parsons et al., 2007; Lane et al., 2008; Szupiany et al., 2009; Riley and Rhoads, 2012; Riley et al., 2015; Gualtieri et al., 2017), bifurcations (e.g., Parsons et al., 2007; Szupiany et al., 2012), canyons (e.g., Alvarez et al., 2017; Tomas et al., 2018; Venditti et al., 2014), deltas (e.g., Czuba et al., 2011) and gravity currents (e.g., Garcia et al., 2007; Garcia et al., 2012). Research has also shown the need to make repeat section measurements (e.g., Szupiany et al., 2007; Jackson et al., 2008) and also to process these data carefully, (Muste et al., 2004; Rennie and Church 2010; Tsubaki et al., 2012; Parsons et al., 2013; Petrie et al., 2013). Such processing must take into account positioning (Rennie and Rainville, 2006) and orientation (Zhao et al., 2014) errors, and the treatment of repeat section measurements (e.g., Szupiany et al., 2007; Jackson et al., 2008).

This paper is concerned with recent observations regarding the inference of secondary flows from aDcp data and concerns regarding the assumption that flow is homogenous in the fluid volumes defined by the acoustic beams emitted from an aDcp and used to calculate any one point estimate (Vermeulen et al., 2014b). Acoustic beams are reflected by suspended particles, which, if moving, cause a Doppler shift in beam frequency, which is then detected at the sensor. This shift is directional so each beam measures the radial velocity, which is the velocity of particle motion parallel to the acoustic path. This can be assumed to be the flow velocity if the particle motion is identical to fluid motion. In order to resolve flow in more than one direction, aDcps require at least three acoustic beams to estimate three Cartesian components of velocity. The radial velocities originating from the beams are traditionally analyzed for a single measurement cycle at a single depth at a time (Vermeulen et al., 2014b). The velocity then applies to the volume of fluid defined by the beams at each depth. Flow within this volume is assumed to be homogeneous. However, as the beams spread from the sensor, depth bins increase in horizontal size (Rennie et al., 2002). This means that: (1) bins further from the sensor are likely to produce less reliable velocities because the bin size is greater and the flow within bins is more likely to be heterogeneous (Gunawan et al., 2011); and (2), even in smaller bins, velocities may be less reliable in zones of strong shear where also the within-bin flow is less likely to be homogeneous. In a river where measurements are made throughout the flow depth, the maximum shear may be close to the bed, where the beam divergence may also be greatest.

One solution to this problem accounts for first order shear within the flow volume (e.g. Marsden and Ingram, 2004) through a Taylor expansion of the coordinate transform used to determine the Cartesian velocity components. Under this solution, flow is allowed to vary linearly within the bin, but the bin's volume becomes potentially larger with distance from the sensor. Vermeulen et al. (2014b) developed and tested a second solution. As explained in detail below, multiple radial (beam) velocity measurements within a single bin are put through a Cartesian transform to obtain a localized within-bin three-dimensional velocity. This method strongly reduces the volume over which homogeneity should be assumed and Vermeulen et al. (2014b) found that this significantly impacted interpretations of secondary velocities in the presence of strong shear. In this paper, we seek to quantify the effects of this method for the measurement of secondary flow in two medium-sized river junctions (c. 60-80 m post-junction channel width). River junctions are associated with very strong shear (e.g. Best and Roy, 1991; Biron et al., 1993, 1996a, 1996b; Sukhodolov and Rhoads, 2001; Rhoads and Sukhodolov, 2004, 2008; Konsoer and Rhoads, 2014; Sukhodolov et al., 2017), as well as well-developed secondary circulation (e.g. Ashmore et al., 1992; Rhoads and Kenworthy, 1995, 1998; Rhoads and Sukhodolov et al., 2001; Lane et al., 2008; Riley and Rhoads, 2012; Riley et al., 2015). Thus, understanding how to process effectively the aDcp data used to describe them is of paramount importance.

Methods for estimating Cartesian velocity components from aDcp data

In this section, we describe the two different methodological approaches used in this study to estimate Cartesian velocity components: (1) Method A, the Vermeulen et al., (2014b) method; and (2) Method B, the conventional method. Common to all methods is the assumption that data are available from repeat measurement of the same cross-section, as has been shown to be critical for obtaining reliable estimates of secondary circulation from aDcp data (Szupiany et al., 2007), particularly when single transect measurements are not close enough together.

Method A: based on Vermeulen et al., (2014b)

Application of the Vermeulen et al. (2014b) method requires mapping of radial beam velocity data onto a predefined mesh. This mesh requires both a bottom topography or bathymetric model, and an upper limit just below the water surface. As the measurements were made using several repeat transects for each cross section, the first step is to define a mean cross section for each set of individual transects (boat tracks). The second step is to define a grid mesh for this mean cross section. Third, all measured beam velocities are projected on to this cross section mesh. Finally, the beam velocities within each mesh cell are then used to resolve a Cartesian velocity for the mesh cell. Errors that influence these steps can be estimated.

The first step is estimation of the mesh extremes, both the lower boundary or bathymetry model and the upper boundary near the water surface. To generate the bathymetry model we use depth soundings collected with the aDcp. We recognize that each beam may register a different distance of the stream bed from the sounder, especially as we are dealing with bathymetrically irregular cross-sections. Specifically, for each bottom track sounding within each transect, we use the UTM coordinates obtained with a coupled differential GPS (dGPS), the range of each bottom track beam return, and the instrument tilt to estimate the bed elevation and horizontal position of each beam impingement point on the bed. These bed positions are combined together to identify an initial mean transect. Provided a point is within a certain distance from the initial mean cross-section, LOWESS interpolation (Appendix A) is applied, which has the effect of defining a bathymetric model that gives most weight to points that appear to be closer to the cross-section. It is important to note that this mean transect is not necessarily orthogonal to the primary flow direction and so will not yield true primary and secondary flow estimates without further correction. We address this below.

Once the initial bathymetric model is defined, we estimate a unique vector using the initial mean transect; that is the principal direction of the scatter cloud of all x and y UTM positions at the bed. This unique vector points in the direction of the largest eigenvector of the covariance matrix of all UTM positions (*t*). We then calculate the mean UTM position

(p_{mean}) for each set of individual transects and the difference between each measured beam position (p_b) and the mean position. The dot product of these obtained values and the unique vector is then used to define the projection of each UTM position in the direction of the unique vector. To identify the final mean cross section, we sum up all individual projected vectors and obtain the best fit to all available data (Figure 1).

To define the upper boundary of the mesh, we estimate the elevation of the water surface. As there is a blanking distance at the surface of the water during the measurement, we then remove this blanking distance, taken as 0.30 m. Thus, the mesh has also a blanking distance and the upper part of the cross-section is, strictly, the upper limit of available data, not the water surface.

“Figure1”

The second step uses the defined bathymetric model and available velocity bins within the measured area (not influenced by side lobes, and below the blanking distance) to define a cross-section mesh. The side-lobe interference is caused by the striking of the channel bed by side-lobe energy from each of the acoustic beams. This side-lobe energy has strong reflections from the bed, which result in echoes that overwhelm the signal from scatters near the bed. The thickness of the side-lobe layer is typically 6-7% of the measured depth (Morlock, 1996).

To generate the mesh, the cross section is initially subdivided into vertical slices with equal widths (Δn). For each slice, the simplest definition of mesh cell thicknesses (Δz) divides each vertical equally. These verticals are converted to non-dimensional σ coordinates using following equation:

$$\sigma = 1 - \left(\frac{p_v.\boldsymbol{k} - \eta}{p_b.\boldsymbol{k} - \eta}\right) \quad \text{(Vermeulen et al. 2014b)} \qquad (1)$$

where p_v stands for velocity measurement positions (m), p_b is the corresponding bed position (m) that is found using velocity measurement horizontal positions and applying the bathymetric model, $\boldsymbol{k}$ is the upward pointing unit vector and η are the water surface fluctuations around the mean water level at which z=0.

However, because of beam spreading and differences in the distance of the sounder from the bed, which varies with position of the sounder, this tends to produce a highly heterogeneous number of measurements in each cell within the mesh. The alternative, adopted here, is to allow mesh cell thickness to vary through the water column such that there is a roughly equal number of beam velocities contributing to each mesh cell (see Figure 2 for a typical distribution).

As the river bed form is varying, to follow its shape, each mesh cell is considered to be a cuboid with 6 edges, two on the left side, two in the middle and two on the right side. To define these edges, the first step is to define the middle point of each mesh cell. Once defined, by calculating the slope for each half part of the mesh cell, edges can be obtained. The mesh cell faces are then calculated on the basis of adjacent verticals and the mesh cell upper and lower boundaries.

To identify the beams that contribute to each mesh cell, an index for each beam velocity is defined, which shows its associated mesh cell, using the projection of each radial velocity onto the estimated mean cross section (Figure 2).

“Figure 2”

In the third step, the radial velocities for each beam (**b**) that contribute to each mesh cell (the N beam velocities) have to be transformed into Cartesian velocities (v_x, v_y and v_z) using:

$$\begin{pmatrix} b_1 \\ \vdots \\ b_N \end{pmatrix} = \begin{pmatrix} q_1 \\ \vdots \\ q_N \end{pmatrix} . \begin{pmatrix} v_x \\ v_y \\ v_z \end{pmatrix} \leftrightarrow \mathbf{b} = Q.\mathbf{u} \qquad (2)$$

where **q** is a unit vector which describes the direction of the acoustic beam.

To obtain the raw beam velocities, we use matrix transformations obtained from the raw data to transform measured velocities in XYZ coordinates into beam velocities. The Vermeulen et al., (2014b) method includes in the transformations an explicit treatment of the random errors due to internal and external factors and the bias (systematic errors) caused by the measurement system and the nature of river flow (Tsubaki et al., 2012). Random errors include those that come from sampling a time-varying flow in the presence of strong gradients and represent a form of aliasing. By adding a combined term of errors ε, (2) becomes:

$$\mathbf{b} = Q\mathbf{u} + \varepsilon \qquad (3)$$

A least squares solution is fitted to (3) that minimizes the sum of the square of the errors. The optimal estimation ($\hat{\mathbf{u}}$) for ($\mathbf{u}$) is then given by the normal equation:

$$\hat{\mathbf{u}} = Q^{+}\mathbf{b} + \varepsilon \qquad (4)$$

where Q^+ can be defined as:

$$Q^{+} = (Q^T Q)^{-1} Q^T \qquad (5)$$

To solve three Cartesian velocity components, we need at least three equations. Each beam measurement in a mesh cell adds an equation. Where enough beam velocities are collected in a mesh cell and the equations are different from each other (beam velocities are measured from different directions), the velocity can be estimated. To check whether this is the case, the matrix describing the system of equations can be analyzed. In the processing we use the rank which indicates how many unknowns can be solved from the system of equations. When the rank is three, the three Cartesian velocities can be solved. Where the rank of the matrix is one or two, the system cannot be solved. Where the system of equations is overdetermined, the obtained solution is a matrix with more equations (rows) than unknowns (columns). The velocity can be solved using the generalized inverse of the matrix and in such a way that the sum of squared errors is minimized. As this combined term of errors also contains information about the turbulence and accuracy of the measurements, we can obtain the covariance matrix of the velocity components:

$$\hat{\varepsilon} = \mathbf{b} - Q\hat{\mathbf{u}} \tag{6}$$

$$\mathrm{var}(\hat{\mathbf{u}}) = \frac{\hat{\varepsilon}^T\hat{\varepsilon}(Q^TQ)^{-1}}{N - 3} \tag{7}$$

and the variance of the velocity across the section can be then estimated as:

$$\mathrm{var}(\mathbf{u}) = \frac{\mathrm{var}(\hat{\mathbf{u}})}{N}$$

(8)

Method B: the standard aDcp method

As the Doppler shift is directional, it can only measure radial velocities. With the standard method, to determine Cartesian velocity components, radial velocities then have to be resolved into three orthogonal velocity vectors. To do so, at least three beam velocities pointed in known directions are required. Also, because the beams are measuring different water profiles along their individual slant ranges, the assumption of horizontal homogeneity must be taken into account. Hence, in the standard method, the three dimensional velocity for each depth bin for each ping can be solved for a typical four-beam system using the following equations (Mueller and Wagner, 2009):

$$V_x = \frac{(b_3 - b_1)}{\sqrt{2}\sin\theta} \tag{9}$$

$$V_y = \frac{(b_4 - b_2)}{\sqrt{2}\sin\theta} \tag{10}$$

$$V_z = \frac{-(b_1 + b_3)}{(2\cos\theta)} = \frac{-(b_2 + b_4)}{(2\cos\theta)}$$

(11)

where V_y is the cross stream velocity assuming beam 3 is pointed upstream, V_x is the streamwise velocity, V_z is the vertical velocity, b_1, b_2, b_3 and b_4 are the radial velocities measured in beams 1,2,3 and 4 respectively and θ is the tilt angle of the beams referenced to vertical. These data should then be corrected for pitch and roll angles, obtained from the internal inclinometer and the heading angle from the internal compass. Velocity outputs are already corrected for ship velocities.

To compare results obtained using Method B with those of Method A, we use the same mean cross section built for Method A, as well as the same bathymetric model and the same mesh. Each measured velocity vector is assigned to the appropriate mesh cell by projecting its 3D position (horizontal position and depth) onto the mean cross section

239 mesh. We then average x, y, and z components of all velocities measured within a mesh
240 cell to obtain the mean velocity vector for the mesh cell.

241 **Methodology**

242 This paper is motivated by the need to acquire three-dimensional data from junctions of
243 tributaries with a main river stem, here the River Rhône, western Switzerland, and so the
244 need to identify methods for reliably obtaining Cartesian velocities from aDcp data. The
245 Rhône tributaries typically have very high bedload transport rates for short periods of time,
246 leading to the formation of very large tributary mouth bars downstream of their junctions
247 with the main river. These bars are maintained for weeks or months such that at lower
248 tributary flow, with negligible sediment supply, there is a legacy effect of previous high
249 momentum tributary events upon junction morphology and secondary flow formation.

250 For this paper, we used a specially-designed rope and pulley system to collect aDcp data
251 from the junction of two tributaries with the Rhône (Figure 3).

252 “Figure 3”

253 The Lizerne is a Rhône tributary of almost 20 km length that flows south-westward from
254 the western slopes of the Tête Noire (2451m) or La Fava (2612m), in the Bernese Alps.
255 This river is heavily regulated for hydropower with sediment extracted upstream of the
256 junction. As a result, there is negligible sediment supply and no evidence of point bar
257 formation. It reaches the Rhône between Ardon and Vétroz, forming a 90° junction angle
258 and it has a bed that is nearly concordant with the Rhône.

259 The Grande Eau is a second tributary of the Rhône River which has a length of 26 km and takes its source on the Vaud side of the Les Diablerets and flows into the Rhône River with a 70° confluence angle, near Aigle. The Grande Eau bed is 1.5 m higher than the Rhône such that it is markedly discordant.

263 In this section, we: (1) describe the aDcp used to collect data; (2) describe how the aDcp was deployed; and (3) outline the analytical approaches used to interpret the results from the different methods. Although the method is valid for any aDcp that has an onboard compass and potential for differential GPS positioning, as is standard with most aDcps, we use a Sontek M9 aDcp in this study.

268 ***The Sontek M9 aDcp***

269 The SonTek M9 aDcp is a nine-transducer system with three acoustic frequencies, configured as two sets of four profiling beams (3 MHz and 1 MHz transducers in Janus configurations) and one vertical beam (0.5 MHz Echo sounder) for depth measurements (SonTek YSI, 2010). It uses these two sets of four beams to provide raw radial velocity samples. These beams are equally spaced at 90º azimuth angles and are projected at an angle θ of 25 º off the vertical axis (SonTek YSI, 2000). For the standard configuration, the four beams encompass a sampling diameter of 93% of the distance from the aDcp (7% of side-lobe) (SonTek YSI, 2000).

277 The output velocities from the SonTek M9 Riversurveyor are either in Cartesian coordinates (XYZ) that are relative to sensor orientation or in Earth coordinates (ENU) for a SonTek system with compass and tilt sensors. These raw velocity data in Earth coordinates or XYZ coordinates are already corrected for the ship motion. To apply

Method A to Sontek output data, as this method is based on radial velocities, it is necessary to transform these output velocities to radial velocities. To do so, we add ship velocities to these output velocities and then apply the inverses of the instrument's matrix coordinate transformations (obtained from MATLAB files output by the SonTek data collection software RiverSurveyor). As the survey is being undertaken using a moving vessel, these radial velocities then have to be corrected again for the boat velocity. There are two key methods for doing this. The first uses the bottom tracking to measure the boat velocity relative to the river bed, under the assumption that the latter is stationary (i.e. there is no bedload transport). The second tracks the boat position using differential GPS (dGPS, e.g. Zhao et al., 2014). In this study, we corrected all raw beam velocities for ship velocities, using dGPS as we could not exclude the possibility of there being bedload transport.

To apply Method B in this study, we use the raw velocity data in Earth coordinates and we correct it for pitch and roll angles, obtained from internal inclinometer and heading angle data for the internal compass. For SonTek M9 aDcps, pitch is a y-axis rotation and roll an x-axis rotation.

Depending on the water depth and velocity, the Sontek M9 firmware changes the acoustic operating frequency and the water profiling mode on-the-fly, thus the number of sampled points in the vertical varies automatically from one profile to the next. Specifically, when the water is shallower than 0.75 m and the maximum velocity is less than 0.4 ms^{-1}, the M9 reports data acquired with a 3 MHz frequency using the pulse coherent mode to obtain a 2cm depth measurement resolution. For deeper situations, this frequency changes to 1 MHz pulse coherent pings using a 6cm aDcp cell size. If the maximum velocity is greater than 0.4 ms^{-1} then SmartPulse (i.e., broadband) mode is utilized, with the 3 MHz beams if depth is less than 5 m and the 1MHz beams if depth is greater than 5m, with the aDcp cell size optimized based on the current water depth. As a result of these on-the-fly changes, each measured profile has a different number of aDcp cells and different aDcp cell sizes. Hence, to correct the aDcp cell size variability, for both methods A and B there is the need to define a cross-sectional mesh and to project the measured velocities to this mesh. For Method A we use the beam velocity vertical positions in a non-dimensionalized coordinate system using equation 1, within the predefined mesh explained in section 2.1.

Deployment of the Sontek M9 in the river junctions

The survey work was undertaken in two junctions of the Swiss River Rhône, the Lizerne-Rhône confluence in August 2017 and the Grande Eau-Rhône confluence in May 2018, using a Sontek M9 vessel mounted aDcp and a specially-designed rope-pulley system (Figure 3c). The survey was spatial, monitoring 11 cross-sections from upstream of the junction to its downstream at the Lizerne-Rhône confluence with a Momentum ratio (Mr) of 0.018 (Figure 3a) and 11 cross-sections at the Grande Eau-Rhône confluence with a Mr of 0.022 (Figure 3b). Table 1 shows the general characteristics of these two confluences on the date of the measurements.

“Table 1”

As proposed previously by Dinehart and Burau (2005), Szupiany et al. (2007), Gunawan et al. (2011) and Vermeulen et al., (2014b) at least five repeats are required to have a robust estimation of secondary velocities. Hence, in this paper, data are processed for cross-section 6 at the Lizerne-Rhône confluence (Figure 3a), and for cross section 3 at the Grande Eau-Rhône confluence (Figure 3b). Identification of the minimum number of repeat transects necessary per cross-section was undertaken using cross-section 9 at the Lizerne-Rhône confluence (Figure 3a), which involves 16 repetitions. We noted that after application of Method A, the standard deviation of velocity stabilized with six repetitions, which is the number we adopt for this study.

Bin position error determination

Application of Method A requires estimation of the error terms in (2). The size of the sampling volume in each beam is determined by the size of the bin used. As the SonTek M9 aDcp uses different bin sizes depending on the water track frequency (section 2.1.3), these volumes could vary. Applying Method A might improve the velocity estimation for large measurement volumes at depth, as it does not rely on the homogeneity assumption. But as bins with a small number of velocity measurements will have greater error, this method can estimate velocities with error. Also, if the beam velocity distribution within each mesh cell is not linear, as averaging is made in the middle of each mesh cell, it can introduce error in velocity estimation. Thus, it is necessary to calculate a minimum necessary mesh cell size when applying Method A.

Method B is inherently limited by spatial averaging due to the potential use of divergent beams and the associated homogeneity assumption. In other words, one must assume that the velocity is homogeneous over the horizontal domain defined by beam divergence (Eq.12). Method A has the advantage that velocities are recorded within an individual beam depth bin, thus no spatial averaging between beams is required. However, in order for Method A to overcome the uncertainty induced by spatial averaging inherent to Method B, it is essential that the bin location is known explicitly. Error in bin location can be induced by dGPS position and or tilt sensor (pitch and roll) errors. We therefore compare possible bin position errors using Method A to beam divergence obtained from Method B to indicate when Method A should be advantageous over Method B.

Beam divergence is the spatial separation of the beams due to the Janus configuration of the beams with beam angles of 25°. This divergence determines the sampling volume that must be considered homogeneous for Method B and can be calculated using equation 12:

$$x_b = 2d\tan\theta \tag{12}$$

where *d* is the depth in *m* and *θ* is the beam angle which for a SonTek aDcp is 25°. The aDcp dGPS is used to reference the velocity measurements in space and to estimate the ship velocity. If dGPS is used for ship velocity, this introduces errors in measurement of the absolute water velocity (because ship velocity is subtracted from the water velocity measured in the reference frame of the aDcp). This uncertainty introduces error in velocity calculations.

To estimate the errors due to dGPS and the tilt sensors, in this study we assume normally distributed random errors with a standard deviation of ±1° for tilt sensors, based on manufacturer specifications, and a normally distributed displacement error measured by the dGPS for the dGPS positions (as a function of satellite configuration during measurement), and we apply a Monte Carlo approach which we run 100 times sampling under these uncertainties. Each time we calculate the estimated secondary velocity differences as compared with the original secondary velocities.

To be able to reduce the uncertainty due to velocity estimation using Method A compared to Method B, the errors induced in Method A related to GPS uncertainty and tilt sensors must be less than the errors in Method B due to beam divergence and the homogeneity assumption. Hence, Method A can be used if the error associated with a minimum aDcp cell size is in between the error due to beam divergence and the maximum estimated error due to the GPS and tilt sensors. Otherwise using this method introduces more error in velocity estimations than using Method B.

Data interpretation

Methods A and B, described above, were applied to the Sontek M9 data, to determine Cartesian velocities (v_x, v_y and v_z). As our interest is in process estimation, here we describe the methods we apply to the Cartesian velocities to estimate processes relevant to junction dynamics. In order to distinguish between primary and secondary components of flow, we need to rotate the initial mean transect. Options for doing this are reviewed in Lane et al. (2000) and we do not assess them here, but rather apply the zero net cross stream discharge definition (Lane et al., 2000). By calculating the mean values of the *x* and *y* velocity components (*U* and *V*), we then calculate the velocity magnitude (*v*). By rotating these velocity components to the direction of the cross-stream velocity, using the unique vector ($\boldsymbol{\sigma}$), primary velocity vectors ($\boldsymbol{v_p}$) and secondary velocity vectors ($\boldsymbol{v_s}$) then can be estimated.

$$\mathrm{v} = \sqrt{\mathrm{U}^2 + \mathrm{V}^2}$$

(13)

$$\begin{pmatrix}\sigma_x \\ \sigma_y\end{pmatrix} = \begin{pmatrix}U \\ V\end{pmatrix}/v \qquad (14)$$

where σ_x and σ_y are sin and cos of the angle between the section angle and east.

$$\boldsymbol{v}_p = \sigma_x \boldsymbol{v}_x + \sigma_y \boldsymbol{v}_y \tag{15}$$

$$\boldsymbol{v}_s = -\sigma_y \boldsymbol{v}_x + \sigma_x \boldsymbol{v}_y \tag{16}$$

However, secondary circulation is all flow that is orthogonal to the primary flow and not just horizontal flow; there should be not net secondary flux in a section; and so correction should also consider vertical velocities. Thus, we extend these relationships to include vertical velocities:

$$\begin{pmatrix} \sigma_{x,1} & \sigma_{x,2} & \sigma_{x,3} \\ \sigma_{y,1} & \sigma_{y,2} & \sigma_{y,3} \\ \sigma_{z,1} & \sigma_{z,2} & \sigma_{z,3} \end{pmatrix} = \begin{pmatrix} U \\ V \\ W \end{pmatrix} / v \tag{17}$$

where: *U*, *V* and *W* are the mean velocities of *x*, *y* and *z* velocity components, respectively and *v* is the magnitude of the velocity which can be obtained using:

$$v = \sqrt{U^2 + V^2 + W^2} \tag{18}$$

$$\boldsymbol{v}_p = \sigma_{x,1} \boldsymbol{v}_x + \sigma_{x,2} \boldsymbol{v}_y + \sigma_{x,3} \boldsymbol{v}_z$$

(19)

$$\boldsymbol{v}_s = \sigma_{y,1} \boldsymbol{v}_x + \sigma_{y,2} \boldsymbol{v}_y + \sigma_{y,3} \boldsymbol{v}_z$$

(20)

$$\boldsymbol{v}_v = \sigma_{z,1} \boldsymbol{v}_x + \sigma_{z,2} \boldsymbol{v}_y + \sigma_{z,3} \boldsymbol{v}_z$$

(21)

To estimate velocity gradients, and to correct for weak curvature with the survey method at the edges of each transect line (e.g. Figure 3), all data have been transformed into row and column coordinates (η and ζ) using the following transformation:

$$\begin{pmatrix} \frac{\partial}{\partial n} \\ \frac{\partial}{\partial z} \end{pmatrix} = \begin{pmatrix} \frac{\partial \eta}{\partial n} & \frac{\partial \zeta}{\partial n} \\ \frac{\partial \eta}{\partial z} & \frac{\partial \zeta}{\partial z} \end{pmatrix} \begin{pmatrix} \frac{\partial}{\partial \eta} \\ \frac{\partial}{\partial \zeta} \end{pmatrix} \tag{22}$$

where *n* and *z* are horizontal and vertical coordinates on the section plane, respectively (Vermeulen et al., 2014b).

Results

Primary and secondary velocities

Primary and secondary velocities estimated using methods A and B for the Lizerne-Rhône confluence appear to be similar at cross-section 6 (Figures 4a and 4b) and the differences in estimated secondary flows are minor. The differences are most pronounced between -10 and 5 m, in the middle of the main channel.

These primary and secondary velocity patterns show higher differences at cross-section 3 of the confluence of Grande Eau-Rhône (Figures 4c and 4d) despite it having a similar momentum ratio to the Lizerne during measurement. Primary velocities differ significantly between methods A and B: (1) at greater distance from the aDcp because the bins contain larger volumes of water assumed to be homogenous; and (2) at the edges of the cross-section where there are more beam velocity measurements (contours in Figures 4c and 4d). Secondary velocity vectors estimated using Method A indicate flow convergence at the surface and flow descending towards the riverbed throughout the centre of the channel (Figure 4c). This is due to a high degree of bed discordance between the Grande Eau and the Rhône, which increases the penetration of the tributary flow into the main channel over the junction, and which forms a zone of high lateral and vertical shear, on the one hand, and main channel narrowing because of penetration of the tributary mouth bar on the other

433 hand. The secondary velocity vectors estimated by Method B show a weaker penetration
434 of the tributary flow into the main channel, which results in a reverse flow towards the bank
435 on the tributary side of the channel at the surface of the mixing interface (Figure 4d). In
436 this case, the core of the secondary circulation is located in the middle of the main channel
437 and closer to the inner bank.

438 “Figure 4”

439 Figure 5 and Figure 6 quantify the differences in primary and secondary velocity patterns
440 estimated using methods A and B, for the Lizerne-Rhône confluence. Figures 5a and 5c
441 and Figures 6a show that almost 4% of mesh cells have a relative difference in primary
442 velocities between methods A and B of more than 10%. These differences can exceed
443 0.2 ms^{-1} and so they are relatively small. Velocity differences are more pronounced in
444 estimated secondary velocities, with almost 82% of mesh cells having a difference of more
445 than 10%, and almost 37% of mesh cells having a difference of more than 50% (Figure
446 5b, 5d and 6b).

447 “Figure 5”

448 “Figure 6”

449 At the Grande Eau-Rhône confluence, these differences are greater as compared with
450 those of the Lizerne-Rhône confluence. Figures 7a, 7c and 8a show that these differences
451 for primary velocities exceed 0.4 ms^{-1} in the zone of high vertical and lateral shear and
452 near the inner bank. Almost 20% of the mesh cells have a relative difference in primary
453 velocities between methods A and B of more than 10%. The secondary velocity
454 differences are more pronounced between these two methods. Figures 7b and 7d show

differences with a magnitude of 0.4 ms^{-1} near the edges and near the bed. Almost all the mesh cells have a difference in estimated secondary velocities between two methods. Figure 8b shows that almost 93% of the mesh cells have a relative difference of 10% between methods A and B. although this value decreases to 55% for a relative difference of 90% between these two methods.

“Figure 7”

“Figure 8”

Velocity gradients

As Figure 9 shows, there is a strong relationship between lateral gradient in secondary velocities and differences between the secondary velocities estimated using methods A and B for both the Lizerne-Rhône and the Grande Eau-Rhône confluences. This is because a stronger velocity gradient increases the probability that the assumption of flow homogeneity within a bin is likely to fail. Indeed, the marked differences between methods A and B at the Grande Eau confluence (Figure 7) are also in a zone of strong lateral shear.

“Figure 9”

Number of repeat transects

One way to reduce data fluctuations due to random errors and turbulence, during the measurement using moving vessel aDcps, is to average by using several repeat transects together in one cross section. As each estimated velocity measurement is a single sample in time, adding in a repeat section adds in an additional estimated velocity measurement. Under [8], this should cause the variance to increase, despite the number of measurements used in its estimation increasing, until the point at which there are enough repeats to capture the effects the range of scales of variation in turbulence impacting the measurement. Then, this variance will become stable. At this stage we can consider the number of repeats as the minimum number required to have a robust estimation of secondary velocity vectors that is to have reached estimates of velocity that are asymptotic on this stable state.

Here we apply both methods A and B to the survey of 16 repeats at cross-section 9 in Figure 3a at the Lizerne-Rhône confluence. To allow a reasonable comparison, three mesh cells in the middle of the cross section, and at three different depths (near the surface, middle depth and near the bed) have been chosen (Figure 11). Results show that by using Method A, after six repeats, a stable variance of the velocity estimator is obtained at the Lizerne-Rhône confluence (Figure 11a). Many more repeats are needed using Method B (Figure 11b) and this is likely because Method B uses fewer measurements per mesh cell. These results also show a higher standard deviation of the velocity estimation near the surface, using Method A and before achieving the stable situation. This can be explained by the fact that near the surface Method A is more sensitive to errors caused by positioning, while near the bed, hence with distance from the sounder, as the beam spread increases, the improvement obtained using Method A is more pronounced (Figure 11a).

“Figure 10”

“Figure 11”

DGPS and tilt sensor uncertainty analysis

As explained above a normally distributed random error has been applied 100 times to both dGPS positioning (by adding a random offset) and tilt sensors (by changing pitch and roll angles randomly) and the secondary velocities have been estimated using Method A for each perturbed dataset. As Figure 12 shows, the magnitude of errors related to dGPS accuracy are higher than those related to tilt sensor accuracy, for both confluences. These values can reach ±0.03 ms^{-1} and confirms the earlier finding of Rennie and Rainville (2006) which showed that GPS corrections can have average errors of about ±0.03 ms^{-1} (Figures 12a and 12c). These magnitudes are also higher near the surface and near the bed for the Lizerne-Rhône confluence (Figure 12a). Near the surface, as there fewer measurements that can contribute to the estimation of aDcp position and tilt, uncertainties in dGPS data will have a greater effect. Near the bed, as the velocity gradient is higher, errors will be greater as well. Figure 12c shows higher magnitudes near the surface at cross-section 3 in Figure 3b for the Grande Eau-Rhône confluence.

Errors related to tilt sensor uncertainty are higher where there is a higher velocity gradient. This is related to the fact that within the mesh cells with higher velocity gradients, as the velocity distribution is not linear, and as averaging is made in the middle of the mesh cell, it is more probable that the velocity will be affected by sensor inaccuracies of bin positioning, and so be in error (Figures 12b and 12d).

“Figure 12”

Homogeneity assumption analysis

Figure13 shows the maximum inhomogeneity allowance, using Method B for both case studies. These results are obtained by dividing the velocity gradient obtained from equation 22 by the divergence of the beams from equation 12. They confirm that, for the homogeneity assumption to be valid and thus error to be minimized using Method B, the maximum mesh cell size, which can be used is as small as 5cm near the bed. Clearly, this is impossible as the configuration of the beams using aDcps always results in beam divergence greater than 5cm.

“Figure 13”

Primary and secondary flow patterns

In this section, we compared estimated primary and secondary velocities using methods A and B for other cross sections in Figure 3 for both river confluences.

Figure 14 shows the results for cross sections 4, 5 and 7 (in Figure 3a) at the Lizerne-Rhône confluence. These cross sections also show similar results in primary and secondary velocity patterns for both methods A and B. Figure15 shows different patterns in primary and secondary velocities estimation using Method A and B for cross sections 4,6 and 8 in Figure 3b at the Grande Eau-Rhône confluence. Method A leads to the identification of a stronger and more coherent tributary penetration at cross-section 4 and weaker upwelling mid-channel, giving the impression of less intense secondary circulation (Figure 15). At section 6, flow towards the true left across the shallow top of the tributary mouth bar is identified and is coherent with Method A. At the channel-scale there is general flow convergence reflecting channel narrowing (Figure 15). When using Method B, these patterns are less coherent and flow is towards the true right in the vicinity of the tributary mouth bar. These patterns are repeated for section 8 (Figure 15).

“Figure 14”

“Figure 15”

Discussion

In this paper we used data collected with boat-mounted aDcp technology at two confluences of the Swiss river Rhône, both with similar and very low momentum ratios (0.018, 0.022) and analysed these using two different methods, A and B, to estimate Cartesian velocity components. Method A is based on a methodological approach developed by Vermeulen et al. (2014b). It differs by treating explicitly each individual beam velocity based on its position within a predefined mesh. Results show that this method reduces the volume over which the flow must be assumed to be homogenous (Fig 13). It can, but not necessarily does, result in differences in estimated primary and secondary velocities as compared with the more traditional method (B in this study), that involves determining velocities by averaging data from the spreading beams. Our results show that these differences are more pronounced in estimated secondary velocities than primary velocities and are higher where there is a greater lateral velocity gradient (Figure 9). The comparison between the two case studies shows that even though both confluences have a very low momentum ratio, as the confluence of the Grande Eau-Rhône has a more complex shear zone, likely due to the effects of bed discordance, and there are more significant differences in the estimation of primary and secondary velocities. This is related to the extent to which spreading of the aDcp measurement beams influences the secondary velocities, particularly in relation to lateral gradients in flow conditions. More standard methods (Method B in this study) are valid if the flow is completely homogenous over the diameter of the fluid column that the beams spread. This diameter varies over depth and is largest near the bed. In the case of the Grande Eau-Rhône confluence where stronger lateral velocity gradients exist in the flow, individual beams will not be measuring

566 homogenous conditions, particularly near the bed and in the zone of high shear near the
567 inner bank, because the spread of the beams may be greater in diameter than the width
568 of the zone of lateral velocity variation. In this case, as Method A involves less spatial-
569 averaging than Method B, it may provide more accurate information on the flow behavior,
570 but such a conclusion really needs a third and independent method to confirm it. At the
571 Lizerne-Rhône confluence, even though the momentum ratio is similar to Grande Eau-
572 Rhône confluence, there is only more localized shear in the flow and a simplified shear
573 zone (Figure 9). In such a situation, using Method B to detect the large scale patterns of
574 secondary flow may be more advantageous, because it involves more spatial averaging.

575 The above discussion suggests that whether or not high rates of later shear influence the
576 potential importance of Method A depends on distance from the aDcp: with more
577 divergence at greater depths, lower levels of lateral shear are likely to be acceptable.
578 Figures 16a and 16b quantifies the relationship between lateral velocity gradient, depth
579 and the magnitude of the relative differences in secondary velocities estimated using
580 methods A and B for the cross-section 6 of the Lizerne-Rhône and cross-section 3 of the
581 Grande Eau-Rhône confluences, respectively. At the Lizerne-Rhône confluence, as the
582 zone of high lateral shear is absent, even though there is a strong relationship between
583 the magnitude of the relative differences in secondary velocities estimated using methods
584 A and B and the depth (Figure 16a), their relationship with the lateral velocity gradients is
585 poor. In contrast, for the case of the Grande Eau-Rhône confluence (Figure 16b), where
586 increasing the lateral velocity gradient and depth results in higher relative differences in
587 secondary velocities. Thus, the need to use Method A will depend on the case being used
588 and the extent to which there is lateral shear at greater distances from the aDcp. This is

why whilst it may be tempting to introduce some kind of shear or velocity gradient threshold to identify when Method A might be preferable, to do so would be misleading as the threshold will also depend on the distance of the shear from the aDcp.

“Figure 16”

Results also confirm that several repeat transects are indispensable to provide a robust estimation of secondary circulation and to reduce the effect of spatial inhomogeneity and temporal variations. Although Method A reduces the minimum number of repeat transects needed to estimate the secondary velocities, a larger number of these minimum repeat transects (6 or more repeats for Lizerne-Rhône confluence) appeared to be required. This is higher than in the earlier findings of Szupiany et al. (2007) and Vermeulen et al., (2014b) who argue that 5 repeats are enough to have a robust estimation of the turbulence averaged velocity. We also note that an even number of repeats may be important to avoid directional bias in dGPS positions.

Since Method A is based on the position of beams, if the bin position errors related to dGPS accuracy as well as sensor tilt are greater than homogeneity errors associated with beam divergence, standard Method B is more reliable. This is likely to be the case particularly in rivers shallower than those studied here and where high resolution is required due to large velocity gradients. In rivers of the scale studied here, and deeper, by increasing the mesh cell size, we can still have sufficient data to estimate velocity vectors, and the effects dGPS and tilt sensor errors have a minor effect. This confirms the earlier findings by Vermeulen et al., (2014b), which showed that Method A provides the greatest improvement where the aDcp cell size is much smaller than the beam spread. We are not yet in a position to identify the depth at which Method A becomes preferable to Method B, and again this will depend on other parameters such as the intensity of shear and so may not be readily generalizable between confluences.

The difficulty of identifying the depths of rivers and intensities of shear that make one method preferable over another precludes adoption of simple quantitative guidance on which method to use when. As both methods have some disadvantages, we argue that both methods should be applied. If they give similar results, then there should be confidence in both. If and where they differ, analysis should be undertaken to identify why, and hence which method is likely to be preferable. Association of the differences in primary and secondary velocities inferred between the two methods with estimates of shear intensity and with estimated tilt and positioning errors should then help decide whether Method A or Method B is preferable in a particular case. This preference may vary between confluences but also through time at a confluence, if shear or flow depth changes significantly between survey dates.

Finally, we wish to emphasise that the impact of averaging is only one element that must be considered in obtaining reliable primary and secondary clow estimates in river confluences. Other issues, such as the rotation method needed to distinguish primary and secondary circulation, remain important and should be considered routinely.

Conclusions

This paper shows the advantage of working with the radial (beam) velocity measurements of an aDcp within each bin prior to averaging them across a given volume of fluid (Method A) as opposed to identify volumes of fluid and assuming bend homogeneity within them (Method B). Such a treatment is important where there are strong velocity gradients in the flow as with river channel confluences. In the first of our case-study confluences, the

Lizerne-Rhône, a very small tributary joined the main river, and the pattern of primary and secondary velocities obtained with methods A and B were relatively similar, more so for primary velocities. But for a second confluence, the Grande Eau-Rhône, with a similar momentum ratio, there were much larger differences. We attributed this to the formation of much stronger shear at this confluence. Method A also appeared to reduce the number of repeat transects needed to estimate secondary velocities reliably. The main downside is that Method A is more sensitive to errors related to positioning. Thus, good dGPS accuracy and precision are required to perform a robust estimation of velocity.

In smaller/shallower rivers, Method B may be acceptable indeed preferable as it is less sensitive to GPS errors. In larger rivers, Method A may be necessary, especially in the presence of strong shear at the confluence. Choice between these methods should be based upon an initial screening of the extent to which there is strong shear in the flow as well as the extent to which bins further from the aDcp are influenced by beam divergence.

Appendix A

The LOWESS model is a locally weighted polynomial regression, which at each point and in the range of dataset, a low degree polynomial is fitted to a subset of the data, using weighted least squares. This polynomial fit gives more weight to points closer to the point whose response is being estimated. The value of the regression function for the point is then obtained by evaluating the local polynomial using the explanatory variable values for that data point. The LOWESS fit is complete after regression function values have been computed for each of the *n* data points. Many of the details of this method, such as the degree of the polynomial model and the weights, are flexible (“Local regression,” n.d.).

Acknowledgements

This paper benefited from constructive and detailed suggestions from two anonymous reviewers and Editor Mike Kirkby. The work was supported by Swiss National Science Foundation Grant 200021_160020. The codes used may be obtained upon request to Gelare Moradi.

References

Alvarez, L. V., Schmeeckle, M.W., Grams, P.E., 2017. A detached eddy simulation model for the study of lateral separation zones along a large canyon-bound river. J. Geophys. Res. Earth Surf. 122, 25–49. https://doi.org/10.1002/2016JF003895.

Ashmore, P.E., Ferguson, R.I., Prestegaard, K.L., Ashworth, P.J. and Paola, C., 1992. Secondary flow in coarse-grained braided river confluences. Earth Surface Processes and Landforms, 17, 299– 312.

Best, J.L. and Roy, A.G., 1991. Mixing-layer distortion at the confluence of channels of different depth. Nature, 350, 411–413.

Biron, P., De Serres, B., Roy, A.G., Best, J.L., 1993. Shear layer turbulence at an unequal depth channel confluence. In: Clifford, N.J., French, J.R., Hardisty J. (editors) Turbulence: Perspectives on Flow and Sediment Transport, Wiley, Chichester, 197–213.

Dinehart, R.L. and Burau, J.R., 2005. Averaged indicators of secondary flow in repeated acoustic Doppler current profiler crossings of bends. Water Resources Research, 41, W09405.

Engel, F.L. and Rhoads, B.L., 2016. Three-dimensional flow structure and patterns of bed shear stress in an evolving compound meander bend. Earth Surface Processes and Landforms, 41, 1211–1226.

Gualtieri, C., Ianniruberto, M., Filizola, N., Santos, R. and Endreny, T., 2017. Hydraulic complexity at a large river confluence in the Amazon basin. Ecohydrology, 10, e1863

Gunawan, B., Neary, V.S., McNutt, J.R., 2011. Ornl Adv Post-Processing Guide and Matlab Algorithms for Mhk Site Flow and Turbulence Analysis, Ornl/Tm-2011/404. doi:10.2172/1034377.

Jackson, P.R., Garcia, C.M., Oberg, K.A., Johnson, K.K. and Garcia, M.H., 2008. Density currents in the Chicago River: Characterization, effects on water quality, and potential sources. Science of the Total Environment 401: 130–143.

Kasvi, E., Vaaja, M., Alho, P., Hyyppä, H., Hyyppä, J., Kaartinen, H. and Kukko, A., 2013. Morphological changes on meander point bars associated with flow structure at different discharges. Earth Surface Processes and Landforms, 38, 577-590.

Kasvi, E., Laamanen, L., Lotsari, E. and Alho, P., 2017. Flow Patterns and Morphological Changes in a Sandy Meander Bend during a Flood-Spatially and Temporally Intensive ADCP Measurement Approach. Water, 9, 106.

Knox, R. L. and Latrubesse, E.M., 2017. A geomorphic approach to the analysis of bedload and bed morphology of the Lower Mississippi River near the Old River Control Structure. Geomorphology, 268, 35-47.

Konsoer, K.M. and Rhoads, B.L., 2014. Spatial-temporal structure of mixing interface turbulence at two large river confluences. *Environmental Fluid Dynamics*, 14, 1043-1070.

Kostaschuk, R.A., Shugar, D., Best, J.L., Parsons, D.R., Lane, S.N., Hardy, R.J. and Orfeo, O., 2009. Suspended sediment transport and deposition over a dune: Río Paraná, Argentina. Earth Surface Processes and Landforms, 34, 1605–1611.

Lane, S.N., Parsons, D.R., Best, J.L., Orfeo, O., Kostaschuk, R. a., Hardy, R.J., 2008. Causes of rapid mixing at a junction of two large rivers: Río Paraná and Río Paraguay, Argentina. Journal of Geophysical Research, 113, 1–16. https://doi.org/10.1029/2006JF000745.

Lane, S.N., Bradbrook, K.F., Richards, K.S., Biron, P.M., Roy, a. G., 2000. Secondary circulation cells in river channel confluences : measurement artefacts or coherent flow structures ? Hydrological Processes, 14, 2047–2071. https://doi.org/10.1002/1099-1085(20000815/30)14:11/12<2047::aid-hyp54>3.0.co;2-4.

Local regression [WWW Document], n.d. URL:https://en.wikipedia.org/wiki/Local_regression (accessed 1.22.18).

Lotsari, E., Kasvi, E., Kämäri, M., and Alho, P., 2017. The effects of ice cover on flow characteristics in a subarctic meandering river. Earth Surface Processes and Landforms, 42, 1195–1212.

Marsden, R.F. and Ingram, R.G., 2004. Correcting for beam spread in acoustic Doppler current profiler measurements. Journal of Atmospheric and Oceanice Technology, 21, 1491–1498.

Morlock, S.E., 1996. Evaluation of Acoustic Doppler Current Profiler Measurements of River Discharge. U.S. Geological Survey Water Resources Investigations Report 95-4218.

Muste, M., Yu, K. and Spasojevic M. 2004. Practical aspects of ADCP data use for quantification of mean river flow characteristics: Part I: Moving-vessel measurements. Flow Measurement and Instrumentation, 15, 1–16.

Parsapour-Moghaddam, P. and Rennie, C.D., 2018. Calibration of a 3D Hydrodynamic meandering river model using fully spatially distributed 3D ADCP velocity data. Journal of Hydraulic Engineering, 144, 04018010.

Parsons, D.R., Best, J.L., Orfeo, O., Hardy, R.J., Kostaschuk, R.A. and Lane, S.N., 2005. The morphology and flow fields of three-dimensional dunes, Rio Paraná, Argentina: results from simultaneous multibeam echo sounding and acoustic Doppler current profiling. Journal of Geophysical Research, 110, F04S03.

Parsons, D.R., Best, J.L., Lane, S.N, Orfeo, O., Hardy, R.J. and Kostaschuk, R.A., 2007. Form roughness and the absence of secondary flow in a large confluence-diffluence, Rio Paraná, Argentina. Earth Surface Processes and Landforms, 32, 155–162.

Parsons, D.R., Jackson, P.R., Czuba, J.A., Engel, F.L., Rhoads, B.L., Oberg, K.A., Best, J.L., Mueller, D.S., Johnson, K.K., Riley, J.D., 2013. Velocity Mapping Toolbox (VMT): A processing and visualization suite for moving-vessel ADCP measurements. Earth Surface Processes and Landforms, 38, 1244–1260.

Petrie, J., Diplas, P., Gutierrez, M. and Nam, S., 2013. Combining fixed- and moving-vessel acoustic Doppler current profiler measurements for improved characterization of the mean flow in a natural river. Water Resources Research, 49, 5600–5614.

Rennie, C.D., Millar, R.G. and Church, M.A., 2002. Measurement of bed load velocity using an acoustic Doppler current profiler. Journal of Hydraulic Engineering – ASCE, 128, 473-483.

Rennie, C.D. and Millar, R.G., 2004. Measurement of the spatial distribution of fluvial bedload transport velocity in both sand and gravel. Earth Surface Processes and Landforms, 29, 1173-1193.

Rennie, C.D., Rainville, F., 2006. Case study of precision of GPS differential correction strategies: influence on aDcp Velocity and discharge estimates. Journal of Hydraulic Engineering, 132, 225–234.

Rennie, C. D., and Church, M., 2010. Mapping spatial distributions and uncertainty of water and sediment flux in a large gravel bed river reach using an acoustic Doppler current profiler, Journal of Geophysical Research – Earth Surface, 115.

Rhoads, B.L. and Kenworthy, S.T., 1995. Field measurements of flow structure at a high-angle asymmetrical stream confluence. Geomorphology 11, 273–293.

Rhoads, B.L. and Kenworthy, S.T., 1998. Time-averaged flow structure in the central region of a stream confluence. *Earth Surface Processes and Landforms*, 23, 171-191.

Rhoads, B.L., and Sukhodolov, A.N., 2001. Field investigation of three-dimensional flow structure at stream confluences: 1. Thermal mixing and time-averaged velocities. Water Resources Research, 27, 2393-410.

Rhoads, B.L., and Sukhodolov, A.N., 2004. Spatial and temporal structure of shear layer turbulence at a stream confluence. Water Resources Research, 40, W06304.

Rhoads, B.L., and Sukhodolov, A.N., 2008. Lateral momentum flux and the spatial evolution of flow within a confluence mixing interface. Water Resources Research, 44, W08440.

Riley, J.D. and Rhoads, B.L., 2012. Flow structure and channel morphology at a natural confluent meander bend. Geomorphology, 163, 84-98.

Riley, J.D., Rhoads, B.L., Parsons, D.R. and Johnson K.K., 2015. Influence of junction angle on three-dimensional flow structure and bed morphology at confluent meander bends during different hydrological conditions. Earth Surface Processes and Landforms, 40, 252–271.

Shugar, D.H., Kostaschuk, R., Best, J.L., Parsons, D.R., Lane, S.N., Orfeo, O. and Hardy, R,J., 2010. On the relationship between flow and suspended sediment transport over the crest of a sand dune, Río Paraná, Argentina. Sedimentology 57: 252–272.

SonTek YSI, 2000. Acoustic Doppler Profiler (ADP ®) Principles of Operation.

SonTek YSI, 2010. RiverSurveyor S5/M9 System Manual 115.

Sukhodolov, A.N. and Rhoads, B. L., 2001. Field investigation of three-dimensional flow structure at stream confluences 2. Turbulence. Water Resources Research, 27, 2411-2424.

Sukhodolov, A. N., Krick, J., Sukhodolova, T. A., Cheng, Z., Rhoads, B. L. and Constantinescu, G. S., 2017. Turbulent flow structure at a discordant river confluence:

783 Asymmetric jet dynamics with implications for channel morphology. Journal of
784 Geophysical Research: Earth Surface, 122(6), 1278-1293.
785 https://doi.org/10.1002/2016JF004126.

786 Szupiany, R.N., Amsler, M.L., Best, J.L. and Parsons, D.R., 2007. Comparison of fixed-
787 and moving vessel measurements with an aDp in a large river. Journal of Hydraulic
788 Engineering, 133, 1299–1309.

789 Szupiany, R.N., Amsler, M.L., Parsons, D.R. and Best, J.,L., 2009. Morphology, flow
790 structure, and suspended bed sediment transport at two large braid-bar confluences.
791 Water Resources Research, 45, W05415.

792 Szupiany, R.N., Amsler, M.L., Hernandez, J., Parsons, D.R., Best, J.L., Fornari, E. and
793 Trento, A., 2012. Flow fields, bed shear stresses, and suspended bed sediment
794 dynamics in bifurcations of a large river. Water Resources Research, 48, W11515.

795 Tomas, G., Bleninger, T., Rennie, C.D., Guarneri, H., 2018. Advanced 3D mapping of
796 hydrodynamic parameters for the analysis of complex flow Motions in a submerged
797 bedrock canyon of the Tocantins River, Brazil. Water (Switzerland) 10, 1–19.
798 https://doi.org/10.3390/w10040367.

799 Tsubaki, R., Kawahara, Y., Muto, Y. and Fujita, I., 2012. New 3-D flow interpolation
800 method on moving ADCP data. Water Resources Research, 48, 1–15.

801 Venditti, J.G., Rennie, C.D., Bomhof, J., Bradley, R.W., Little, M., Church, M., 2014. Flow
802 in bedrock canyons. Nature 513, 534–537. https://doi.org/10.1038/nature13779.

Vermeulen, B., Hoitink, A.J.F., van Berkum, S.W. and Hidayat, 2014a. Sharp bends associated with deep scours in a tropical river: The river Mahakam (East Kalimantan, Indonesia). Journal of Geophysical Research, Earth Surface, 119, 1441–1454.

Vermeulen, B., Sassi, M.G. and Hoitink, A.J.F., 2014b. Improved flow velocity estimates from moving-boat ADCP measurements. Water Resources Research, 50, 4186–4196.

Vermeulen, B., Hoitink, A.J.F. and Labeur, R.J., 2015. Flow structure caused by a local cross-sectional area increase and curvature in a sharp river bend. Journal of Geophysical Research, Earth Surface, 120, 1771-1783.

Zhao, J., Chen, Z., and Zhang, H., 2014. A robust method for determining the heading misalignment angle of GPS compass in ADCP measurement. Flow Measurements and Instrumentation, 35, 1–10.